FE-2028-7

MASTER

KINETICS AND MECHANISM OF DESULFURIZATION AND
DENITROGENATION OF COAL-DERIVED LIQUIDS

Sixth Quarterly Report, September 21, 1976—December 20, 1976

By
Bruce C. Gates
James R. Katzer
Jon H. Olson
Harold Kwart
Alvin B. Stiles

November 1977
(TIC Issuance Date)

Departments of Chemical Engineering and Chemistry
University of Delaware
Newark, Delaware

U. S. DEPARTMENT OF ENERGY

FOSSIL ENERGY

DISCLAIMER

DISCLAIMER

Portions of this document may be illegible in electronic image products. Images are produced from the best available original document.

NOTICE

KINETICS AND MECHANISM OF DESULFURIZATION AND

DENITROGENATION OF COAL-DERIVED LIQUIDS

Sixth Quarterly Report for Period

September 21, 1976, to December 20, 1976

Prepared by:

Bruce C. Gates, James R. Katzer,
Jon H. Olson, Harold Kwart, and Alvin B. Stiles

Departments of Chemical Engineering and Chemistry
University of Delaware
Newark, Delaware 19711

Date Published

December 22, 1976

Prepared for

Fossil Energy
Energy Research and Development Administration
Washington, D.C.

Under Contract No. E(49-18)-2028

I.   <u>ABSTRACT</u>

Two high-pressure flow microreactors continue to function effectively for studies of the hydrodesulfurization of dibenzothiophene, methyl-substituted dibenzothiophene and also for studies of the hydrodenitrogenation of quinoline. The construction of the badly needed third microreactor unit now is complete.

The hydrodesulfurization of dibenzothiophene has been examined in the flow system in a totally reproducible fashion which is free from catalyst deactivation for extended periods. The reaction is first-order in dibenzothiophene, and all of the reaction products except H_2S are sulfur free.

A program for determining the kinetics and reaction network of methyl-substituted dibenzothiophenes was started. For example, the rate for hydrodesulfurization of 4,6-dimethyldibenzothiophene is about one-fifth the rate for dibenzothiophene. The hydrocarbon reaction products except H_2S are sulfur free; therefore, the initial point of attack is concluded to be the C-S bond.

The hydrodenitrogenation of quinoline was examined further by replacing white oil with hexadecane; this substitution permits the determination of the nitrogen-free reaction products by gas chromatography. These studies show that the C-N bond is broken after at least the heterocyclic ring and preferably both rings are hydrogenated. The hydrogenolysis reactions are rate limiting for the overall process of nitrogen removal. Further, since one of the two major reactions for hydrogenolysis, the conversion of 1,2,3,4-tetrahydroquinoline to o-propylaniline, exhibits decreasing reaction rate with increasing hydrogen partial pressure, the overall hydrodenitrogenation has maximum rate at about 1600 psi hydrogen partial pressure.

The hydrodenitrogenation of acridine is slower than that of quinoline. The reaction network shows that the molecule must be hydrogenated before nitrogen removal occurs at a significant rate.

Aged catalyst samples from a proprietary fixed-bed coal liquefaction process and from the II-coal process were examined with scanning electron microscopy and an electron microprobe. Coal mineral matter penetrates circa 100 μm into the catalyst of each sample, and the fixed-bed catalyst also is covered with a 10-15 μm crust of deposited material.

TABLE OF CONTENTS

TABLE OF CONTENTS (cont)

LIST OF TABLES

LIST OF FIGURES

LIST OF FIGURES (cont)

LIST OF FIGURES (cont)

II. OBJECTIVES AND SCOPE

The major objectives of this research are as follows:

i) To develop high-pressure liquid-phase microreactors for operation in pulse and steady-state modes to allow determination of quantitative reaction kinetics and catalytic activities in experiments with small quantities of reactants and catalyst.

ii) To determine reaction networks, reaction kinetics, and relative reactivities for catalytic hydrodesulfurization of multi-ring aromatic sulfur-containing compounds found in coal-derived liquids.

iii) To determine reaction networks, reaction kinetics, and relative reactivities for catalytic hydrodenitrogenation of multi-ring aromatic nitrogen-containing compounds found in coal-derived liquids.

iv) To obtain quantitative data characterizing the chemical and physical properties of aged hydroprocessing catalysts used in coal liquefaction processes and to establish the mechanisms of deactivation of these hydroprocessing catalysts.

v) To develop reaction engineering models for predicting the behavior of coal-to-oil processing and of catalytic hydroprocessing of coal-derived liquids and to suggest methods for improved operation of hydrosulfurization and hydrodenitrogenation processes.

vi) In summary, to recommend improvements in processes for the catalytic hydroprocessing of coal-derived liquids.

SCOPE

A unique high-pressure, liquid-phase microreactor is
being developed for pulse (transient) and steady-state modes
of operation for kinetic measurements to achieve objectives
ii) through iv). The relative reactivities of the important
types of multi-ring aromatic compounds containing sulfur
and nitrogen are being measured under industrially important
conditions (300-450°C and 500-4000 psi). The reaction net-
works and kinetics of several of the least-reactive multi-
ring aromatic sulfur-containing and nitrogen-containing
compounds commonly present in coal-derived liquids will be
determined. Catalyst deactivation is an important aspect
of the commercial scale upgrading of coal-derived liquids.
Accordingly, the chemical and physical properties of com-
mercially aged coal-processing catalysts are being determined
to provide an understanding of catalyst deactivation; these
efforts can lead to improved catalysts or procedures to
minimize the problem. To make the results of this and
related research most useful to ERDA, reaction engineering
models of coal-to-oil processing in trickle-bed and slurry-
bed catalytic reactors including deactivation will be developed
to predict conditions for optimum operation of these processes.
Based on the integrated result of all of the above work,
recommendations will be made to ERDA for improved catalytic
hydrodesulfurization and hydrodenitrogenation processing.

III.   SUMMARY OF PROGRESS TO DATE

     This summary is organized to parallel the task statements of the contract. A milestone chart is provided at the end of this section.

Microreactor Development

     Three continuous-flow, liquid-phase, high-pressure micro-reactors have been built and operated under this contract. The work in this report confirms the success of these microreactors; the data from the batch autoclave runs are effectively identical to data from the flow microreactors. Task 1 has been completed.

Hydrodesulfurization

     The hydrodesulfurization of dibenzothiophene (DBT) has been examined with a liquid-phase, high-pressure microreactor and in batch, stirred autoclave experiments. The range of data collected thus far shows that the reaction network is the direct reduction of DBT to hydrocarbon products; the reaction rate is first-order in the concentration of DBT. The principal product of the reaction is biphenyl; phenylcyclohexane and bicyclohexane have been iden-tified tentatively as the other two hydrocarbon reaction products.

     The study of the relative reactivities of methyl-substituted dibenzothiophene has begun. In particular, hydrodesulfurization of 4,6-dimethyldibenzothiophene is about 1/5 the rate for hydro-desulfurization of DBT. Further, there are no organic products containing sulfur; the first point of attack is the C-S bond. The reduction in reaction rate is presumed to be caused by severe steric blocking of the reactive sulfur atom by the protruding methyl groups.

Catalytic Hydrodenitrogenation

     The hydrodenitrogenation of quinoline has been studied to yield a nearly complete identification of the reaction network and partial identification of the rate parameters in this network. The network under catalytic conditions is as follows:
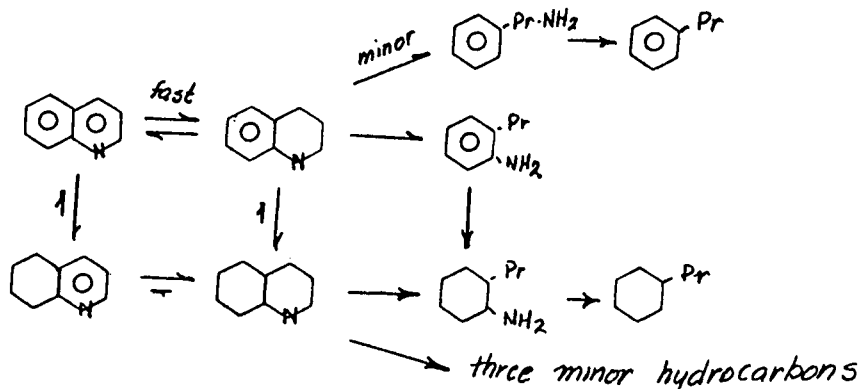
This network shows that usually both the benzene and pyridine
rings are saturated before the C-N bond in the (now) piperidine
ring is broken. Thus, the HDN of quinoline requires a large
consumption of hydrogen before the N atom is removed from the
hydrocarbon backbone. This reaction network is similar to the
one proposed by Goudriaan (1974). The temperature sensitivity of
the rate constants shows that the hydrogenation of the complete
ring structures has very low activation energy whereas the ring-
opening hydrogenolysis has an activation energy in the range of
20 to 35 Kcal/gmole. The overall activation energy for nitrogen
removal is about 25 Kcal/mole, and therefore the hydrogenolysis
reactions are rate determining in the temperature and pressure
range investigated.

The total rate of HDN shows a maximum with respect to hydrogen
partial pressure. However, the only individual reaction in the net-
work which decreases in rate with hydrogen partial pressure is the
conversion of 1,2,3,4-tetrahydroquinoline to ortho-n-propylaniline;
therefore, this reaction dominates the overall network at high pressure.

The HDN of acridine is more complex than that of quinoline
because the number of hydrogenated intermediates formed before
hydrogenolysis is much greater. This reaction network will be
described in the next progress report; the overall reaction rate for
acridine is much lower than for quinoline. The network for the
HDN of carbazole has not yet been identified because a separation
scheme for the reaction products is in the beginning stages.

Catalyst Deactivation

A variety of physical techniques have been used to identify
the aging processes for catalysts used in synthetic liquid fuel
processes. Thus far catalyst samples from three processes have
been examined: a proprietary fixed-bed process, Synthoil, and
H-Coal. The spent fixed-bed catalysts show the formation of an
external crust which appears to be formed by columnar grain growth
combined with the deposition of coal mineral matter, particularly
clays and rutile. This external crust is absent from the H-Coal
catalyst. The interior of the catalyst is altered by several
processes: coking, reactive deposition of mineral matter, passive
deposition of mineral matter, and crack enhancement. These four
processes are found in catalysts from all three processes. Coking
fills the micropore volume of the catalyst. Reactive deposition
of mineral matter penetrates about 200 μm from the outer surface
into the interior of the catalyst. The concentration profile is
approximately exponentially decreasing from the surface. Passive
cementing occurs within 50 μm of the surface unless the cracks
have been enlarged by grain growth; this deposition yields
irregular concentration profiles. Finally, grain growth can occur

inside the catalyst near the surface and tends to increase these cracks. When the surface cracks become a significant portion of the pore volume, passive deposition can penetrate further into the interior of the catalyst.

Microreactor Engineering

The use of moments as a tool in interpreting pulse data from microreactors has been extended to fairly complex reaction networks. This work is now complete. The complex data for quinoline and acridine reactions have been reduced to rate parameters by extension of nonlinear regression analysis.

	0	1	2
Year			

ACCOMPLISHMENT

A. APPARATUS CONSTRUCTION

1st High-Pressure
Microreactor
Completed   month 6

2nd High-Pressure
Microreactor
Completed   month 10

Batch Reactors
Completed   month 4

**B. MICROREACTOR
STUDIES OF HDS & HDN**

Definition of reaction
procedures and opera-
ting conditions   month 8

Choice of HDN
Catalyst   month 8

Reaction Studies For:

| Benzothiophene | month 6 | month 12 |

Quinoline

Dibenzothiophene   month 12   month 18   75%

Carbazole   started

| Naphthobenzothiophene | month 18 | month 24 |
| Acridine | 15% | month 24 | month 28 |

Higher molecular
weight and methyl-
substituted nitrogen
and sulfur compounds   month 12 started   month 28

Reaction Kinetics,
Reaction Networks and
Inhibitor Studies of
Least Reactive Sulfur
and Nitrogen Compounds   month 18   month 28

HDS-HDN:
Simultaneously,
Effect of Inhibitors   month 16   month 3

13

0	1	2

Year

C. CATALYST DEACTIVATION
   SYNTHOIL
   CATALYST:

   Physical
   Properties   month 6

   Chemical
   Properties   month 6   10%   *no catalyst available*   until 5/77   month 16

   Other Deacti-
   vated Cata-   90%   month 26
   lysts   month 10

   Catalyst
   Deactivation
   Studies   start   month 14   month 30

D. REACTION ENGINEERING
   Reactor Models
   for Pulse and Flow   75
   Microreactors   month 14

   Process Reaction
   Engineering   5
                           month 14   month 36

14

---

 *Time Plan and Milestone Chart as Presented in Proposal.
**Hatching indicates that activity indicated is under
  active investigation; number in hatched region indicates
  the precentage completed; crosshatching indicates that
  the task has been completed.

CUMULATIVE EXPENDITURES [*]

Quarter

Item	First	Second	Third	Fourth	Fifth	Sixth
Personnel	$5,807	$20,740	$37,396	$53,418	$91,593	$112,666
Travel	28	528	1,152	1,152	1,521	2,458
Supplies & Expenses	4,674	10,007	19,582	25,735	37,291	42,341
Occupancy & Maintenance	6,110	9,208	10,108	10,634	13,755	13,920
Equipment	610	17,978	30,704	34,930	50,614	54,013
Information Processing	--	--	--	97	154	375
Transfers (Overhead)	--	10,202	20,035	38,710	75,839	93,287

*Includes encumbrances

15

IV.   DETAILED DESCRIPTION OF TECHNICAL PROGRESS

A.   HYDROPROCESSING MICROREACTOR DEVELOPMENT

The first two high-pressure liquid-phase flow microreactors are in routine operation, and data appear later in this report. The third microreactor is almost completely constructed, and it is expected to be in routine operation as well within a few weeks. This third unit is the final one, and the equipment construction is therefore almost complete.

B.   CATALYTIC HYDRODESULFURIZATION

1.   Experimental

a.   Liquid-phase high-pressure flow microreactor

During this quarter the assembly of the third microreactor almost has been completed. The third microreactor will enable us to proceed full time with the planned studies of the kinetics and reaction networks of methyl-substituted dibenzothiophene hydrodesulfurization simultaneously with dibenzothiophene.

All the experiments with the high-pressure liquid-phase flow microreactor covered in this report were carried out under the same conditions described in detail previously (see Fifth Quarterly Report). These operating conditions are summarized briefly below:

·Catalyst: HDS 16A; mass: 25 mg; volume of reactor bed: 0.325 ml; length of bed: 4.1 cm; catalyst-particle size = 149-178 μm.

·Pretreatment: catalyst sulfided _in situ_ with 10% H_2S in H_2 for 2 hours at 400°C.

·H_2 saturation pressure: 1000 psig.

·Reaction temperature: 300°C.

·Liquid flow rate: 1.2 cm^3/hr unless otherwise specified

·Reactant mixture (unless otherwise mentioned):   0.1225 wt% dibenzothiophene in n-hexadecane solvent.

b. Batch reactor experiments: dibenzothiophene
    hydrodesulfurization

Two experiments were carried out using a one-liter autoclave
reactor. Based on an evaluation of the earlier operating exper-
ience with hydrodenitrogenation, the following procedure was
adopted:

The catalyst was presulfided at 400°C for two hours and cooled
to room temperature under 10% H_2S in H_2 flow. After adding 15 cm^3
of n-hexadecane or reactant mixture to the injection loader, the
catalyst was added to the loader. An additional 15 cm^3 of reactant
mixture or pure n-hexadecane then was added, and the total mixture
was injected into the autoclave.

The reactant mixture in the autoclave was prepared by purging
with hydrogen at room temperature and then bringing the charge
to reaction temperature under the desired hydrogen partial pressure.

The experimental conditions were the following:

·Catalyst: HDS 16A, 80-100 mesh.

·Catalyst mass: Run 8:667 mg
                 Run 9:220 mg.

·Reaction temperature : 300°C.

·Hydrogen pressure: Run 8:280 psig.
                     Run 9:1000 psig.

·Reactant mixture: ~0.3 wt% dibenzothiophene in n-
                    hexadecane

·Volume of reactant mixture: Run 8:320 cm^3.
                              Run 9:350 cm^3.

2. Results and Discussion

a. Hydrodesulfurization of dibenzothiophene

(i) Liquid-phase high-pressure microreactor.

Blank experiments

The hydrodesulfurization activity of an empty reactor and
a reactor filled with quartz chips (previously used to dilute
the catalyst) was determined. In both experiments the reactor
was subjected to the same pretreatment used in earlier experiments
(2 hrs at 400°C with 10% H_2S in H_2). Less than 1% dibenzothiophene
hydrodesulfurization conversion was observed with an empty reactor.
The reactor filled with quartz chips showed a conversion level of
8% based on the disappearance of dibenzothiophene. After 70
hours only 3% conversion was observed (Figure 1). Under the
same conditions, a run with 25 mg of catalyst led to 65-80%

sulfur removal.

Although the hydrodesulfurization activity of quartz chips is not large compared with that of the Co-Mo/γ-Al$_2$O$_3$ catalyst, its effect would be pronounced when small amounts of catalyst were used for initial rate determinations. Consequently, the use of another inert was necessary.

The quartz chips were therefore replaced by alundum. As shown in Figure 1, the hydrodesulfurization activity of a reactor filled with alundum (90 mesh) under our experimental conditions corresponds to less than 1% conversion of dibenzothiophene. Based on this result, alundum is to be used in future experiments as the inert material in the catalyst bed.

Reproducibility tests

As mentioned in the Fifth Quarterly Report, reproducibility tests were carried out without mechanical stirring of the reactant mixture during the saturation with hydrogen. We have repeated these experiments after the saturator problem was eliminated.

Seven independent runs were carried out, each with fresh catalyst and reactant mixture. Quartz chips were used as (supposedly inert) packing material to dilute the catalyst in the early runs 1 to 5. Alundum was used as a diluent in runs 6 and 7 (Figure 3)

Examination of the results leads to the following conclusions: Run 1 shows a sharp decline in hydrodesulfurization activity of the catalyst. The rate of deactivation became consistently less pronounced with each successive run. Runs 6 and 7 were carried out with alundum used as packing material, and less than a 5% decline in activity was observed during 110-hour runs (Figure 3). The same conversion is obtained in run 5 when the HDS activity of the quartz chips is taken into account.

We attribute the steep decrease in activity observed in run 1 to an insufficient purging of the reactant mixture used in previous runs (see Fifth Quarterly Report) due to stirrer malfunctioning. The malfunction probably introduced some unidentified catalyst poison into the microreactor lines*. The fact that with each run the rate of deactivation decreased substantially indicates a slow purging of the unidentified poison from the microreactor lines.

The reproducibility finally achieved in runs 5, 6, and 7 is quite satisfying, especially when one takes into account that these are completely independent experiments with variables including hydrogen saturation pressure, sulfiding procedure, catalyst amount, length of catalyst bed, reactor temperature, and GC analysis.

*There is further support for the argument that the deactivation is attributable to the feed; namely, all runs had the same initial activity.
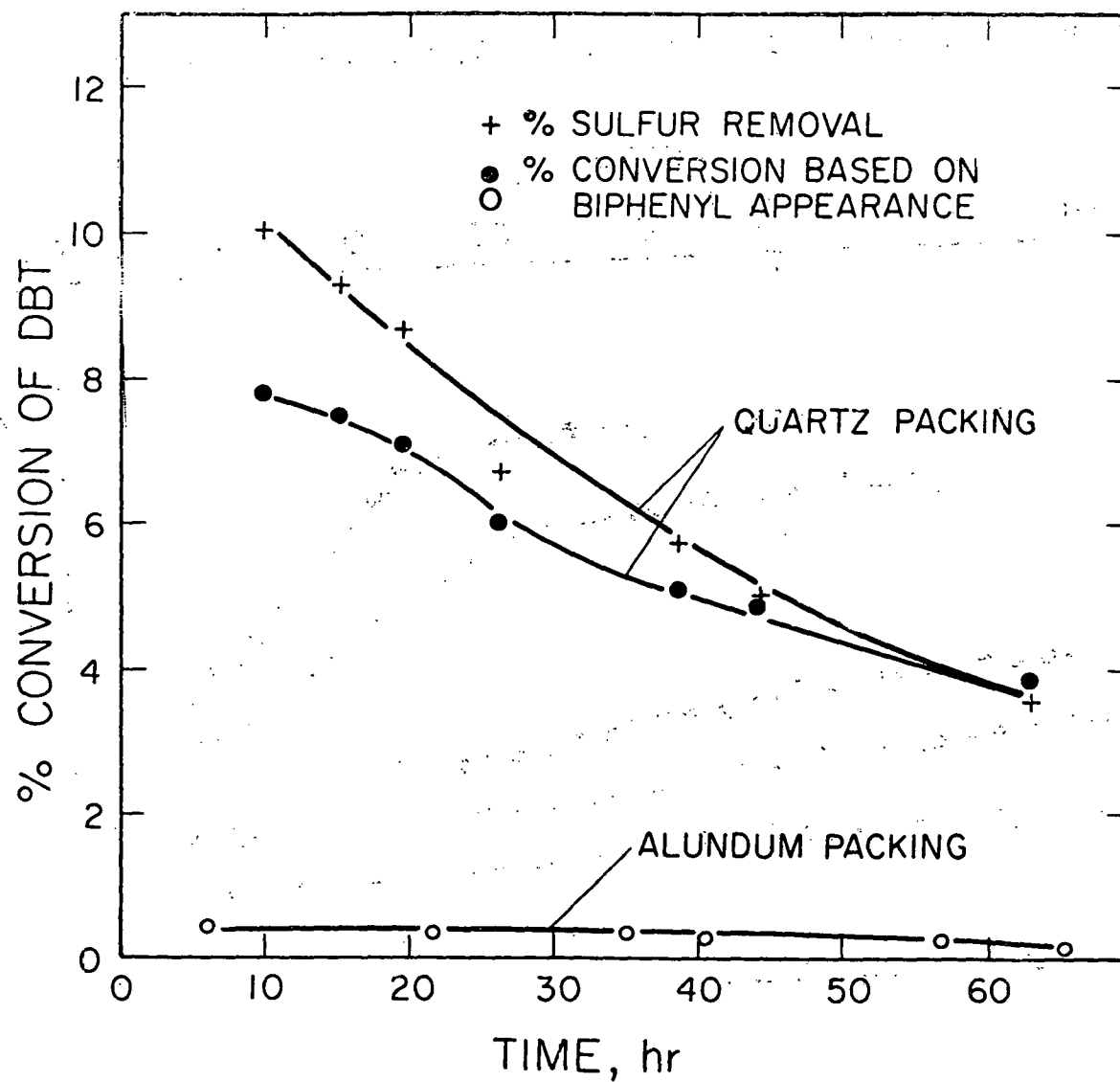
Figure 1. Blank Runs for HDS of Dibenzothiophene (DBT). Run conditions were T = 300°C, 1000 psig hydrogen saturation pressure and reactant mixture: 0.123 wt % DBT in n-hexadecane.
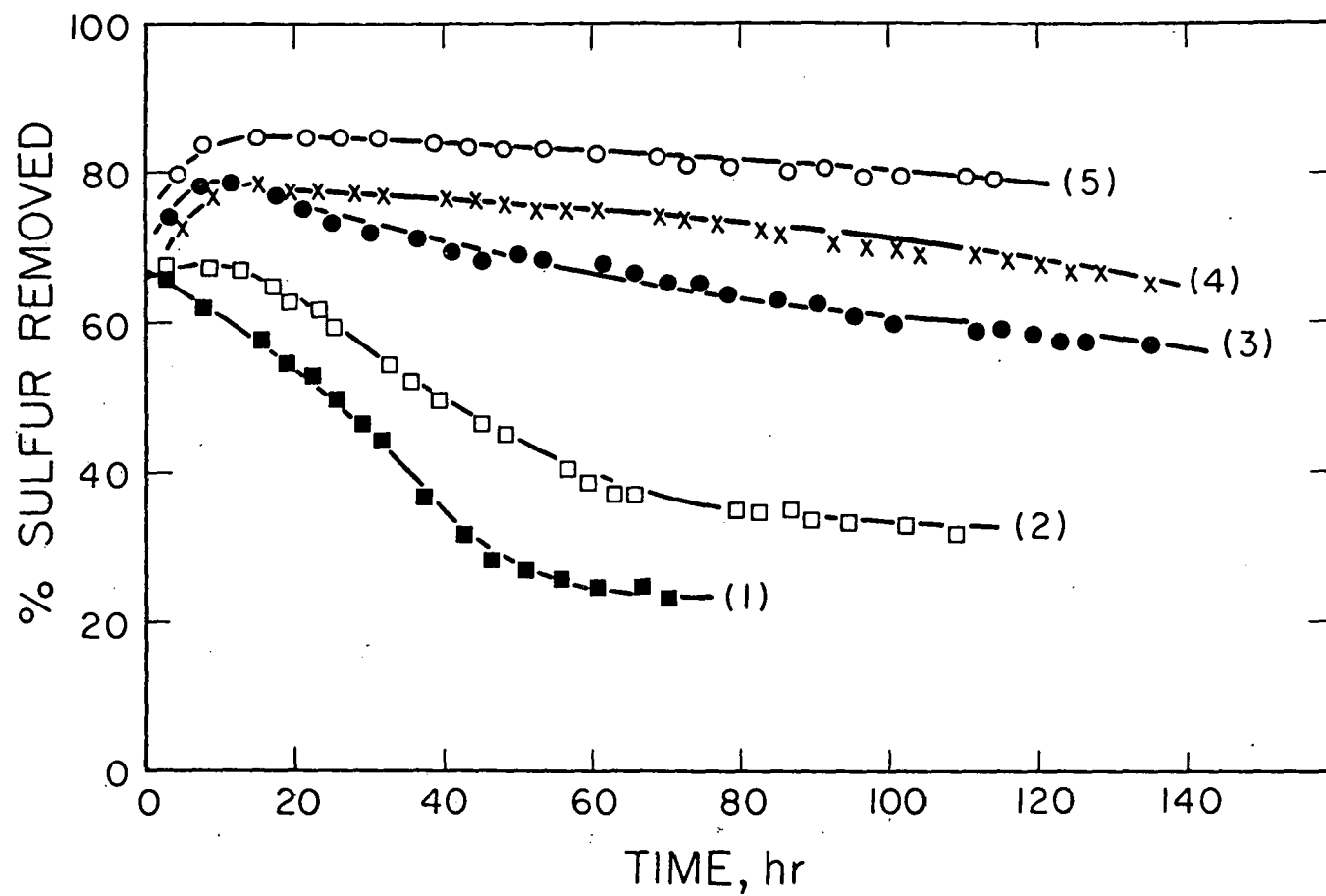
Figure 2. Preliminary Reproducibility Tests. DBT HDS at 300°C with Standard Feed. The catalyst was diluted with quartz chips.
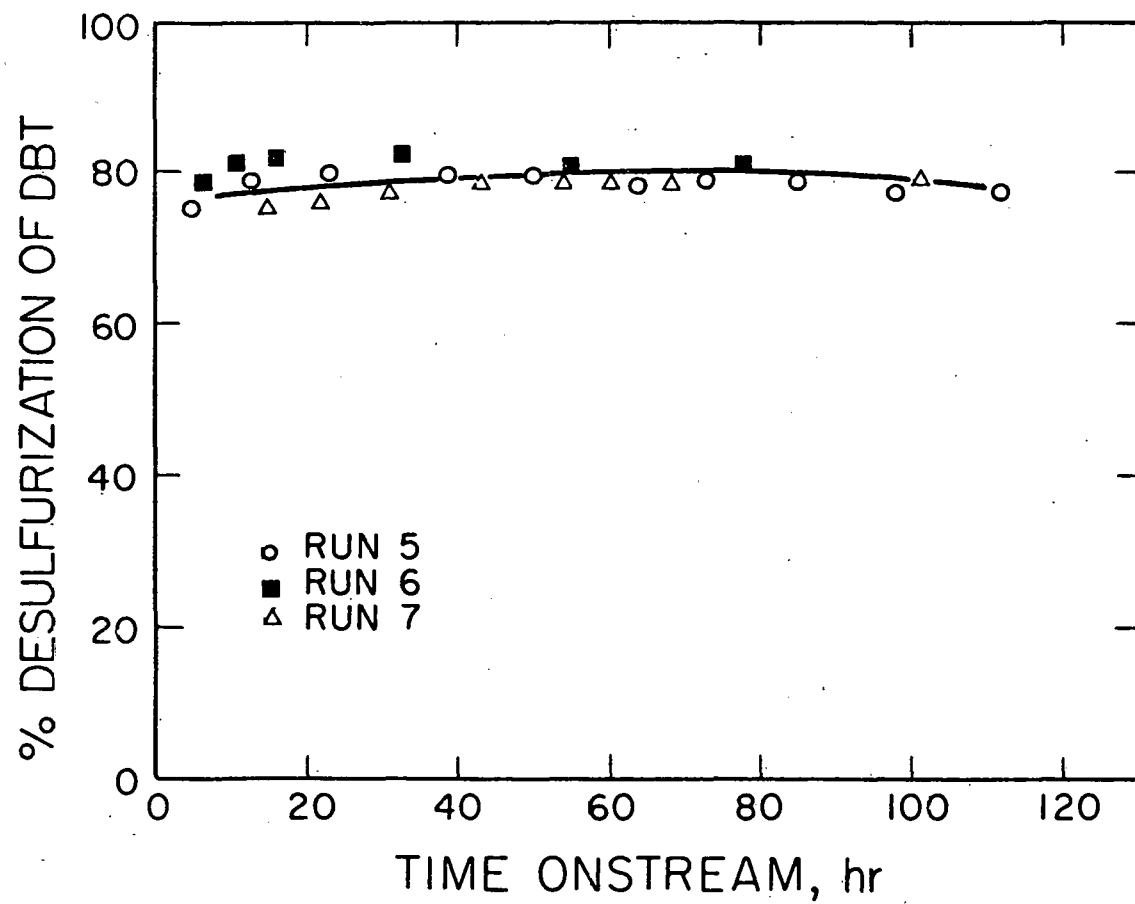
Figure 3. Reproducibility Test Results. HDS of DBT at 300° under Standard Conditions.
  The catalyst in runs 6 and 7 was diluted with alundum.

(ii)   Batch reactor experiments

As mentioned in the literature review of dibenzothiophene hydrodesulfurization (see Fourth Quarterly Report), different intermediates and reaction products have been reported. Recently, Urimoto and Sakikawa (1972), in their study of dibenzothiophene hydrodesulfurization catalyzed by MoS_2 in a batch reactor, identified products such as 1, 2, 3, 4-tetrahydrodibenzothiophene, 1, 2, 3, 4, 10, 11-hexahydrodibenzothiophene, and perhydro-dibenzothiophene. No hydrogenated dibenzothiophenes were reported by Landa and Mrnkova (1966), however. Moreover, o-mercaptobiphenyl was identified by Urimoto and Sakikawa and detected in very low concentrations (~100 ppm) by Rollmann (1976).

The high pressure flow microreactor results of this work have shown that in agreement with the data of Landa and Mrnkova for DBT HDS, hydrogenated dibenzothiophenes were not produced in detectable amounts, nor was o-mercaptobiphenyl detected in our experiments.

In order to investigate more thoroughly the reaction pathway of sulfur removal from DBT, two batch experiments were carried out with two different hydrogen partial pressures. The results of these runs were desired to check the performance of the flow reactors and to confirm the nature of the products. The batch reactor runs were carried out with the same catalyst previously used in flow experiments (HDS-16A; Co-Mo/Aℓ_2O$_3$, 80-100 mesh and at the same temperature of 300°C). In order to facilitate product identification, relatively high DBT concentrations around 0.3 wt% were used, compared to 0.12 wt% in the flow microreactor exper-iments.

## Blank reactor tests

A run was performed without catalyst using a reactant mixture of 0.3 wt% DBT in n-hexadecane with a hydrogen partial pressure of 1000 psig at 300°C. The results show that there was no measurable sulfur removal activity associated with the reactor walls. In a complementary experiment, significant sulfur removal was obtained in a run with catalyst under the same conditions.

Product identification

The products of DBT hydrodesulfurization found in two batch reactor runs at 280 and 1000 psig hydrogen partial pressure were analyzed with the GC using the flame ionization detector and the sulfur-specific detector. The results show that, in agree-ment with high-pressure flow-microreactor data, no sulfur-containing species other than unreacted DBT could be detected. Biphenyl was the major hydrocarbon product, accounting for 90% and 75% of the DBT reacted at 280 and 1000 psig hydrogen partial pressure,

respectively. More thorough analysis of the reaction products is planned for the coming quarter. The approach will be to concentrate the products and use GC-MS techniques as a means of identification.

Preliminary kinetics

Figures 4 and 5 show results of the batch reactor experiments and indicate that a first-order kinetics in dibenzothiophene accounts for the conversion in each run. (The pseudo first-order reaction rate constant incorporates hydrogen partial pressure as a constant.)

For comparison, corresponding plots assuming zero-order kinetics are given in Figures 6 and 7. The data of run 8 do not give a linear fit which would conform to a zero-order kinetic equation, and although the results of run 9 give a linear fit, the intercept is incorrect. Clearly, the first-order kinetics give the better representation of the data.

Comparison of flow and batch reactor data

Pseudo first-order rate constants were calculated from both batch reactor and flow microreactor. The rate constant calculated from the appropriate microreactor data was compared to value extracted from the data of run 8, which was chosen since it was carried out using the same feed hydrogen concentration used in the microreactor experiments. The results shown in Table 1 indicate close agreement between the two values. This agreement is strong evidence of the accuracy of the data and is especially satisfying in view of the differences in catalyst sulfiding procedures in the two types of experiments, and the error in the determination of hydrogen concentration in the feed (see the Third Quarterly Report, p. 72).

b. Hydrodesulfurization of 4,6-dimethyldibenzothiophene

The studies of substituent effects on dibenzothiophene HDS catalyzed by $Co-Mo/\gamma Al_2O_3$ catalyst have been initiated. A preliminary run was carried out with the high-pressure flow microreactor. The reactant mixture contained 0.140 wt% 4,6-dimethyldibenzothiophene in n-hexadecane, which corresponds to the same sulfur content as was used in the standard DBT solution previously described. All other reaction parameters were kept the same as described earlier.

Figure 8 shows the relative hydrodesulfurization reactivity of 4,6 dimethyldibenzothiophene compared to dibenzothiophene. Only 25% sulfur removal was obtained from the substituted com-
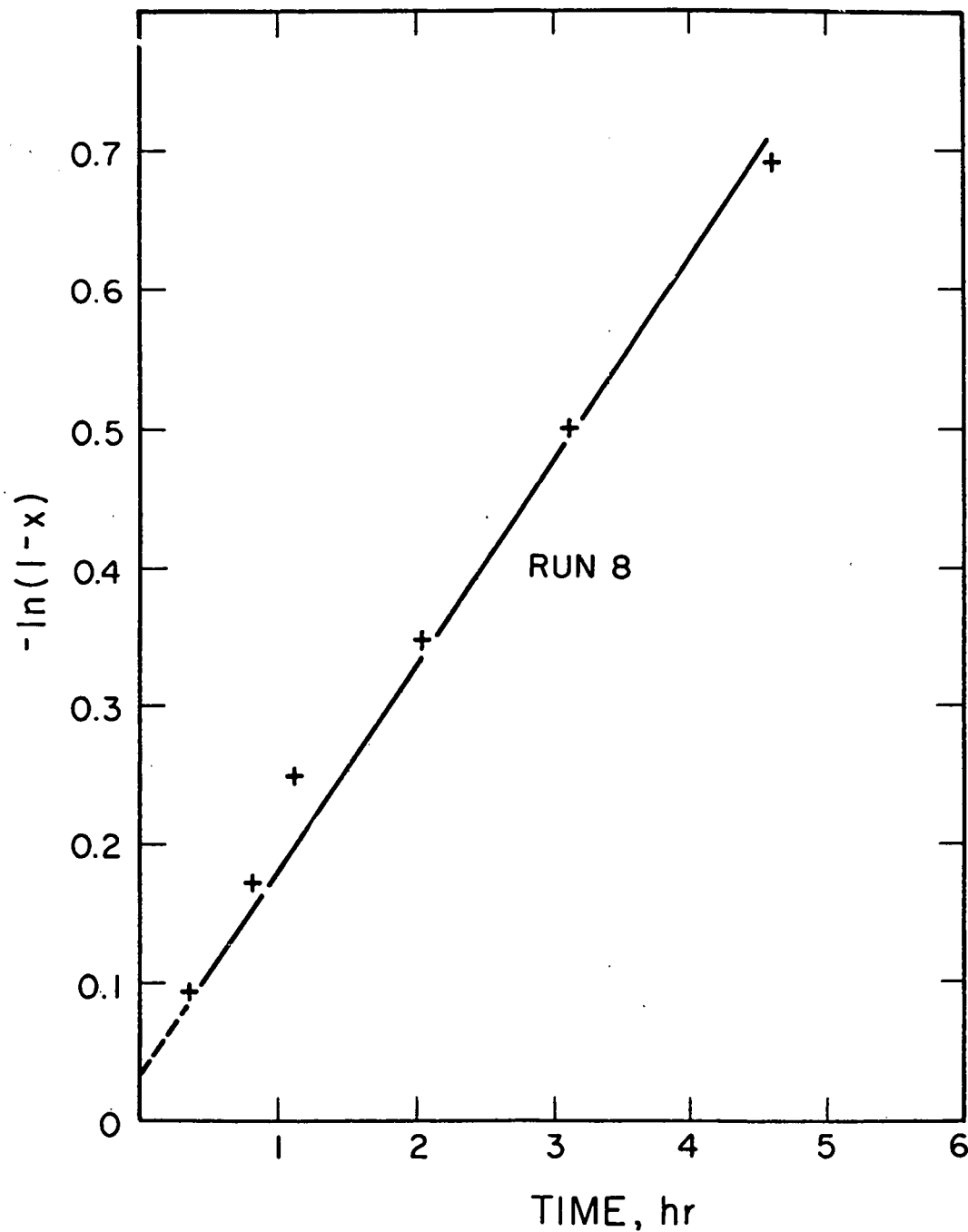
Figure 4.   Pseudo First-Order Kinetics in HDS of DBT in a Batch Reactor at 300°C and 280 psig of H_2.   See text for experimental details.
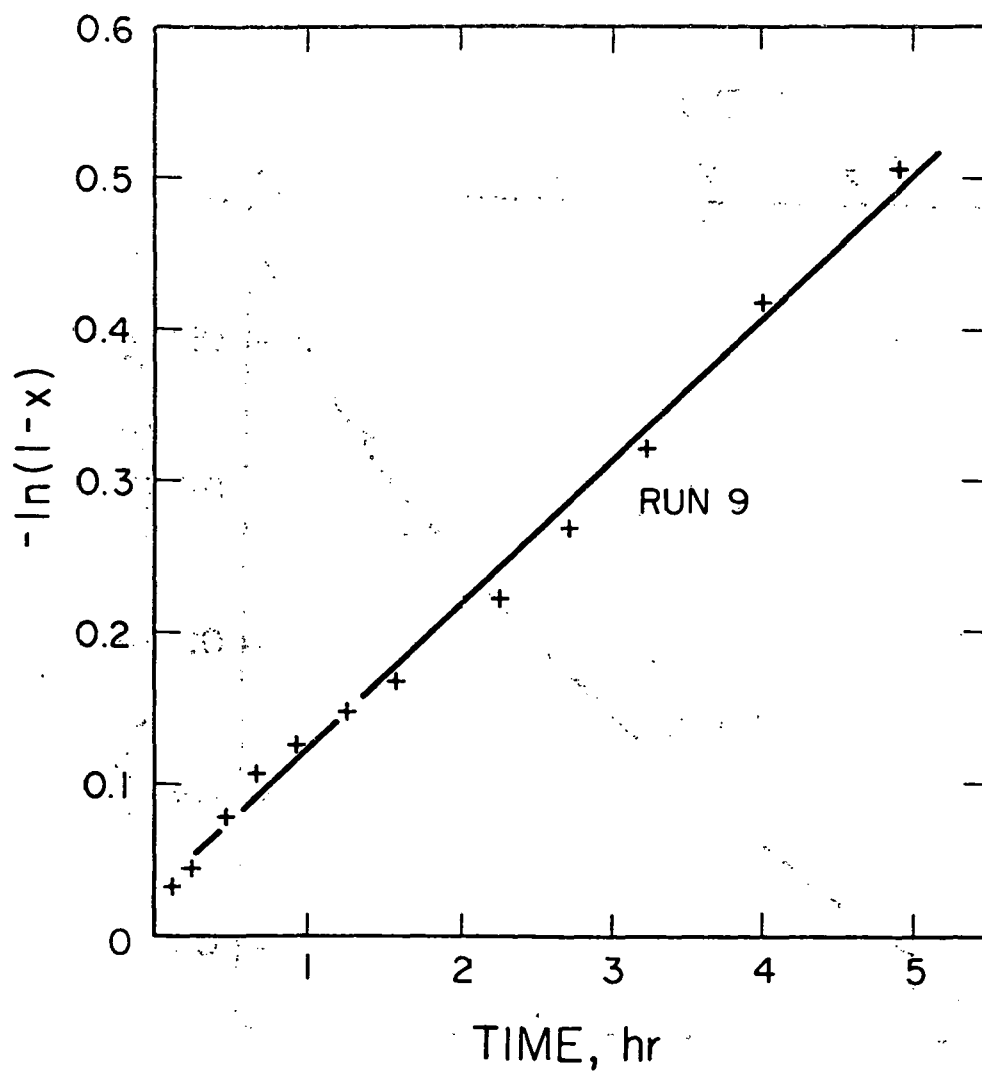
Figure 5. Pseudo First-Order Kinetics of HDS of DBT at 300°C and 1000 psig of H_2. See text for experimental details.
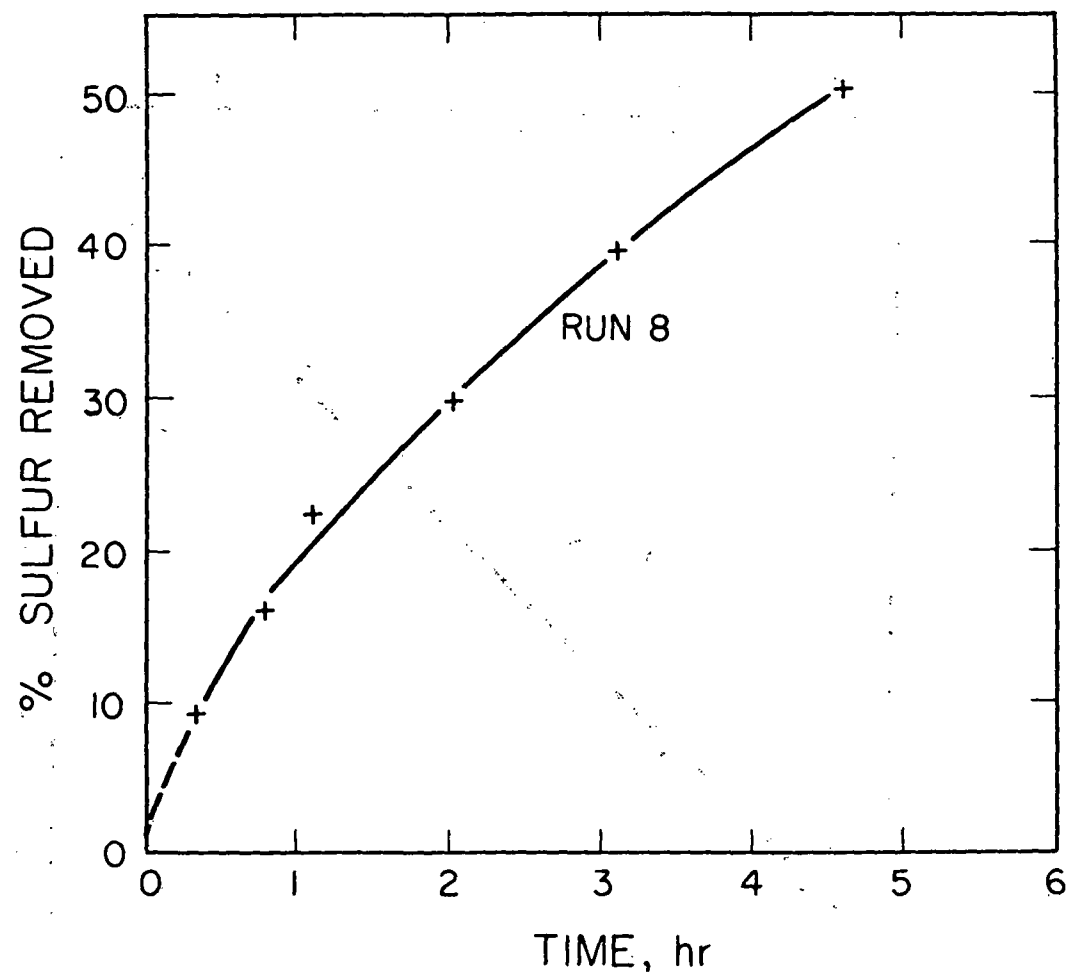
Figure 6. Test for Zero-Order Kinetics of HDS of DBT at 300°C and 280 psig of H_2. See text for experimental details.
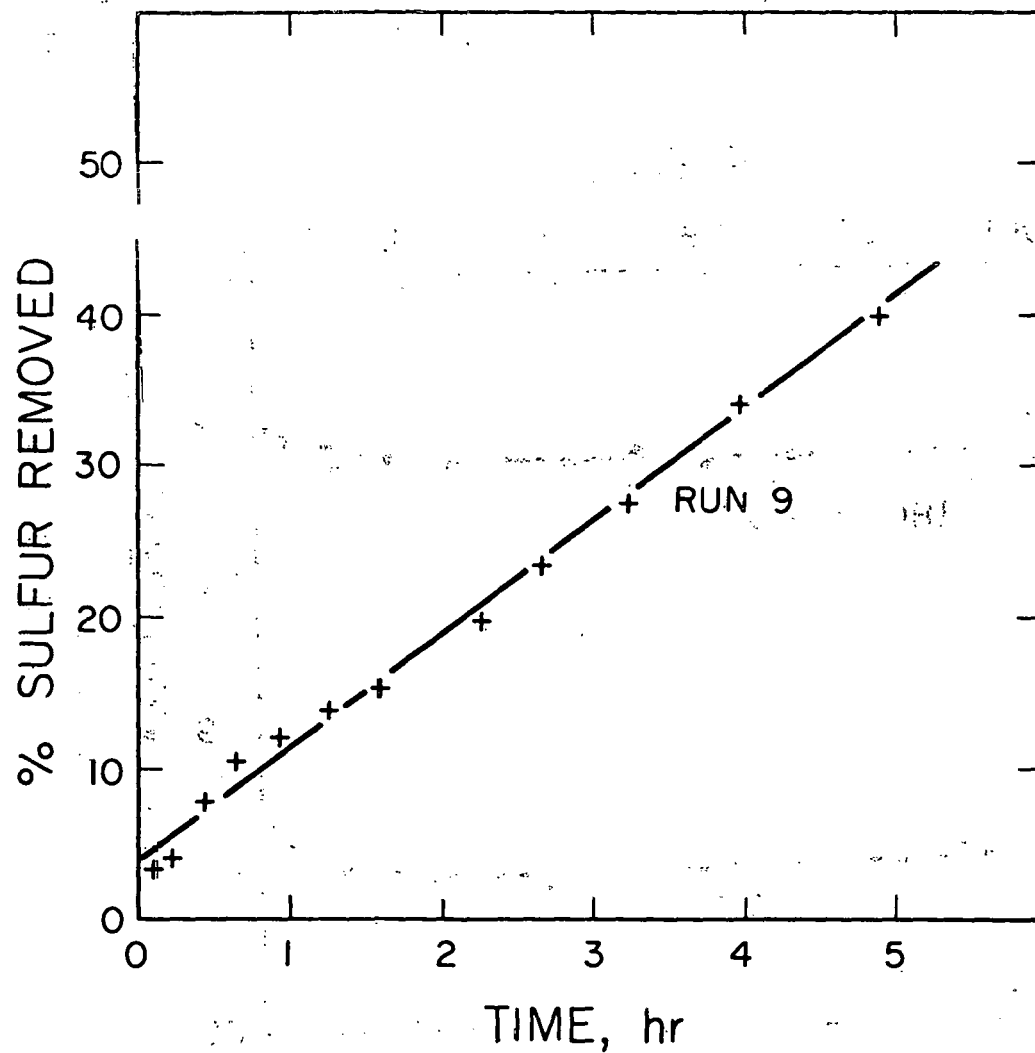
Figure 7. Test for Zero-Order Kinetics of HDS of DBT at 300°C and 1000 psig of H_2. See text for experimental details.
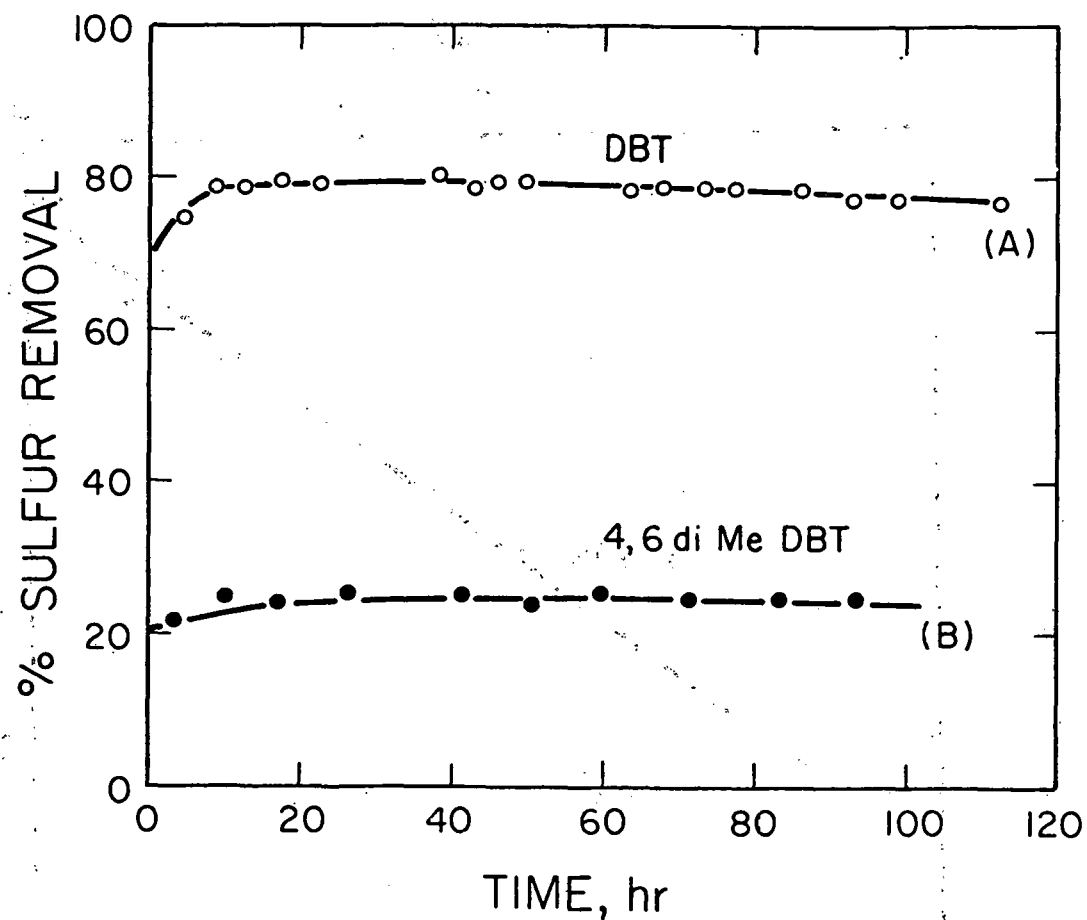
Figure 8. Relative Reactivities of Dibenzothiophene and 4,6-Dimethyldibenzothiophene in the Presence of Co-Mo/γ-Al$_2$O$_3$ at 300°C and a Hydrogen Saturation Pressure of 1000 psig. The catalyst was 0.025 g of HDS 16A (in situ sulfided). The feed flow rate was 1.2 cm^3/hr. The reactant mixtures were (a) 0.122 wt % DBT in n-hexadecane and (b) 0.140 wt % diMeDBT in n-hexadecane.

TABLE 1

FIRST-ORDER RATE CONSTANTS FOR HDS OF DBT

DETERMINED FROM FLOW AND BATCH EXPERIMENTS

(See the text for details of the experiments)

	K^1 (ml/g cat. hr)
Flow microreactor	75
Batch reactor run #8	67

The rate constant is defined by the following equations:

$$\text{Flow reactor } \ln C = \left(\frac{W}{F} K^1\right)$$

$$\text{Batch reactor } \ln C = \left(\frac{W}{V}t \, K^1\right)$$

where W = weight of catalyst, g
      F = flow rate of solution, ml/hr
      V = volume of solution (batch), ml
      K^1 = rate parameter, ml/g cat hr
      C = fraction of DBT remaining
      t = time, hr

pound under the conditions at which dibenzothiophene experienced 80% conversion. The decrease in reactivity upon incorporation of the methyl groups can be explained in terms of steric hindrance caused by the presence of methyl groups close to the sulfur atom which restrict the access of the organic sulfur atom to the active site (anion vacancy) on the catalyst surface:
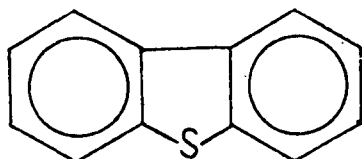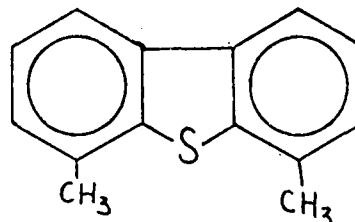
Dibenzothiophene   4-6-Dimethyldibenzothiophene

It is noteworthy that in agreement with dibenzothiophene data, no measurable deactivation of the catalyst was observed during a 94-hour run.

Preliminary analysis with the sulfur-specific detector has shown that 4,6-dimethyl DBT is the only sulfur compound detected in the HDS reaction products. Identification of desulfurized products is underway.

3.   Progress in synthesis and characterization of sulfur- and nitrogen-containing reactants

4-Methyldibenzothiophene was synthesized by the following route:
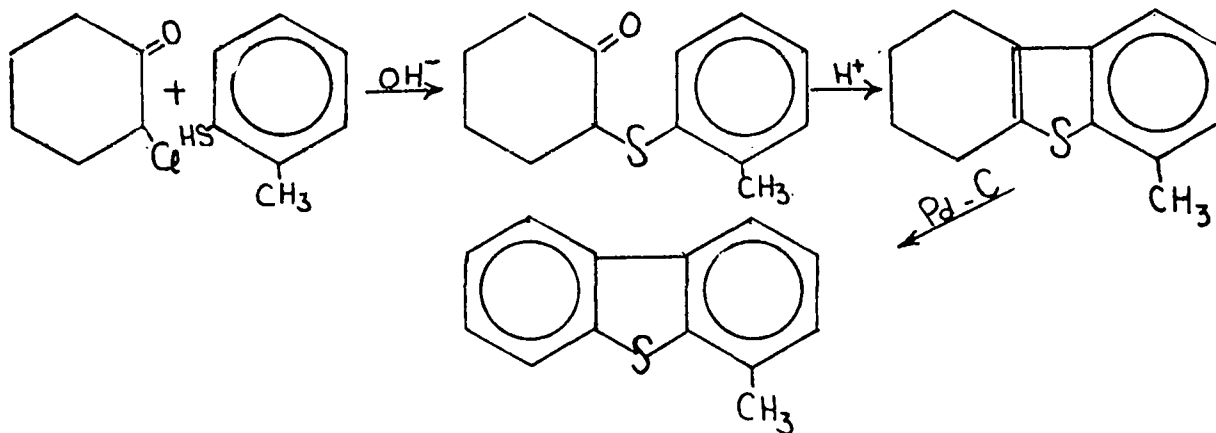
1,2,3,4-Tetrahydrodibenzothiophene was obtained by a similar procedure using o-chlorocyclohexanone and benzenethiol:
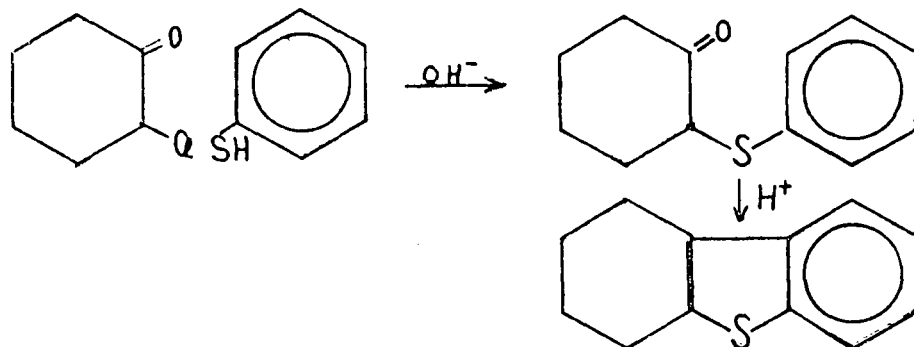
1,2,3,4,10,11-Hexahydrodibenzothiophene was prepared from tetrahydro compound as follows:
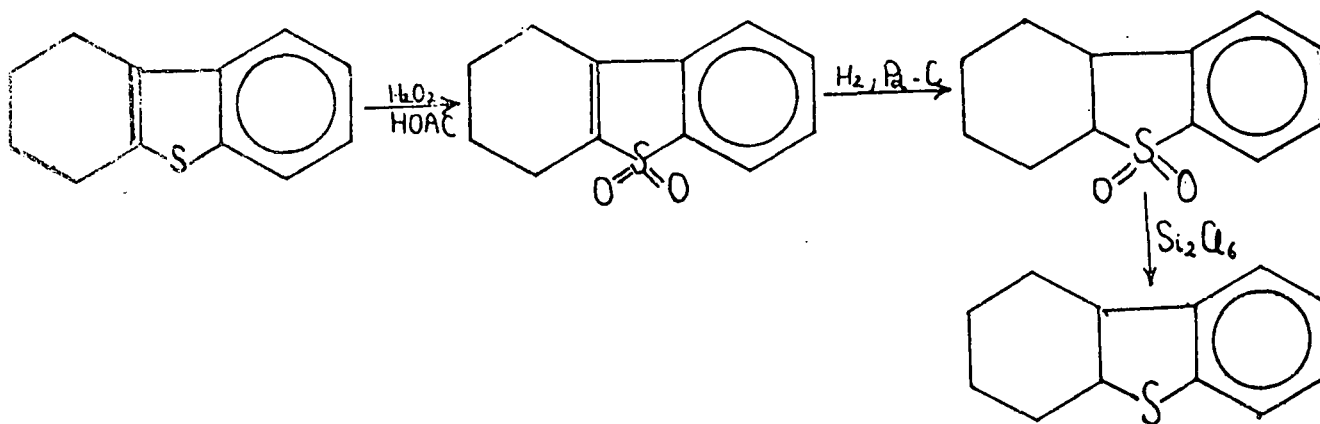
4,6-Dimethyldibenzothiophene, which had been obtained earlier in 95% purity, was further purified by sublimation and fractional crystallization, and a 100% pure product (by glc) was obtained.

C.   CATALYTIC HYDRODENITROGENATION

1.   Analytical Procedure for Acridine

Both internal and external standards for the acridine system calibration were tried unsuccessfully. When quinoline was used as an internal standard, non-linear response plots were obtained for concentration vs. response area for a packed glc column. When a 50m OV101 WCOT (capillary) column was used, however, the use of a calibration curve was feasible.

Several solutions of acridine in white oil were prepared. Figure 9 shows the results obtained on the Perkin-Elmer gas chromatograph model 3920B with the nitrogen-specific detector. The application of such a calibration curve to compounds with differing molecular structures was confirmed using solutions of sym octahydroacridine in white oil.

For the analysis of the reactor product samples for a given run, the curve is verified and/or regenerated before the samples are processed on the gas chromatograph.

2.   Acridine Conversion Catalyzed by Ni-W/Al$_2$O$_3$

Two runs were made at 2000 psi and different temperatures in the one-liter autoclave. Figures 10 and 11 show the respective concentration vs. time plots. Table 2 shows the percent conversion relative to initial acridine concentration for the two runs.

It appears that acridine disappearance during reaction is very rapid and follows first-order kinetics; tetrahydroacridine and octahydroacridine, on the one hand, and perhydroacridine and symoctahydroacridine, on the other, seem to be interconverted in reversible reactions. Temperature has a marked effect on the total nitrogen removal rate.

3.   Carbazole Extraction Procedure

The carbazole reaction products were divided into low boilers (glc retention times up to 10 min) and high boilers (between 10 and 25 min) as judged on a 50m OV101 WCOT column. This separation was achieved using a 60 cm x 6 cm dry chromatography column. Neutral alumina (activity 111/20mm) with UV indicator was used as packing material. The white oil (WO) solution was run through the column, followed by 500 cm^3 of hexane to free the column of the oil carrier. With a UV lamp, 2 distinct zones were detected. Extraction of the products with ether and chromatography on a WCOT column using the nitrogen-specific detector yielded the chromatograms shown in Figures 12 and 13.

TABLE 2

PERCENT PRODUCT DISTRIBUTION RELATIVE TO
INITIAL ACRIDINE CONCENTRATION
AT REACTION TIME OF 10 HRS.

Compound	2000 psig	
	T = 332°C	T = 357°C
Acridine	0	0
Tetrahydroacridine	0.6	0
Octohydroacridine	11.6	1.6
Symoctahydroacridine	8.0	20.0
Unidentified	-	0
o-Methylenecyclohexyl-Aniline	8.76	3.01
Perhydroacridine	64.9	30.1
Total Nitrogen Removed	6.14	45.4

Catalyst: $Ni-W/Al_2O_3$
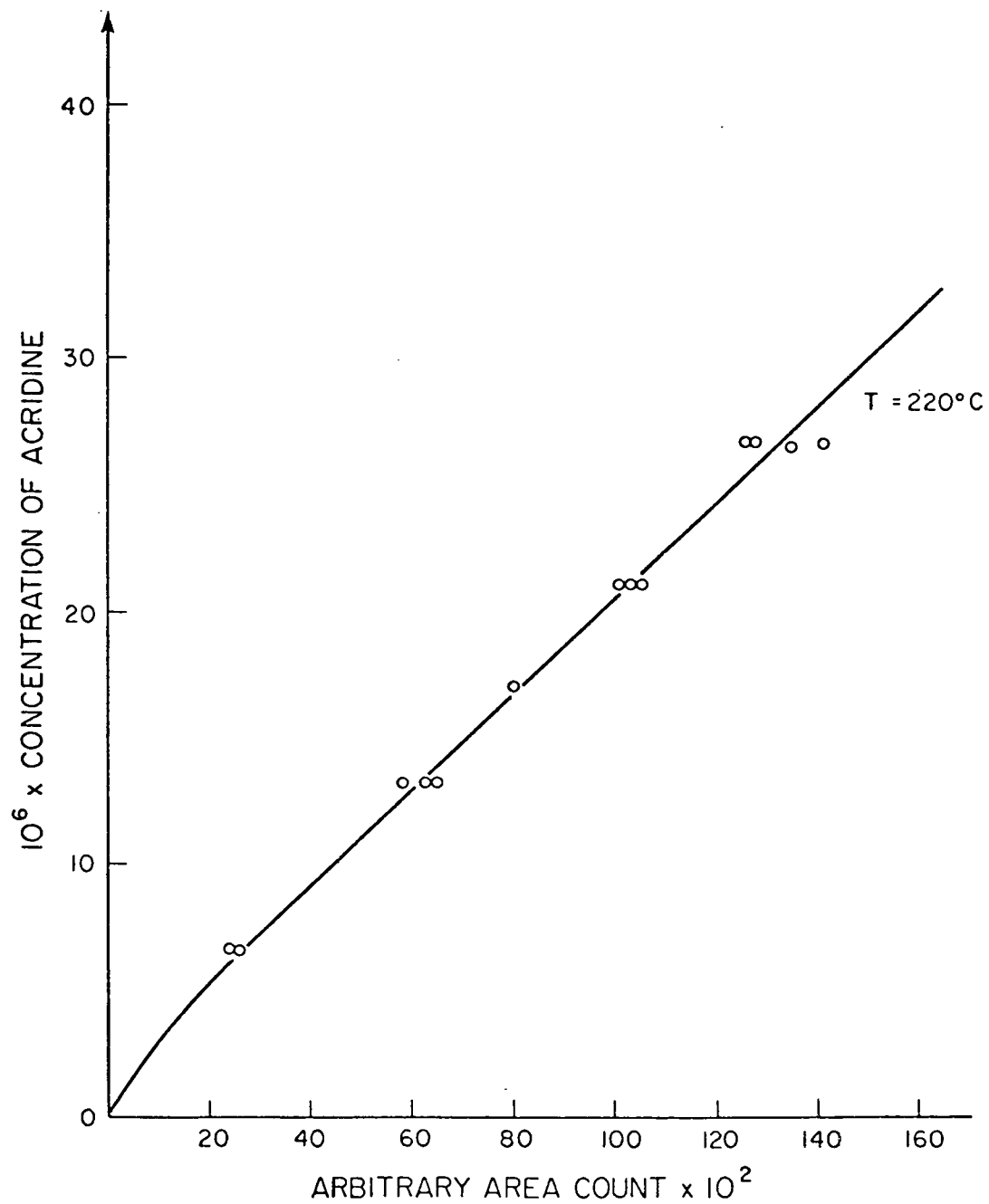
Figure 9. Wall-Coated Open Tubular Column Calibration Curve for Acridine
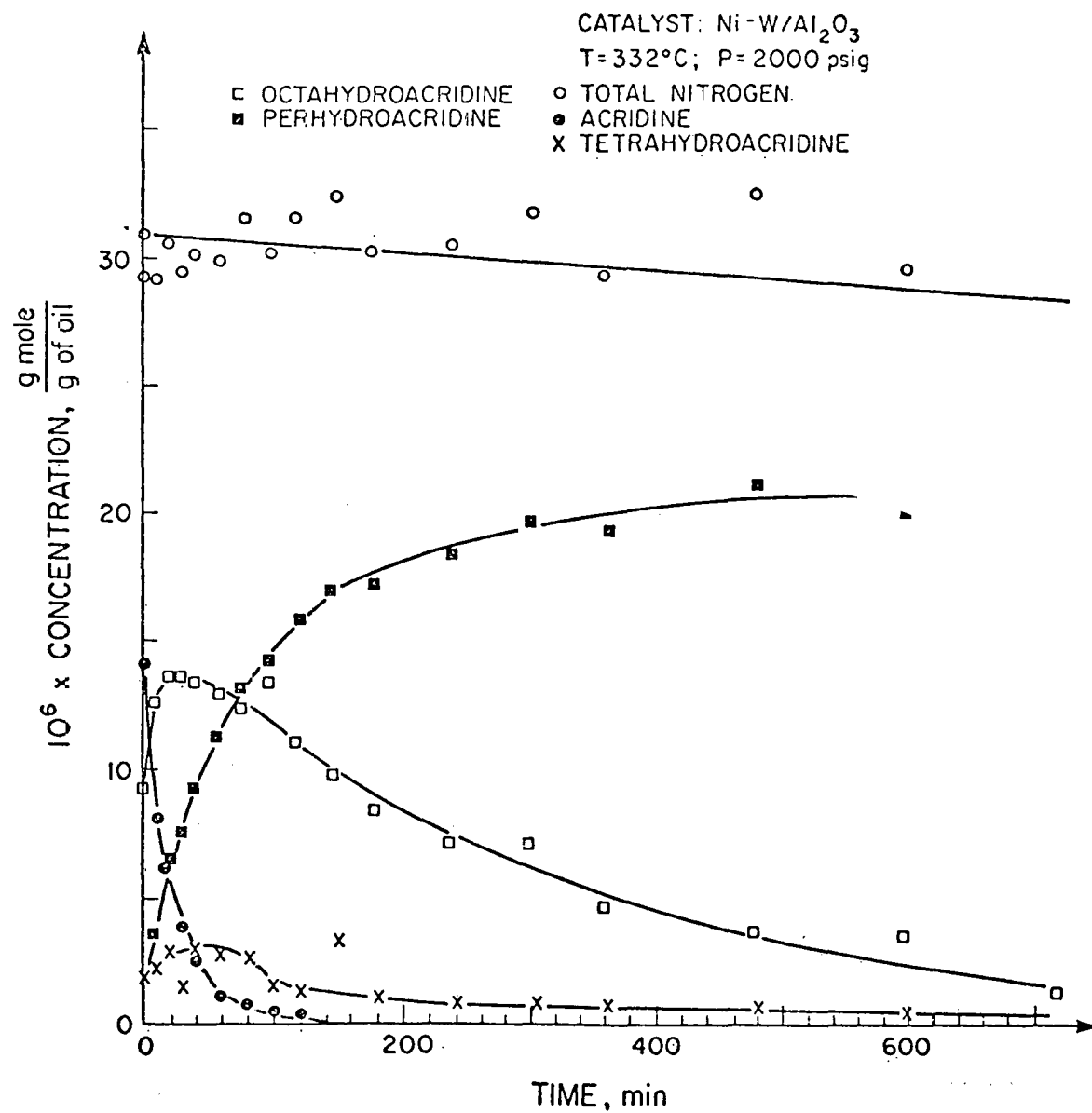
Figure 10. Batch Run for Acridine at 332°C.

CATALYST: Ni-W/Al$_2$O$_3$
T = 357°C; P = 2000 psig

o TOTAL NITROGEN
⊙ ACRIDINE
x TETRAHYDROACRIDINE
□ OCTAHYDROACRIDINE
▣ SYM OCTAHYDROACRIDINE
△ UNKNOWN
▲ PERHYDROACRIDINE
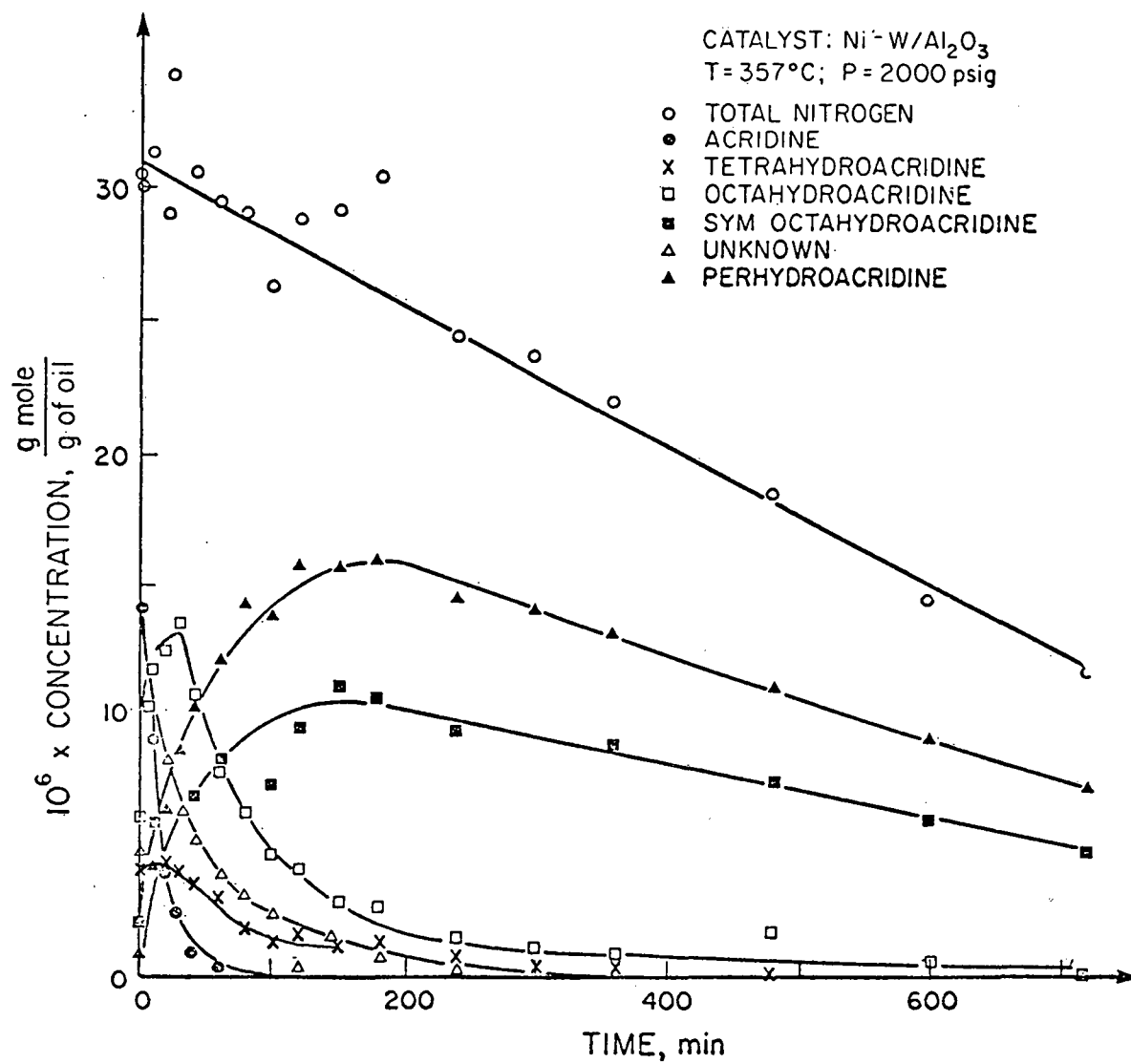
Figure 11. Batch Run for Acridine at 357°C.
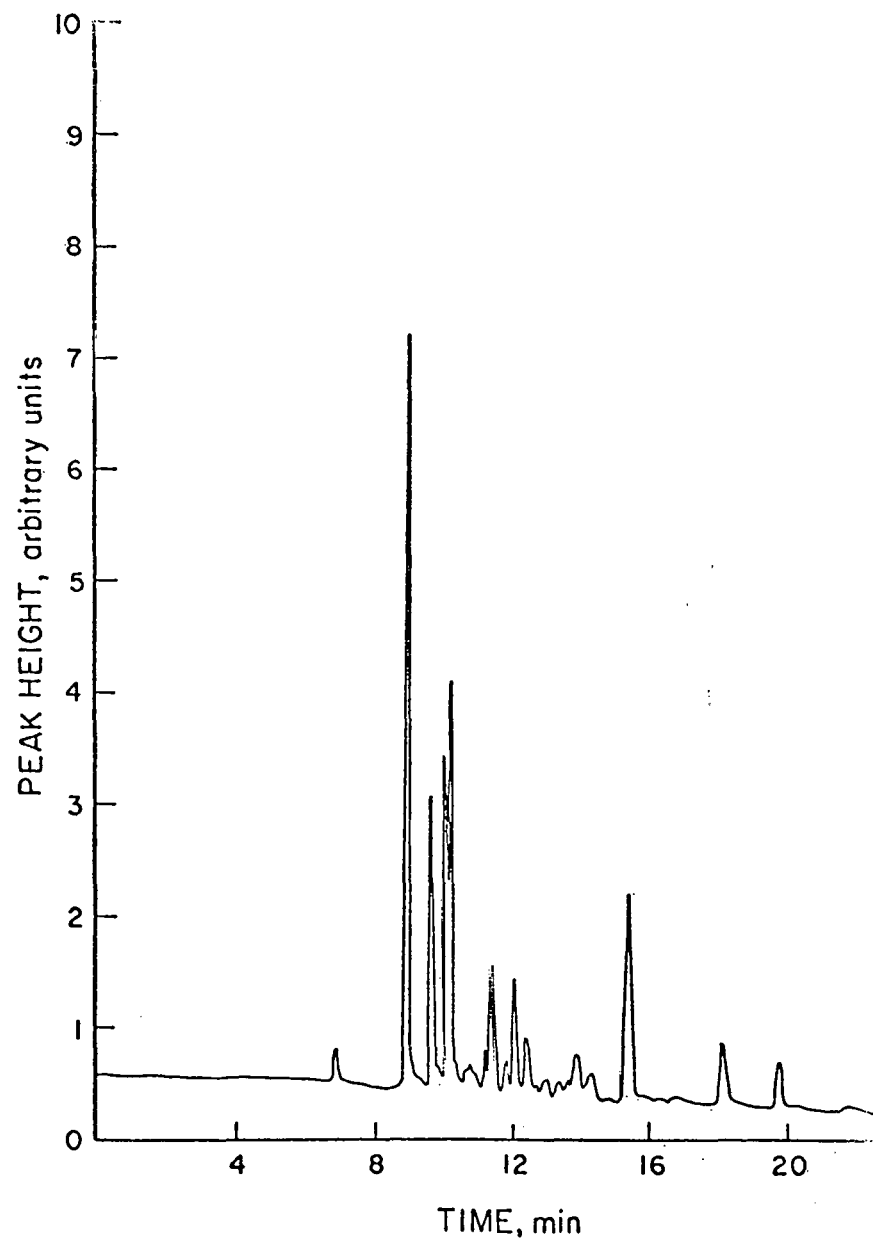
Figure 12. Gas Chromatography of Carbazole - Low Boilers.
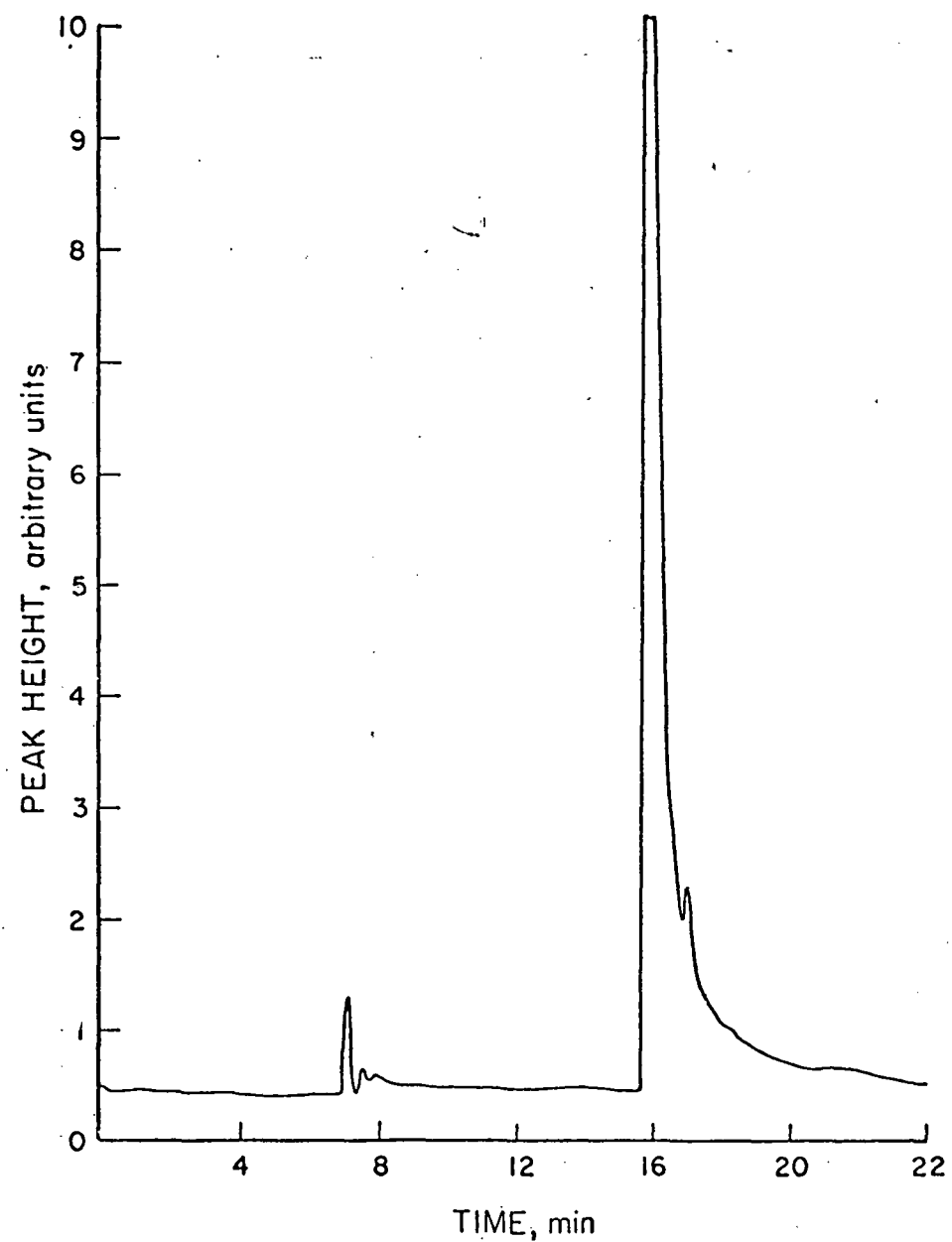
Figure 13. Gas Chromatography of Carbazole - High Boilers

4. Hydrodenitrogenation of Quinoline

a. Literature Review of Quinoline Hydrodenitrogenation

(i) Introduction

Quinoline is a representative multiring heterocyclic nitrogen-containing compound, containing both a benzene ring and a pyridine ring. Understanding of the mechanism of quinoline hydrodenitrogenation might be expected to provide the information required for understanding the hydrodenitrogenation of higher-molecular-weight heterocyclic nitrogen-containing compounds found in coal-derived liquids.

Thermodynamics of Quinoline Hydrodenitrogenation

Quinoline has a planar structure. The dimensions of the molecule are estimated those shown below:
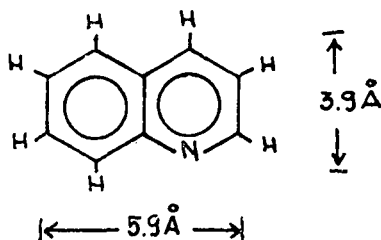
Quinoline is a basic compound, having a pK_a of 4.94. The pK_a values of some related compounds are listed for comparison in Table 3. These data show that hydrogenation of the pyridine-ring increases the basicity strongly (e.g., pK_a for pyridine; $pK_a = 11.1$ for piperidine). Hydrogenolysis of the saturated nitrogen-containing ring decreases the basicity (e.g., $pK_a = 11.1$ for piperidine; $pK_a \sim 10$ for n-butylamine).

Quinoline hydrodenitrogenation is an exothermic reaction,

TABLE 3 *

Nitrogen Compounds Classified According to Basicity

Compound	pK_a (H_2O)
Piperidine	11.1 **
Cyclohexylamine	10.6 **
t-butylamine	10.65**
Ammonia	9.27
Imidazol	7.03
2-Methylpyridine	6.5
Acridine	5.60
Pyridine	5.23
5,6-Benzquinoline	5.15
Isoquinoline	5.14
Dimethylaniline	5.10
6,7-Benzquinoline	5.05
Quinoline	4.94
N-Methylaniline	4.78
3,4-Benzacridine	4.70
Aniline	4.63**
2,3-Benzacridine	4.52
1,10-Phenanthroline	4.27
7,8-Benzquinoline	4.25
2,2-Bipyridine	4.23
Quinazoline	3.51
Phthalazine	3.47
1,2-Benzacridine	3.45
Phenanthridine	3.30
4,7-Phenanthroline	3.12
1,7-Phenanthroline	3.11
Cinnoline	2.70
Pyrazole	2.53
Thiazole	2.53
Pyridazine	2.33
Benztriazole	1.6
Pyrimidine	1.30
Indazole	1.3
Phenazine	1.23
Diphenylamine	0.85
Quinoxaline	0.8
Pyrazine	0.6
Pyrrole	0.4
Indole	...
Propionitrile	-0.8
Carbazole	<-1

*Richter et al. (1952)
**Roberts et al. (1971)

The reaction equilibrium is favored by low temperatures and high pressures. The overall reaction equilibrium constant for the HDN of quinoline (calculated by the group contribution method) is shown in Figure 14 (Cocchetto⁴Satterfield, 1976). At temperatures less than 500°C, the reaction equilibrium constant becomes greater than zero.

Reaction Kinetics

In the literature there is not detailed kinetic information spanning a significant range of reaction temperature or hydrogen partial pressure. The literature reports that the reaction is first order with respect to the total nitrogen content (Flinn et al., 1963; Abou-Gheit and Adbou, 1973) and strongly inhibited by reaction intermediates and ammonia (Cox and Berg, 1962). In a study reported by Flinn et al. (1963), quinoline was blended with a middle distillate having a low impurity concentration and contacted with an unspecified commercial $Ni-W/Al_2O_3$ catalyst and hydrogen at 1000 psi and 315°C. The hydrogenation reaction was suggested to be rate determining, and hydrogen partial pressure was an important processing variable; increased hydrogen partial pressures up to 6,000 psi increased the rate of nitrogen removal from heavy petroleum gas-oil feed-stocks.
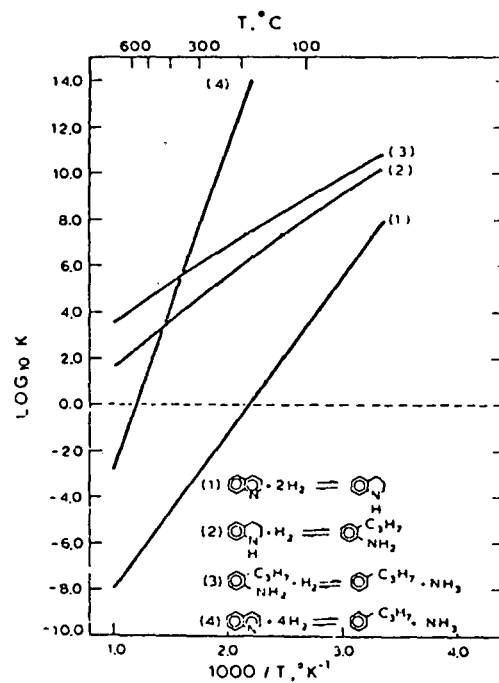
Figure 14. Thermodynamics of quinoline HDN. (Cocchetto & Satterfield, 1976)

The first-order kinetics in total nitrogen were also reported by Cox and Berg (1962). Their experiments were carried out at relatively low pressure (250 psig), 370°C, and with feed containing an aromatic solvent.

From pilot plant experiments, Haensel et al. (1963) determined a product of less 0.05 ppm nitrogen; the feed was 1,200 ppm of quinoline in white oil. The HDN reaction was retarded by polycyclic aromatic hydrocarbons. Therefore, the remaining nitrogen in a technical methylnaphthalene feed which contains primarily quinoline processed under similar conditions was 48 ppm.

Reaction Network

It is well known that the C=N bond is much stronger than the C-N bond (Table 4). For the HDN of pyridine-like compounds, the reaction is expected to proceed through saturation of the nitrogen-containing ring followed by the rupture of the saturated nitrogen-containing ring. The nitrogen is then removed from the resulting amine or aniline. A reaction network was suggested by Goudriaan (1974) (Figure 15), but experimental results are lacking in this reference. Some reaction intermediates, including 1,2,3,4-tetrahydroquinoline, 5,6,7,8-tetrahydroquinoline, and primary amines have been isolated by Deolman and Vlugter (1963) for the quinoline reaction in the presence of an oxidic Co-Mo/Al_2O_3 catalyst. Detailed kinetics and reaction network were not reported by these workers.

HDN of quinoline in paraffin oil was investigated by Aboul-Gheit and Adbou (1973), who used an oxidic Co-Mo/Al_2O_3 catalyst at 2,000 psig and 300-400°C. Without isolation of the reaction intermediates, the authors proposed the following reaction network:
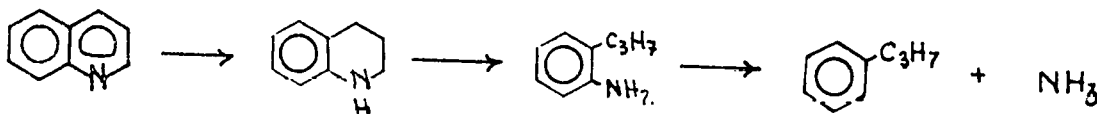
The quinoline HDN reaction was found to be a first order with respect to total nitrogen and to have an activation energy of 30 kcal/mole.

Influences of S and Other Compounds

In industrial petroleum processes, catalytic hydrotreating simultaneously removes sulfur and nitrogen. In general, sulfur

Pyridine reaction network (Sonnemans, 1973)
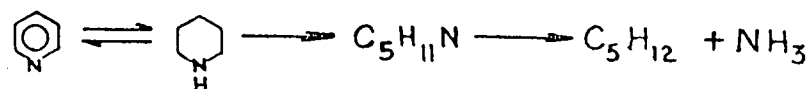
Quinoline reaction network (Goudriaan, 1974)
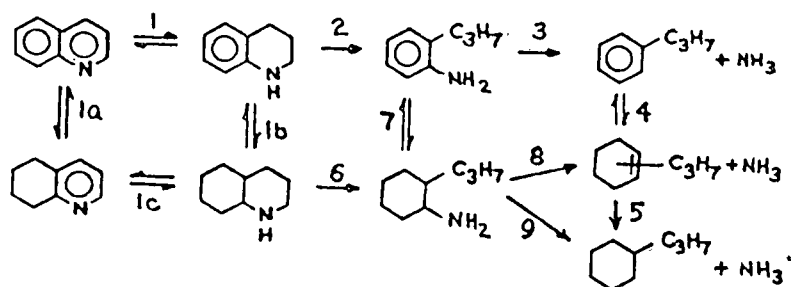
Figure 15. Hydrodenitrogenation Reaction Networks for Pyridine and Quinoline.

removal is faster than the nitrogen removal, corresponding to the weaker bonding between carbon and sulfur atoms (Table 4). Under industrial operating conditions, the catalyst becomes a sulfide rather than an oxide (Thomas, 1970). Although there are no specific data for quinoline HDN, the presence of sulfur-containing compounds seems to maintain the HDN activity (Doelman and Vlugter, 1963; Hatch, 1969; Goudriaan, 1973).

Recently Rollmann (1976) studied the simultaneous removal of S, N, and O from a synthetic feed in a trickle-bed reactor with commerical hydrotreating catalysts. The relative reactivities were as follows:

> sulfides > p-alkyl phenols > benzothiophenes >
> quinoline ~ o-alkyl phenols ~ indoles ~ benzofurans ~
> naphthalenes > dibenzofurans >> mono-nuclear aromatics

The roles of sulfur and oxygen compounds in the HDN process are not well understood. The state of the catalyst (the extent of sulfiding) may be affected by the sulfur contents cr oxygen contents. H_2S and H_2O may influence the acidity of the catalyst and the degree of sulfiding (and therefore activity).

Nondestructive Hydrogenation of Quinoline

The nondestructive hydrogenation of quinoline preceding HDN is relatively fast compared to HDN. Typical hydrogenation catalysts, such as Pt and Pd, are active for the reaction at low temperatures and pressures, such as 200°C and 1 atm. It is well known that the catalytic hydrogenation of quinoline, isoquinoline, and their homologs occurs preferentially in the nitrogen-containing ring (Vierhapper & Eliel, 1976; Freifelder, 1963). In strongly acidic solution, hydrogenation on the benzene ring is predominant. Hydrogenation of quinoline in neutral media (e.g., absolute ethanol) yields 94.5% 1,2,3,4-tetrahydroquinoline with PtO_2 catalyst at room temperature and 50 psig (Vierhapper and Eliel, 1976). At similar conditions, the hydrogenation of quinoline in strong acid (12 N HCl) yields 70% of 5,6,7,8-tetrahydroquinoline.

Both substitutions on the benzene ring and on the nitrogen-containing ring affect the rate of formation of 1,2,3,4 tetrahydroquinoline and 5,6,7,8-tetrahydroquinoline.

Further hydrogenation of quinoline or tetrahydroquinoline requires relatively severe conditions. The reaction conditions used to prepare decahydroquinoline have an effect on the distribution between the cis and trans forms that are formed. Adkins and Cramer (1930) carried out the hydrogenation in the presence of nickel on kieselguhr and obtained tetrahydroderivitives at 150°C and 160 atm after 1-4 hours; but they obtained a mixture of trans and cis dehydroquinoline operating at 175°C and 170 atm for 6-8

TABLE 4

Bond Energies in Polyatomic Molecules

Bond	Energy*	Bond	Energy*	Bond	Energy*
C-H	99	N-H	93	S-H	83
C-C	83	C-N	73	C-S	65
C=C	146	C=N	147	C=S	128
C≡C	200	C≡N	213		

---

*Bond Energy given in kcal/mole.

Source: Roberts, Stewart and Caserio, Organic Chemistry, Benjamin, Menlo Park, CA, 1971.

hours. It might be expected that the cis isomer would be deaminated on the catalyst surface, with the isomerization product subsequently converted into the trans isomer. In acidic media and at high temperatures, the isomerization and consequently higher yields of the trans isomer would be favored. Recently Vierhapper and Eliel (1975) reported a simple method to prepare trans-decahydroquinoline in 90% yield by the reduction of 5,6,7,8-tetrahydroquinoline with sodium in ethanol.

b. Experimental results: quinoline HDN in a batch reactor

(i) Effects of hydrogen partial pressure

The effects of hydrogen partial pressure ranging from 300 psi to 2000 psig in the batch reactor on the apparent first-order rate constants are shown in Figures 16-18. The hydrogen partial pressure effects have been reported in previous reports, and the new data at a higher pressure (2025 psig) provide additional confirmation, falling on the lines which were extrapolated from the lower pressure data. High hydrogen partial pressure leads to rapid formation of 5,6,7,8-tetrahydroquinoline from quinoline. Further hydrogenation of 5,6,7,8-tetrahydroquinoline to give decahydroquinoline is a slow reaction even at very high hydrogen partial pressures (Figure 16). Confirming data from the flow microreactor (with quinoline in white oil saturated at 1500 psig with hydrogen) show that 5,6,7,8-tetrahydroquinoline is the predominant species left in the liquid phase at 90% total nitrogen removal.

The new data also reveal that hydrogenolysis of decahydroquinoline is independent of hydrogen partial pressure (Figure 17). The rate of hydrogenolysis of 1,2,3,4-tetrahydroquinoline decreases with increasing hydrogen partial pressure.

The effect of hydrogen partial pressure on total nitrogen removal rate is shown in Figure 18. The total nitrogen removal rate passes through a maximum at a hydrogen partial pressure of 1000-1500 psig.

(ii) Effects of temperature

The effects of temperature on quinoline HDN from 300°C to 370°C are summarized in Table 5. As reported in the previous progress report, the activation energies for the hydrogenation reactions are very low; the activation energies for hydrogenolysis reactions are quite high, around 30 kcal/mole.

TABLE 5

Summary of Effect of Temperature on Quinoline HDN Kinetics

Reaction	First-Order Rate Constants $\frac{\text{g of oil}}{\text{g of catalyst min}}$				Approximate Activated Energy
	363°C	342°C	325°C	304°C	kcal/mole
Total N-removal	0.96	0.56	0.42	0.07	25
Quinoline plus 1,2,3,4-tetra-hydroquinoline removal	1.77	0.88	0.63	0.21	25
Quinoline $\xrightarrow{2H_2}$ 5,6,7,8-tetra-hydroquinoline	0.68	0.76	0.65	1.125	very low
1,2,3,4-tetra-hydroquinoline $\xrightarrow{2H_2}$ decahydroquinoline	0.28	0.27	0.26	0.16	very low
5,6,7,8-tetra-hydroquinoline $\xrightarrow{2H_2}$ decahydroquinoline	~0	0.045	~0	0.20	very low
1,2,3,4-tetra-hydroquinoline $\xrightarrow{H_2}$ o-propylaniline	1.21	0.38	0.27	0.0446	35
Decahydro-quinoline $\xrightarrow{H_2}$ HC + NH_3	2.05	1.39	1.30	0.592	20
o-propyl-aniline $\xrightarrow{H_2}$ HC + NH_3	2.31	1.28	0.38	0.20	35

TABLE 5 (cont)

Summary of Effect of Temperature on Quinoline HDN Kinetics

Operating Conditions:

Catalyst: HDS-9A (American Cyanamid)
             Ni-Mo/Al$_2$O$_3$
             Loading ~0.5 wt % catalyst in white oil

Presulfiding conditions: 325°C in 10% H$_2$S/H$_2$ for 2 hr

Solvent: Hydrotreated white oil

Total pressure (approximate H$_2$ partial pressure): 500 psig

Initial Reactant Concentration: ~1 wt % quinoline in white

Reactor: batch autoclave
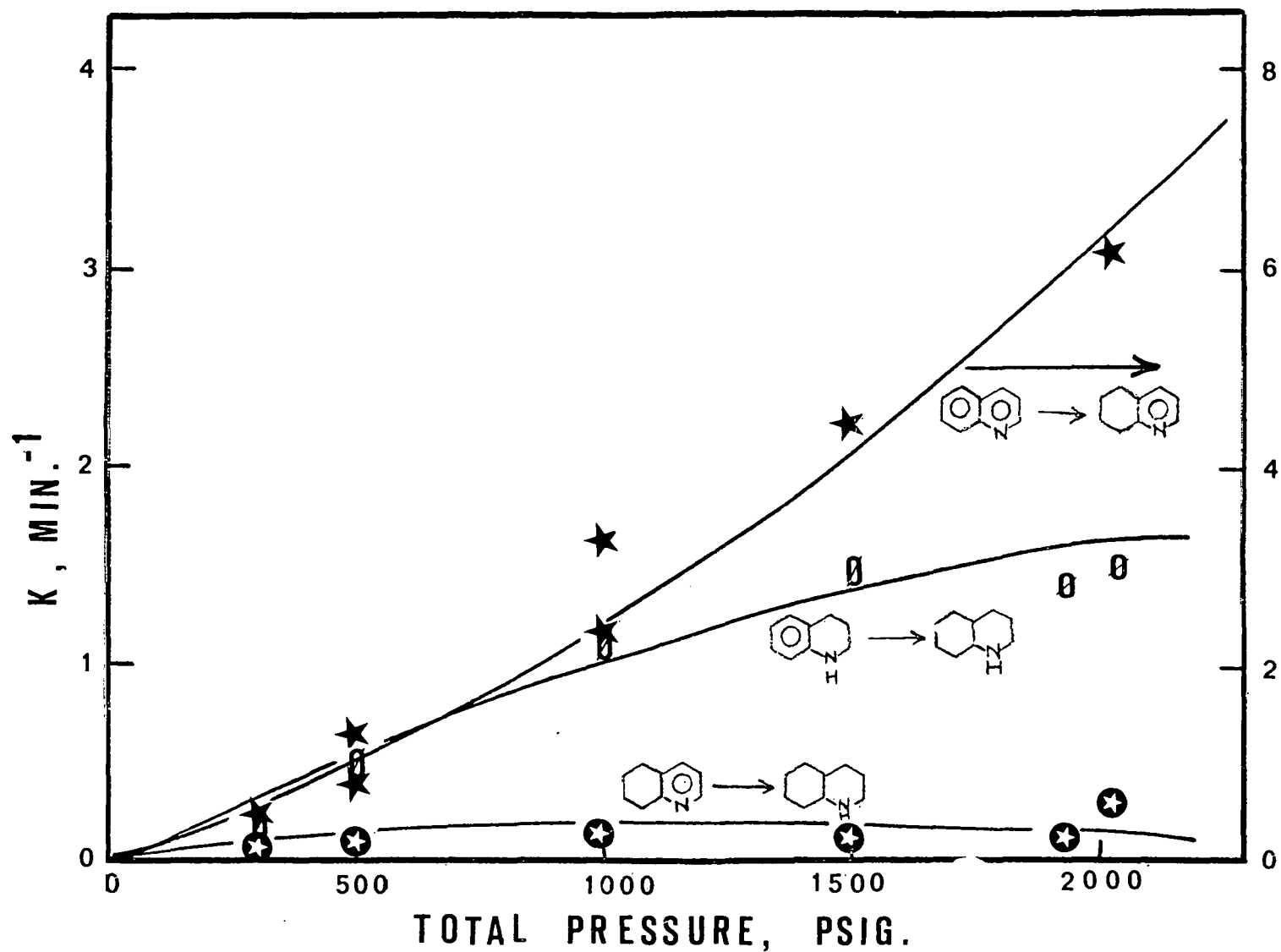
Figure 16. Effect of Total Pressure on Hydrodenitrogenation of Quinoline. Hydrogenation reactions; NiMo/Al$_2$O$_3$ catalyst, 342°C, 0.05 wt% CS$_2$ in white oil, 1.0 wt% of quinoline in white cil.
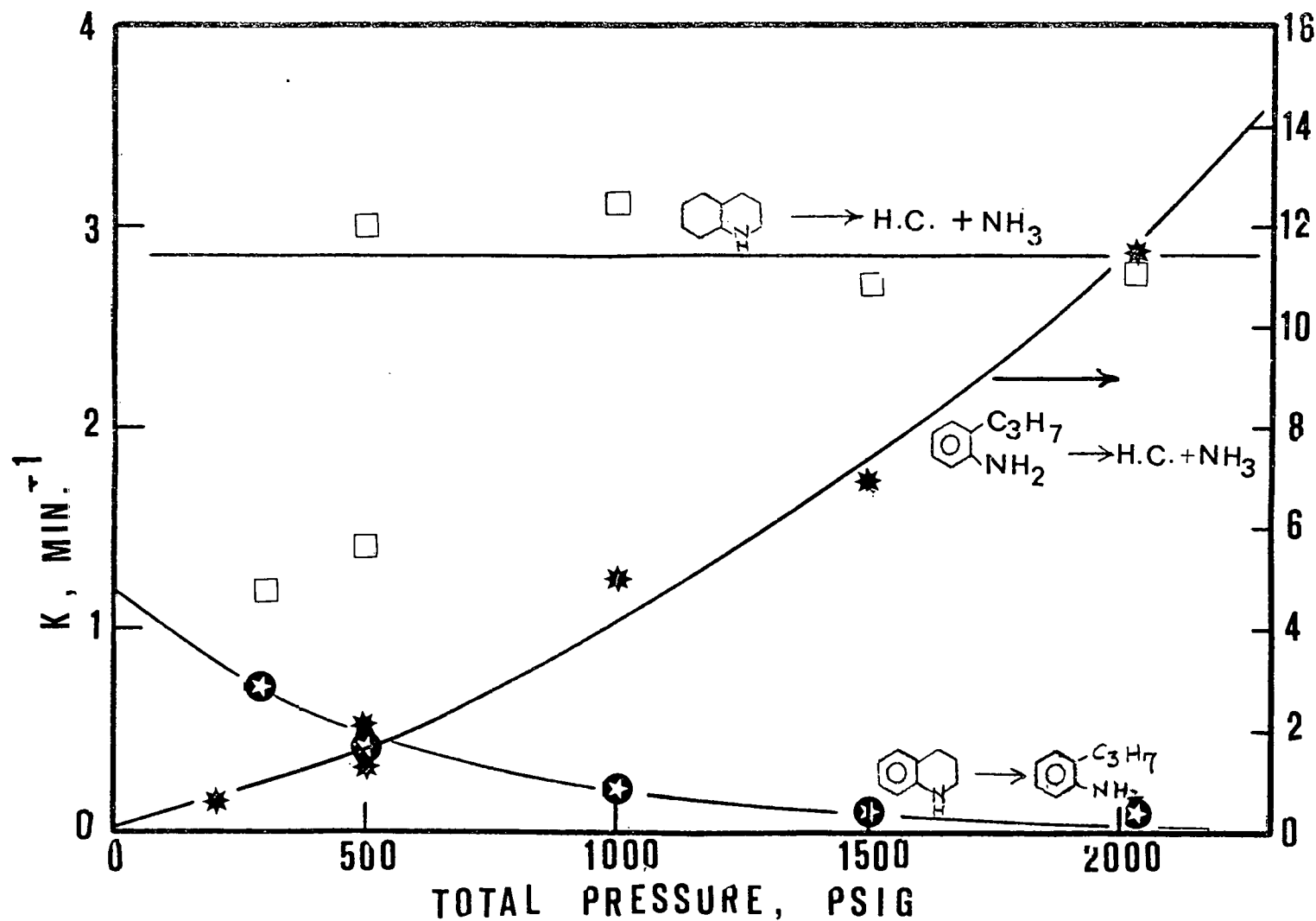
Figure 17. Effect of Total Pressure on Hydrodenitrogenation of Quinoline. Hydrogenolysis reactions; NiMo/Al$_2$O$_3$ catalyst, 342°C, 0.05 wt% CS$_2$ in white oil, 0.5 wt% catalyst in white oil, 1.0 wt% of quinoline in white oil.
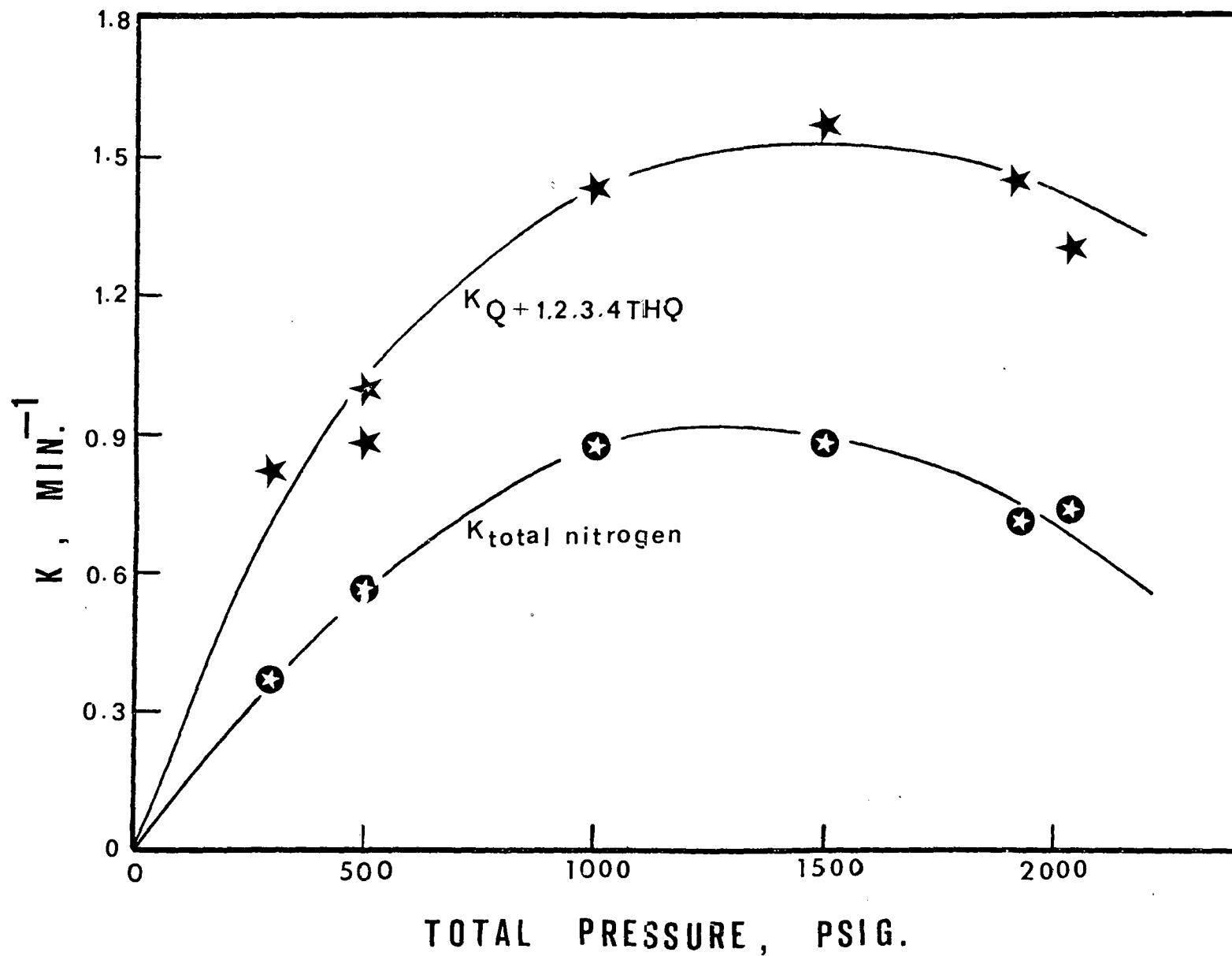
Figure 18. Effect of Total Pressure on Hydrodenitrogenation of Quinoline: presulfided NiMo/Al$_2$O$_3$ catalyst, 342°C, 0.05 wt% CS$_2$ in white oil, 0.5 wt% catalyst in white oil, 1.0 wt% in white oil.

(iii) Effects of the catalyst support

A run with additional support (alumina, Harshaw Al-0104T has been completed to determine the role of the support. The results show that added support alone does not increase the rate of HDN. It is speculated that the hydrogenolysis reactions may occur on the support surface. The acidity of the alumina used in this run may not be strong enough to facilitate the hydrogenolysis reaction substantially. A more acidic support, silica-alumina, will be examined to test this possibility.

(iv) Total hydrocarbon analysis

A run with n-hexadecane solvent instead of white oil has been made in the batch reactor. All reaction products, including hydrocarbons and nitrogen containing compounds, were analyzed with a 6-ft column of 0.1 % of Sp-1000/carbopack C (Supelco, Inc., Bellefonte, PA). Temperature programming from 100°C to 215°C was used with the FID detector. The detailed GC operating conditions are listed in Table 6.

The results of hydrocarbon analyses show that, besides n-propylbenzene and n-propylcyclohexane, there were three unidentified hydrocarbons present in the product. Only trace amounts of benzene or cyclohexane were observed. These results are consistent with our kinetic observation that only a small amount of 1,2,3,4-tetrahydroquinoline is converted into n-propyl aniline:
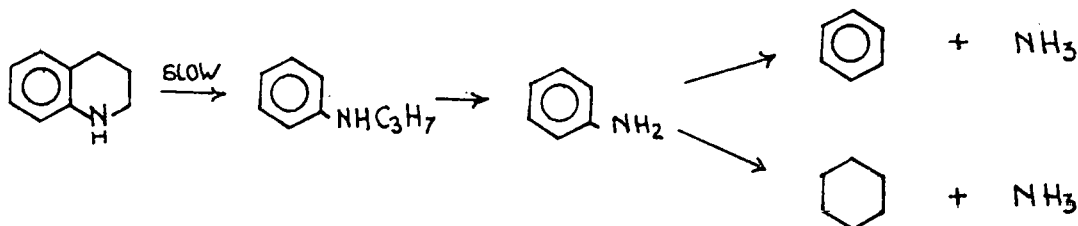
It also implies that nitrogen removal through cyclohexamine is not kinetically important, i.e.,
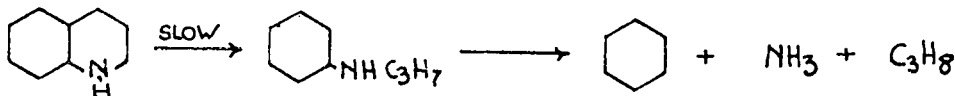
The major hydrocarbon product in the liquid phase was n-propyl-cyclohexaneamine. This implies that the major nitrogen removal

TABLE 6

Gas Chromatographic Analysis of Quinoline

HDN Products in n-Hexadecane

Conditions:

Column:	1/8", 6-ft 0.1% SP1000/carbon pack
He:	set pressure 100 psi, 30 cm^3/min
H_2	30 psig
Air:	50 psig
Instrument:	Perkins-Elmer 3920B

Temperature Programming:

Initial temp:	100°C
Initial hold:	2 min
Rising rate:	16° c/min
Final temp:	225°C or 215°C
Final hold:	16 min

Results:	for final temp = 225°C	for final temp = 215°C
Compound	Retention time, min	
C_6H_{12}	2.3	2.2
C_6H_6	3.5	3.1
$C_6H_{11}C_3H_7$	9.41 (9.0)	8.9
$C_6H_5C_3H_7$	9.7 (9.5)	9.3
1,2,3,4-tetrahydro-quinoline		18.7 (18.7)
o-propylaniline	13.6	18.9
Decahydroquinoline	10.4	14.9 (14.30)
Quinoline	15.8	25.8 (24.0)

occurs through the following reactions:
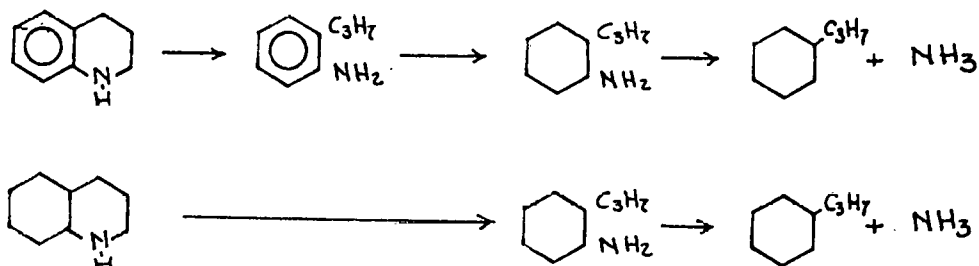
This result reveals that hydrogenation of o-propylaniline occurs before the ammonia is removed. This conclusion has been discussed in the previous progress report.

The small amount of propylbenzene observed in the current study suggests that some of the 1,2,3,4-tetrahydroquinoline is converted into 1-phenylpropyl amine, i.e.,
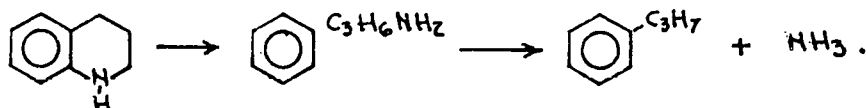
The three unidentified hydrocarbons may include $C_6H_{11}C_2H_5$, $C_6H_{11}CH_3$, $C_6H_5C_2H_5$, or $C_6H_5CH_3$. This suggestion implies that the C-C bond in the decahydroquinoline may be broken before the C-N bond is broken.

(v) Computer programs for kinetic analysis

Currently, Marquardt's nonlinear regression method is being routinely used to analyze the reaction kinetics. An improved program which combines Marquardt's method and the Runge-Kutta-Gill integration method has been developed to handle more complex reaction kinetics. The multi-response regression method is based on that developed by Himmelblau et al. (1967). The programs are to be reported in a subsequent report.

c. Experimental results: quinoline HDN in a flow microreactor

A 425-hr run to characterize quinoline HDN in a flow micro-reactor has been completed. Reaction conditions are summarized in Table 7.

Preliminary results of the product analysis have been obtained, and concentration profiles of major intermediate compounds have been plotted as a function of inverse space velocity in Figure 19. The conditions of a similar run previously carried out in batch autoclave reactor are given in Table 8.

The basis for comparing data from the batch autoclave reactor and those from the flow microreactor was as follows:

(catalyst conc) x (time) is equivalent (space velocity)$^{-1}$

$$\frac{g \text{ of catalyst}}{g \text{ of oil}} \quad hr \qquad\qquad \frac{g \text{ of catalyst } hr}{g \text{ of oil}}$$

batch autoclave   flow microreactor
    reactor

The flow microreactor data correspond to data taken at about 1-4 hrs in the batch reactor. The plots for ln (percent total nitrogen remaining) vs. time or (space velocity)$^{-1}$ for the two reactor systems are given in Figure 20. A more detailed analysis of the kinetics will be presented in the next progress report, but it can already be seen from Figure 20 that the data from the two reactors are in good agreement. This result strengthens that mentioned earlier for HDS experiments, and taken together, the combined results provide a convincing demonstration of the successful design and operation of the flow microreactors and of their appropriateness for the planned kinetic studies.

TABLE 7

Reaction Conditions for Quinoline Hydrodenitrogenation

in a Flow Microreactor

● Reactant mixture:

Quinoline in white oil ~2.03 x 10^{-5} $\frac{g\ mole}{g\ of\ oil}$

● Hydrogen saturation pressure:

~2000 psig at 25°C with ~1% H_2S

● Catalyst:

2.58 x 10^{-2} g of Ni-Mo/Al_2O_3

In situ sulfided with 10% H_2S/H_2 for 2 hr at 325°C

● Reaction temperature:

342°C

● Space velocity:

50 - 212 $\frac{g\ of\ oil}{g\ of\ catalyst\ hr}$

● Reactor pressure:

~2500-3000 psig

TABLE 8

Reaction Conditions for Quinoline Hydrodenitrogenation

in a Batch Autoclave Reactor

- Reactant mixture:

    Quinoline in white oil $\sim 2.1 \times 10^{-5} \frac{g \text{ mole}}{g \text{ of oil}}$

    CS_2 ~ 0.05 wt %

- Hydrogen partial pressure:

    500 psig at 342°C

- Reaction temperature:

    342°C

- Catalyst:

    Ni-Mo/Al$_2$O$_3$ $4.8 \times 10^{-3} \frac{g \text{ of catalyst}}{g \text{ of oil}}$
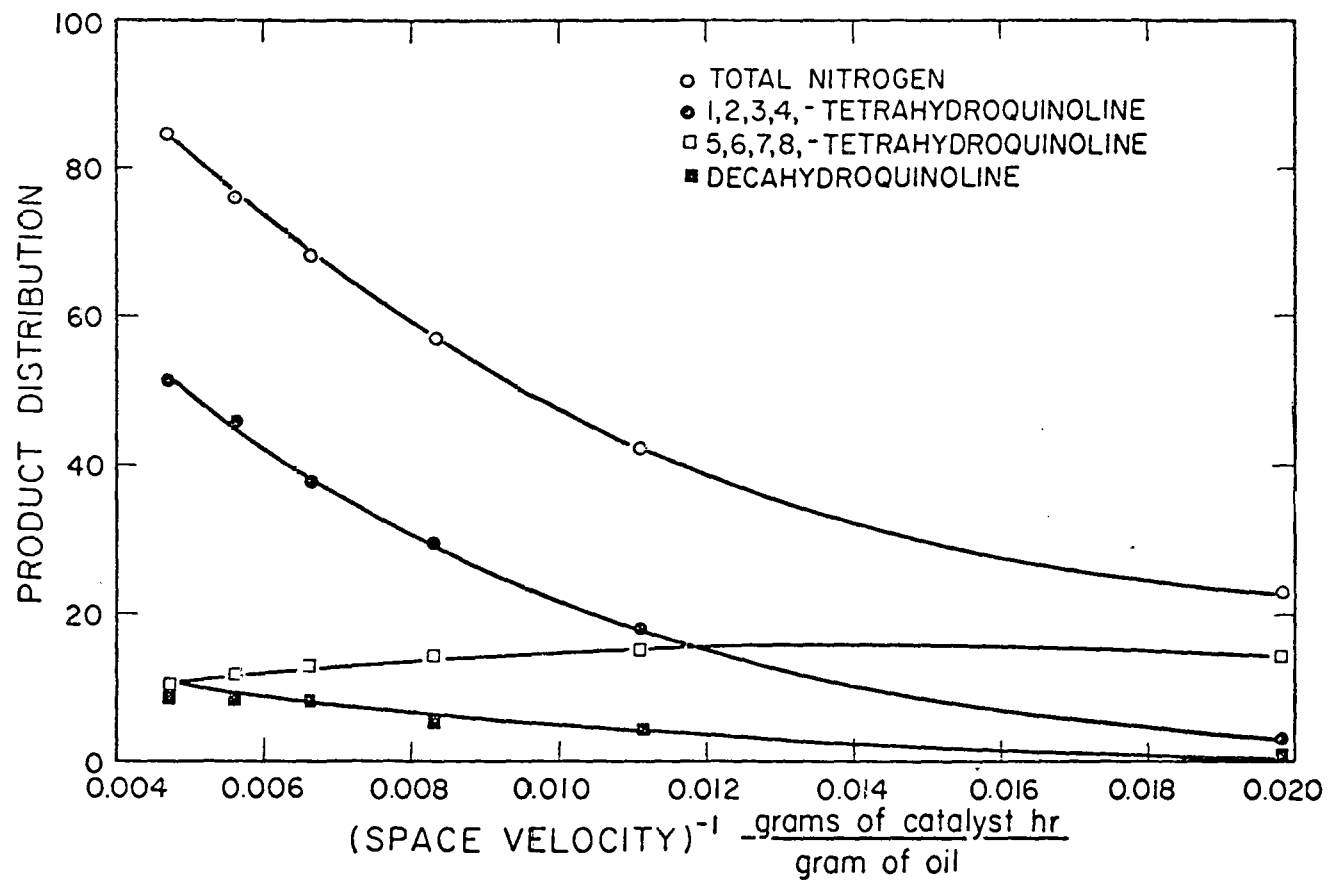
    Sulfided externally at 325°C for 2 hr

Figure 19. Quinoline HDN in a Flow Microreactor; see Table 7 for details.
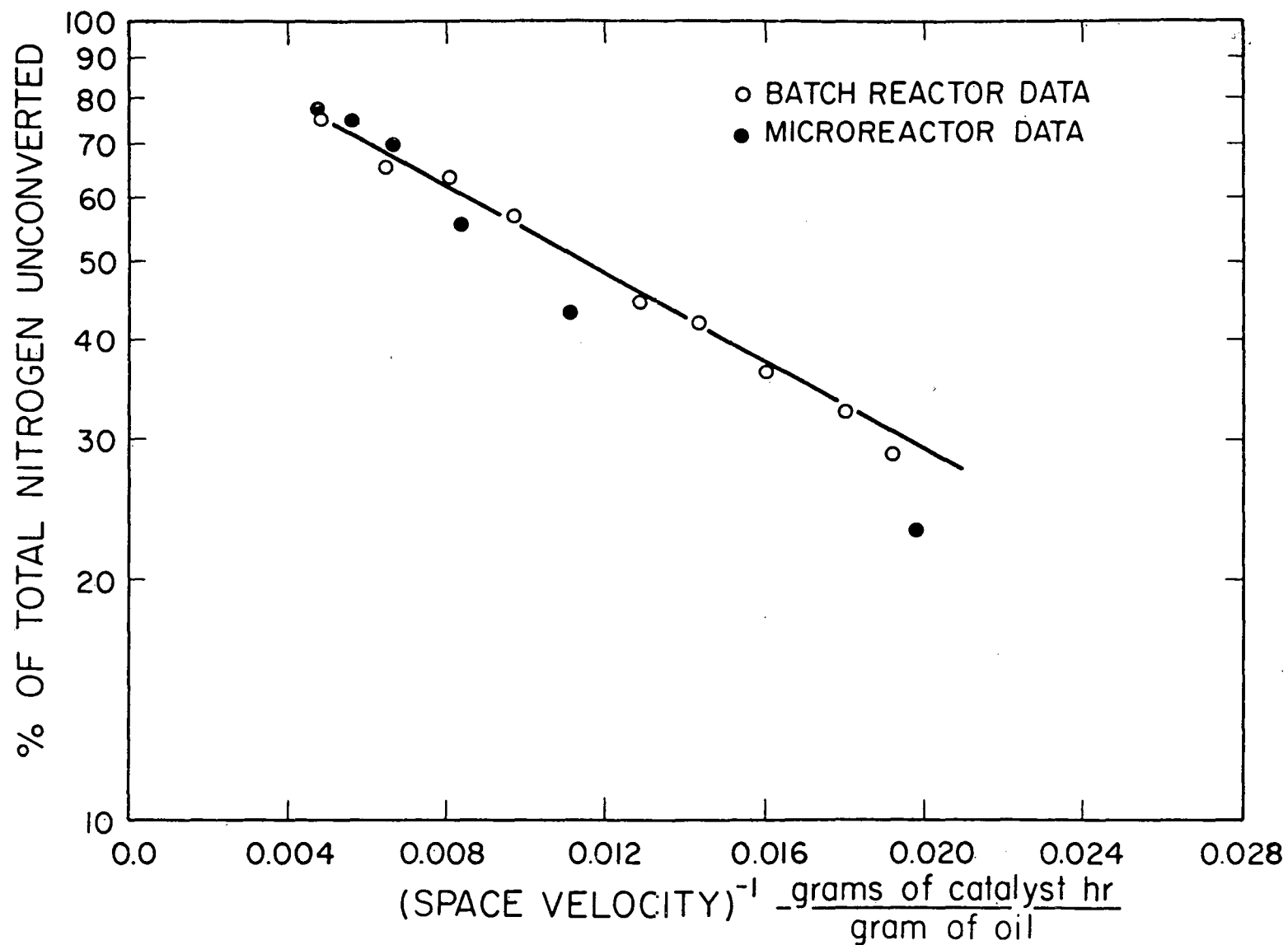
Figure 20. Comparison of Quinoline Conversion Data from a Batch Reactor and a Flow
Microreactor. See Tables 7 and 8 for details.

5. Progress in synthesis and characterization of nitrogen-containing reactants

1-Methylcarbazole has been synthesized as follows:
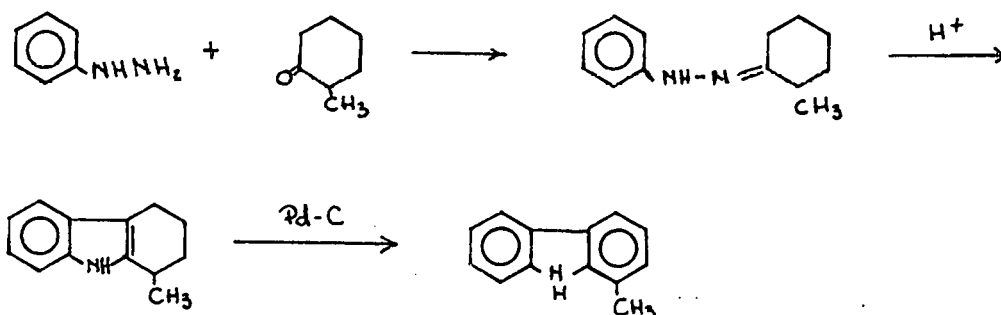
2-Mercaptobiphenyl was prepared by reduction of 2-biphenyl xanthate, which was obtained from 2-aminobiphenyl
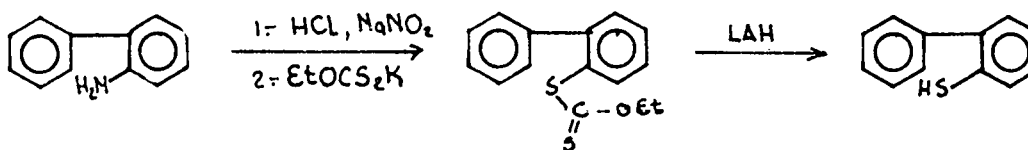
The preparation of 5,6,7,8-tetrahydroquinoline was attempted by the partial dehydrogenation of decahydroquinoline:
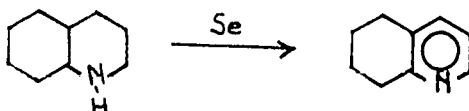
However, the chromatogram of the reaction product indicated the presence of at least six compounds which are difficult to

separate. An alternative route involving the partial hydrogenation of quinoline in acid medium is underway:
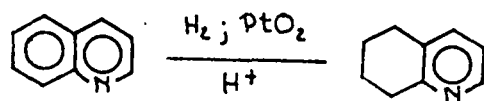
Any decahydroquinoline formed would be separated by acetylation.

The synthesis of 1,2-benzocarbazole has been undertaken by the following method:
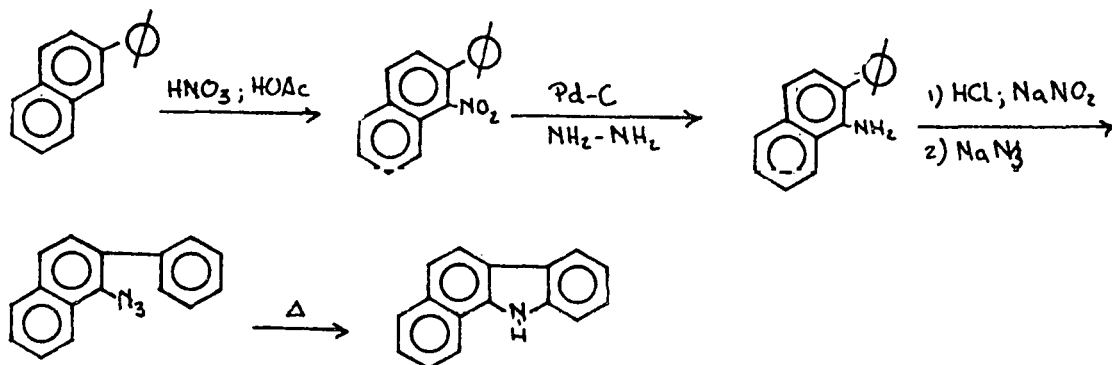
2-phenyl-1-naphthylamine has already been prepared.

The following compounds will be synthesized by the methods indicated below:

Benz[c]acridine:
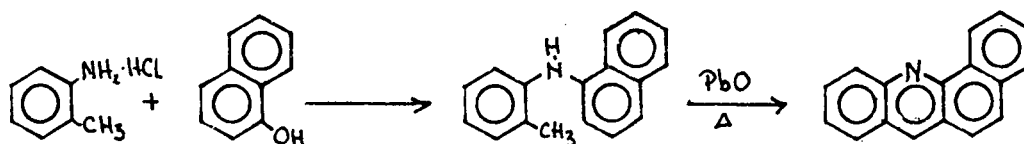
(Ref: Chem. Abstr. 55:15488E [Tada et al. Kyoritsu Yakka Daigaku Kenkyu 5, 16 (1961)]).

Benz[a]acridine:
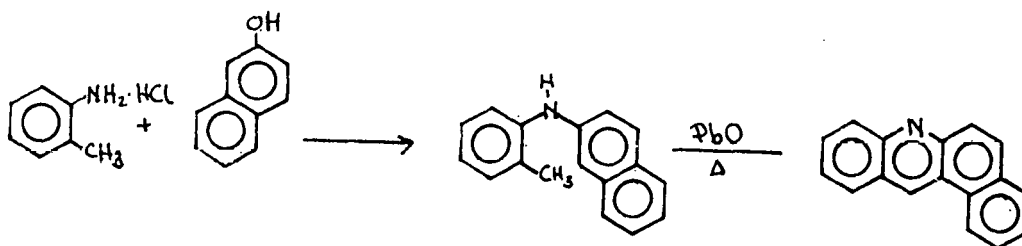
(Ref: Chem. Abstr. 55:15488E)

Dibenz[c,h]acridine:
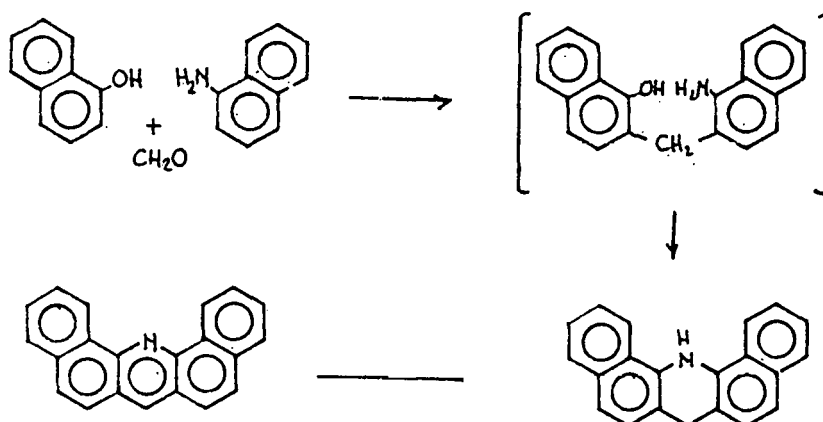
Ref: 1) Ullman and Fetvadjian, Ber. 36, 1027(1903).
      2) Jacquigon Pierre, Bull. Soc. Chim. Fr. 6, 2131(1973)

2,5,8-Trimethyl-1,4,7,9b-Tetrazaphenalene:
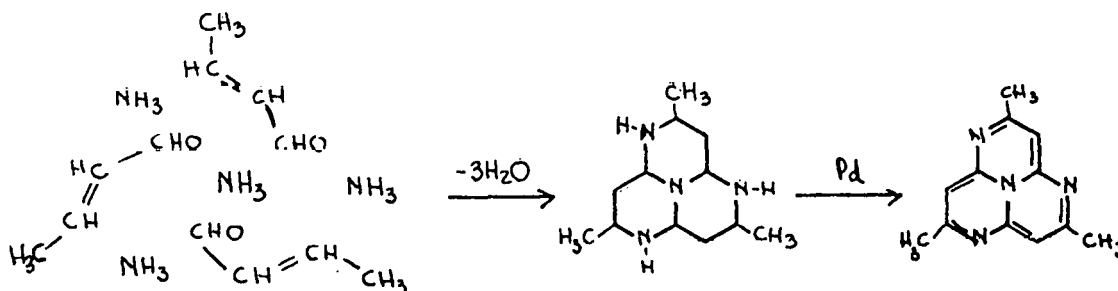
Refs: 1) M. Delepine, Compt. Rend. 216, 649(1943)
       2) L. van Winkle et al., J. Org. Chem. 31, 3300(1966)
       3) W. Crinzel and F. Kuffner, Monatshefte für Chemie,
           101, 1037(1970)

Perhydroacridine:

Trans-Sym-Trans.
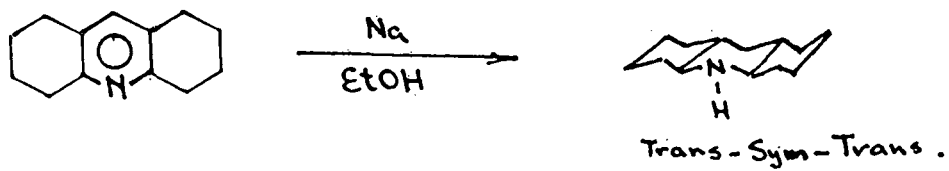
Ref: W. Vierhapper and L. Eliel, J. Org. Chem. 41, 2734
      (1975).

D. SURFACE PROPERTIES AND POISONING PROFILES OF AGED COAL HYDROPROCESSING CATALYST

This section reports a continuation of studies of aged catalysts taken from coal hydroprocessing processes. The first portion of this investigation was presented in the First Quarterly Progress Report in which the deposition of coal mineral matter on the Harshaw 0402T catalyst used in the Synthoil process was described. The current work shows that the deposition of coal mineral matter is a general phenomenon in the hydroprocessing of coal slurries.

Six aged catalyst samples were used in this phase of the program. The first three catalyst samples were supplied on a confidential basis from industry. The process uses a fixed-bed reactor containing a proprietary promoted molybdenum-containing catalyst. The samples were taken from the inlet, middle, and outlet sections of the reactor after the completion of a normal run cycle. The exact processing conditions and analysis of the coal are not available. We tentatively believe that the system operates with process conditions similar to those of the synthoil process using East Coast coal; however the maximum temperature in the reactor probably is less than 400°C. These catalyst samples will be designated as PP (for proprietary process) in the remainder of this report.

The second series of catalysts was supplied by Mr. C. A. Battista of Hydrocarbon Research, Inc. (HRI). The catalyst samples were used in the H-Coal process in runs made under ERDA support. The catalyst is American Cyanamid HDS-1442a 1/16 inch extrudate and was used as received. The run conditions for the three samples are:

1. Temperature: 825-850°F
2. Pressure: 2500-2700 psig
3. Start-up solvent: anthracene

The three catalysts were run with Illinois No. 6 Burning Star Mine Coal; the analysis of the coal used in HRI run 130-78 is given in Table 9. The data in this table are representative of the specifications for all of the runs.

The three samples were taken from runs of differing duration and severity. The values of these parameters are given below:

HRI Run Number	Space Velocity lbs coal/(cu ft reactor hr)	Run Duration hrs
130-73	70	534
130-78	78	274
130-79	30	603

TABLE 9

BURNING STAR MINE ILLINOIS NO. 6 COAL OF THE H-COAL CATALYST

	Run 130-73	Run 130-78	Run 130-79
Moisture, wt %	2.92-3.21	2.25	1.75-2.39
Approximate, dry basis, wt %			
Ash	10.68-10.98	10.88	10.73-10.86
Volatile matter	37.80-38.64	41.79	36.06
Fixed carbon	50.45-51.52	47.33	53.21
Ultimate analysis, dry basis, wt %			
Carbon	69.24-70.11	69.52	68.65-69.20
Hydrogen	4.43-4.79	4.71	4.36-4.63
Nitrogen	1.13-1.45	1.25	1.20-1.23
Sulfur	3.45-3.61	3.34	3.37-3.53
Chlorine	0.00	0.02	0.03
Ash	10.68-10.98	10.88	10.73-10.86
Oxygen (difference)	9.62-10.48	10.28	10.65-11.40
BTU (dry basis)	12,307	12,695	12,621
Sulfur types			
Pyritic	0.96-1.47	1.65	1.48-1.56
Sulfate	0.08-0.24	0.00	0.01-0.03
Organic	1.89-2.29	1.69	1.77-1.85
Total	3.44-3.51	3.34	3.34-3.36
Mineral analysis, wt % ignited basis			
Phosphorous pentoxide	0.12	0.08	0.02
Silica	50.71	48.26	47.38
Ferric oxide	20.09	18.33	19.29
Alumina	14.95	19.70	17.65
Titania	0.10	0.90	0.77
Lime	6.25	5.70	6.45
Magnesia	1.17	0.86	0.75
Sulfur trioxide	3.99	2.61	4.60

TABLE 9 (cont)

BURNING STAR MINE ILLINOIS NO. 6 COAL OF THE H-COAL CATALYST

	Run 130-73	Run 130-78	Run 130-79
Potassium oxide	1.73	2.02	1.77
Sodium oxide	0.44	0.68	0.72
Undetermined	0.45	0.86	0.60
Iron, wt % of dry coal	1.40-1.50	1.48	
Screen size (4.S.S.)			
+50	1.67-4.13	3.48	3.69-5.55
50/70	2.32-4.11	4.64	3.98-5.35
70/100	5.56-7.66	7.78	7.17-9.79
100/140	8.17-11.26	10.77	12.20-13.66
140/200	10.23-12.89	10.74	13.73-14.69
200/325	22.19-24.32	27.39	18.94-22.40
325/pan	35.63-50.04	35.20	29.51-39.33

These catalyst samples will be designated by the HRI run number. A sample of fresh HDS-1442A catalyst was examined along with the three samples of aged catalyst.

The pellets were analyzed with a scanning electron microscope (SEM) equipped with an energy dispersive x-ray analyzer (EDAX) and with an electron microprobe at the facilities of Micron, Inc., of Wilmington, Delaware. One set of samples was prepared for analysis by mounting the pellet in epoxy support, followed by grinding and polishing to yield a radial and transverse section, and finally removing external non-mineral matter with plasma etching. The second set of samples was prepared by fracturing the catalyst radially and transversely, mounting the broken piece on a post, and cleaning the surface with plasma etching. The EDAX analyzer provides qualitative analysis of elements above sodium in atomic mass; these data were used to guide the subsequent microprobe studies.

Representative SEM results are shown in Figures 21 to 23 for the three catalyst samples taken from the inlet, middle, and outlet sections of the PP fixed-bed reactor, and Figures 24 to 27 show the typical electron microprobe x-ray images for both H-coal runs 130-73, 130-78, 130-79 and fresh catalysts. Figures 28 to 37 show the electron microprobe concentration profiles for each specific pellet. Each figure is accompanied by a detailed caption. Therefore, only the general results will be described in the following section.

Proprietary Catalyst

All PP catalyst samples have a thin layer of about 10-20 μm thick of inorganic crust which covers essentially all of the surface. Since the pellet from the outlet section was examined first, more information was gathered for this sample. The results for this sample are typical of the surface properties for all the samples of this catalyst.

The catalyst pellet in the inlet section is covered with a crust 10 um thick which is analyzed to be primarily iron, sulfur, and calcium. Cobalt and molybdenum were also found in the crust in minor quantities. The trace amounts of silicon, titanium, aluminum, magnesium, nickel, and phosphorus varied, depending on the location examined. The penetration depth of the inorganic elements was found to be greater than 200 um into the interior of the catalyst for most of the elements concerned. The quantitative amount of deposition was found to be much higher than that in the middle and outlet sections of the reactor.

The catalyst pellet in the middle section of reactor has a 20 um crust which is thicker than the crust found in the inlet section. This result may be caused by the inhomogeneity of the catalyst. The crust was made up primarily of iron, sulfur, calcium, and molybdenum with minor and trace amounts of aluminum,

silicon, titanium, cobalt, and nickel. The amounts of these trace elements varied, depending on the location analyzed. The penetration depth of the inorganic elements was found to be less than 150 µm, except for calcium, sodium, and sulfur. The deposition of iron was much lower than that in the inlet section.

In the outlet section the elements of crusts varied significantly with the location analyzed. Some crust was found to be primarly of rod-like crystals (Figure 23a,b), which were analyzed to be ferrous sulfide, and others were found to be made up of rectangular bars, which were found to contain calcium, aluminum, molybdenum, and silicon. Titanium, magnesium, potassium, zinc, cobalt, and manganese were present only in trace amounts. The penetration depths of the inorganic elements were found to be less than 100 µm within the interior of the catalyst, except for sodium and sulfur.

The nature and location of the deposits suggest the following possibilities for the sources of these elements in the PP catalyst. The elements aluminum and molybdenum are known to be from the catalyst, and the nickel and cobalt appear to be promoters deposited together onto the molybdenum catalyst. Sodium may have been added to control catalyst acidity. The catalytically active material is quite heterogeneous and apparently can migrate into the deposited external crust.

The external crust is not less than 10 µm thick and can be much thicker (~1mm) in some regions in which presumably the fluid turbulence is low or the catalyst has chipped away. Further, the external crust can penetrate down cracks in the catalyst. These cracks grow during aging, and therefore formation of the crust contributes to the attrition and ablation of the catalyst. The external crust appears to be better defined in the outlet PP sample than in the inlet and middle PP samples. The structure within the crust suggests the deposition by columnuar grain growth of ferrous sulfide and perhaps calcium sulfide as well as the direct deposition of mineral oxides of the clays in coal. The formation of the external crust clearly reduces the availability of the catalyst.

The exterior crust contains aluminum, calcium, silicon, titanium, magnesium, and minor amounts of manganese and zinc. These elements are all present in clays and rutile. Since these inorganic oxides are not reactive under process conditions, they apparently are attached to the surface by cementing. The cemented position of the elemental traces appears as sharp spikes on the exterior of the catalyst.

In addition to the cementing process, there is an apparent reductive deposition of some of the elements deeper into the interior of the catalyst. In the most simple first-order process

the conversion of a precursor P to a deposit D

$$O \approx \frac{\partial P}{\partial t} = \frac{\partial}{\partial x} D_{eff} \frac{\partial P}{\partial x} \quad - \quad k\, P$$

$$\frac{\partial D}{\partial t} = \quad\quad\quad\quad + \quad k\, P$$

suggests that the deposited profile should have the form

$$D(x, t) = P_0\, e^{- \left(\frac{k x^2}{D}\right)^{1/2}} (kt)$$

Thus a simple reductive deposition should yield an exponential decay in the concentration of the deposited product. The titanium and silicon signals appear to follow this form after the surface deposition contribution is removed from the signals.

The previous work with the Synthoil catalyst established the formation of $Fe_{14}S_{15}$ on the catalyst surface. The formation of this compound is indicated by a high correlation between the sulfur and iron signals. On this basis the formation of FeS_x has advanced 125 μm into the apparent interior of the PP inlet catalyst sample and is confined to the exterior of the PP middle and outlet samples. In addition, there is an exponential decay of the iron signal toward the catalyst interior, which does not correlate with the sulfur signal. The exponential portion of the iron signal appears to indicate a reduction product of the form described above.

The SEM investigation of the PP samples showed very large variations in the thickness of the external crust. The microprobe scans were taken on what appeared to be thin sections of the crust of approximately the same thickness. The microprobe data indicates that the FeS_x deposition penetrated well into the PP inlet sample, a result not apparent in the SEM investigation. The molybdenum concentration profiles for the three samples vary by a factor of two, and the sulfur level correlates with the molybdenum concentration quite well. On this basis it appears that the PP outlet sample also experienced surface undermining from mineral deposition. In particular, the section 50 μm interior from the surface is high in aluminum, magnesium, calcium and oxygen, and low in molybdenum, sulfur, nickel and cobalt. Therefore, the surface interior appears to be filled with coal clays, and therefore deposition appears to destroy the catalyst physically. This result appears to be general.

H-Coal Catalyst

The SEM studies of the H-coal catalysts, in contrast to the PP or Synthoil catalysts, show that there is little external crust on any of the spent samples. This result indicates that the inherent "wet grinding" of the catalyst in the H-coal process removes the external crust. Secondly, the extruded catalyst is filled with large cracks and smaller but still visible macropores; this void structure improves the availability of the catalyst interior to reactants. The SEM work shows that the large interior voids fill in with coal mineral matter during reaction.

The electron microprobe analyses show evidence for traces of external crust. In particular, run 130-79 exhibits a small amount of FeS_x and run 130-73 shows a minute quantity of silicon. Thus, external cementing and crystal growth is nearly absent in the H-coal process.

The electron microprobe analysis of the catalyst interior of the H-coal process shows modes of deposition which are similar to those in the PP and Synthoil systems. For example, runs 130-78 (short run time, high concentration of coal in slurry) and 130-73 (long run time, high slurry density) both exhibit penetration of FeS_x approximately 50 μm with the catalyst. The formation of FeS_x is established by spikes of the iron and sulfur signal at the same position in the catalyst. In contrast, highly localized concentrations of FeS do not appear in run 130-79 (long run time, low slurry density). The penetration of calcium and silicon into the catalyst appears to occur by three processes: (a) a highly localized deposition 10 μm into the interior of the surface, (b) a highly localized penetration deeper into the catalyst to the depth of significant FeS formation, and (c) a decaying exponential penetration. The first two results are consistent with a general penetration of coal mineral matter into the cracks of the catalyst; when the cracks grow, the penetration is deeper. The last result suggests penetration of the mineral matter of smallest size into the macropore of the catalyst. Finally, the titanium and iron signals also show an exponentially decreasing pentration to a depth of about 200 μm. The titanium signal additionally exhibits the formation of a dense deposit just below the surface.

The cobalt and molybdenum signals of the fresh and spent H-coal processes show that the cobalt is added to the catalyst separately from molybdenum (Figure 33, the fresh catalyst). The concentration of molybdenum and cobalt show substantial local variations in all of the samples, and the cobalt may be sintering as the runs progress. The sintering or surface diffusion would appear to be a permanent loss of activity.

Summary

These studies lead to the following general conclusions about the catalytic formation of liquid fuels from coal:

1. Only a very small fraction of the mineral matter in coal remains on the catalyst. For the H-Coal process this fraction is less than 0.005.

2. Coal mineral matter appears to be attached by direct cementing at the surface and by a reactive penetration to greater depth into the catalyst.

3. The formation of FeS often leads to the destruction of the catalyst support. The formation of FeS appears to increase the size of the cracks in the catalyst near the surface. These cracks also can fill with other coal mineral matter (primarily clays).

4. An external crust of mineral matter forms on catalyst in fixed-bed reactors. This crust is nearly absent from the catalyst from a slurry, stirred-tank reactor.
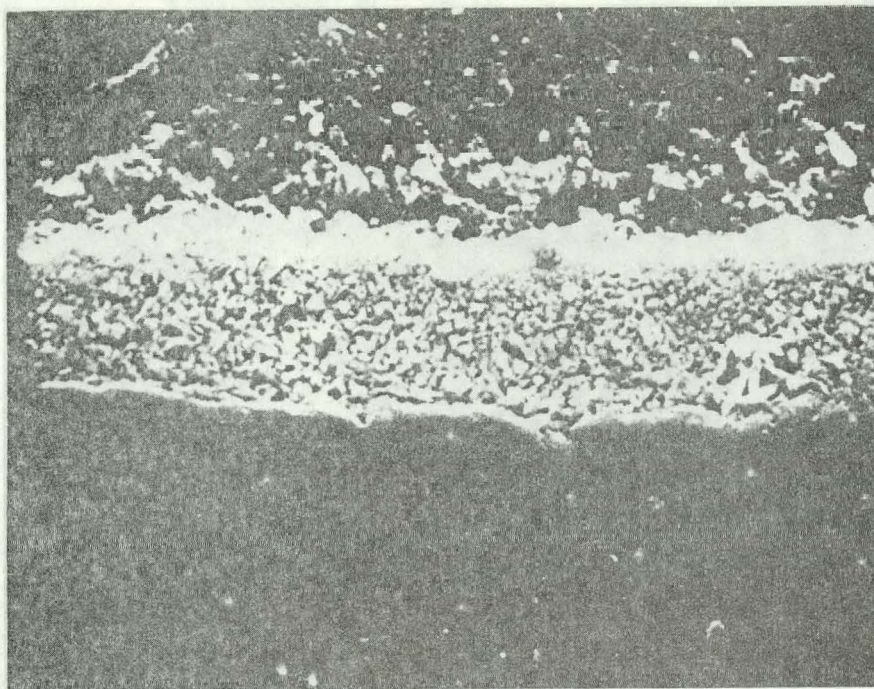
10 μm
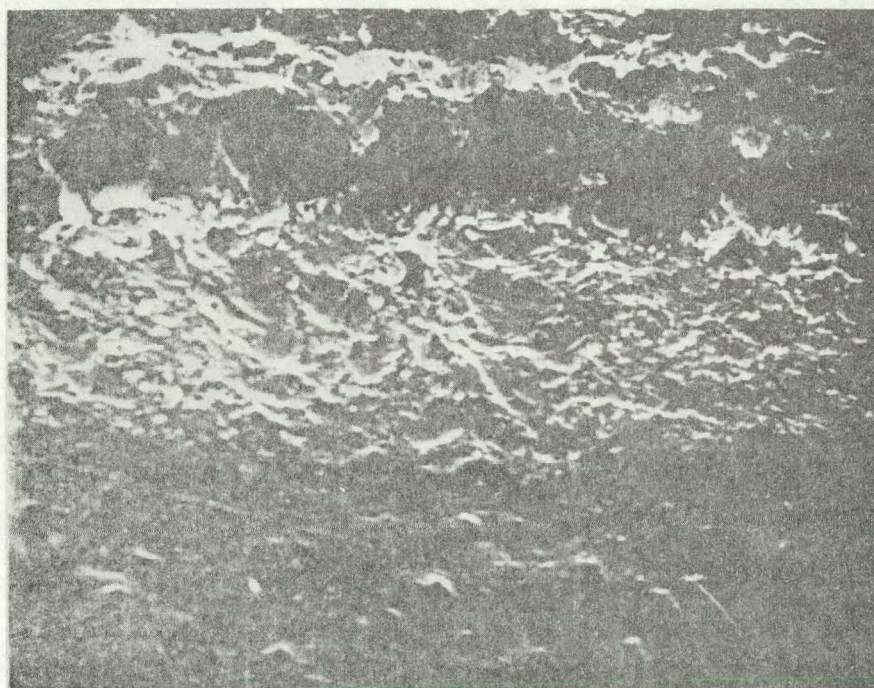
10 μm

Figure 21. SEM of the Inlet PP Catalyst -- The upper picture shows
the crust on the exterior of radial-sectioned catalyst. The crust
is 10 μm thick, which is less than that found in the middle section
of a reactor. The crust was determined by EDAX to be primarily of
calcium and ferrous sulfide with traces of aluminum, silicon and
magnesium. The lower picture shows the deposition effect on the
transverse-sectioned catalyst. The upper part of the picture is
part of the mounting material. EDAX results show that the crust
is composed of ferrous sulfide with small amounts of calcium and
traces of aluminum, silicon and magnesium.

10 μm
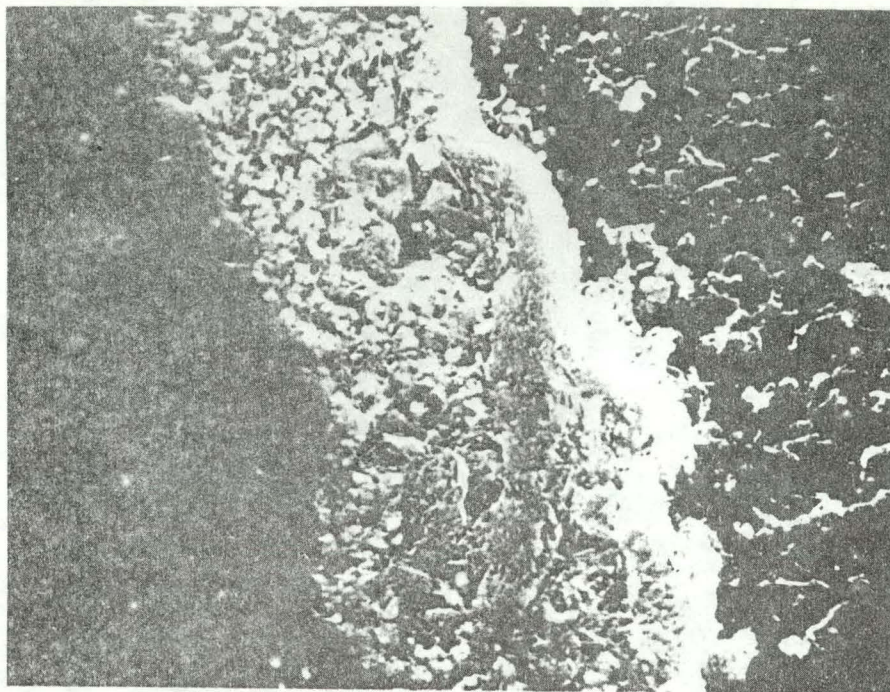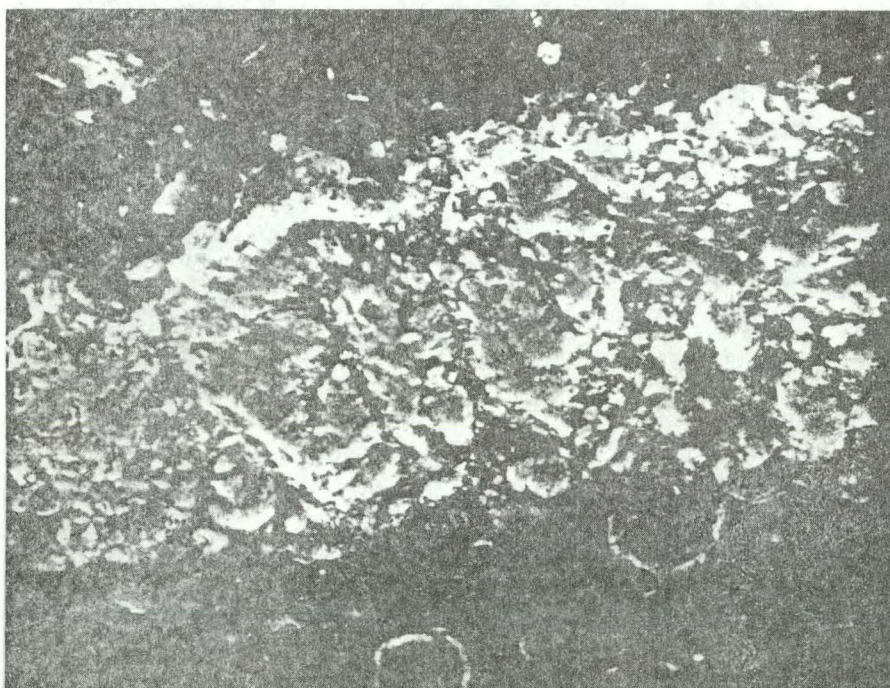
10 μm

Figure 22. SEM of the Middle PP Catalyst -- The upper picture shows
a crust with 20 μm thickness. The catalyst is sectioned along
the radial plane. The crust was shown by EDAX to be made up
primarily of molybdenum and ferrous sulfide, with small amounts
of calcium and traces of aluminum, silicon and titanium. The
lower micrograph shows the typical crust material in transverse
section. EDAX results show that the crust was primarily ferrous
sulfide with small amounts of calcium and traces of aluminum and
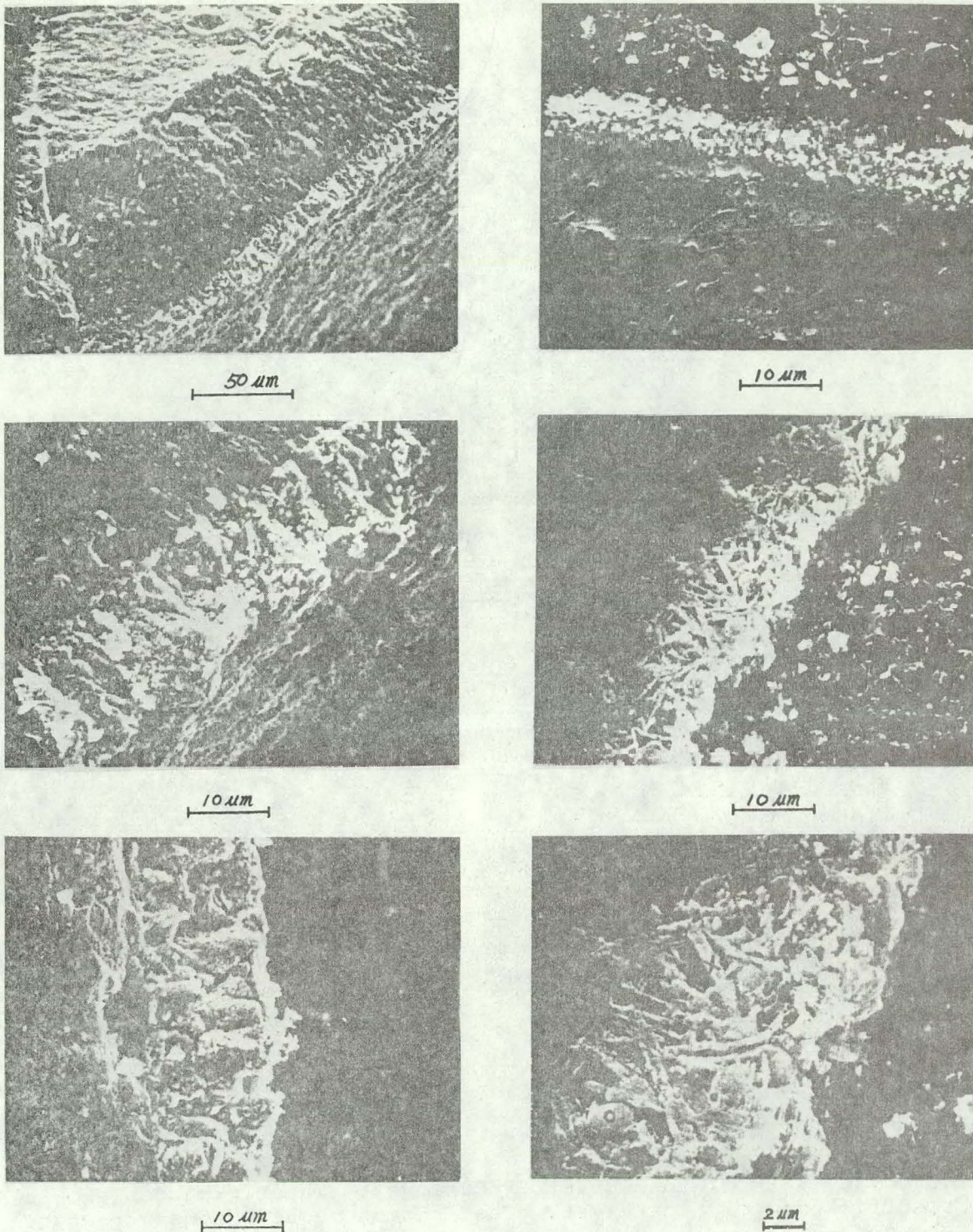silicon.

Figure 23a. SEM of the Outlet PP Catalyst -- The upper left picture shows a typical fractured and plasma etched catalyst particle. The crust is 15 μm thick, a little smaller than the crust on the middle section. EDAX results show the crust was primarily ferrous sulfide and molybdenum with trace amounts of calcium, silicon, aluminum and magnesium. The right pictures show a polished section of catalyst. The area marked (X) is shown by EDAX to be made up primarily of calcium with small amounts of sulfur, aluminum and silicon. The area marked (O) was determined by EDAX to be primarily calcium and silicon with traces of aluminum, sulfur, iron and magnesium.
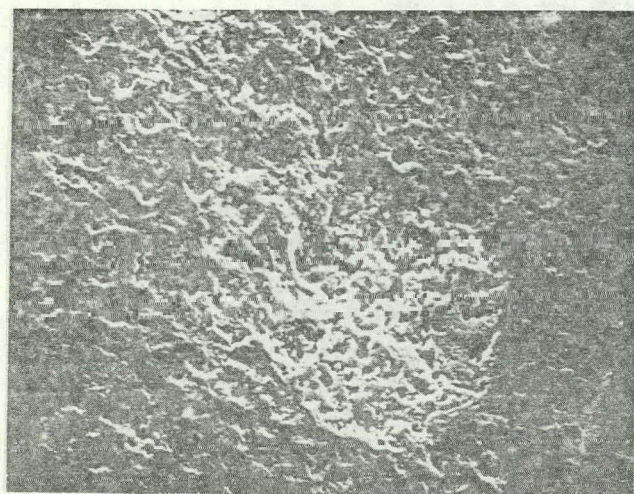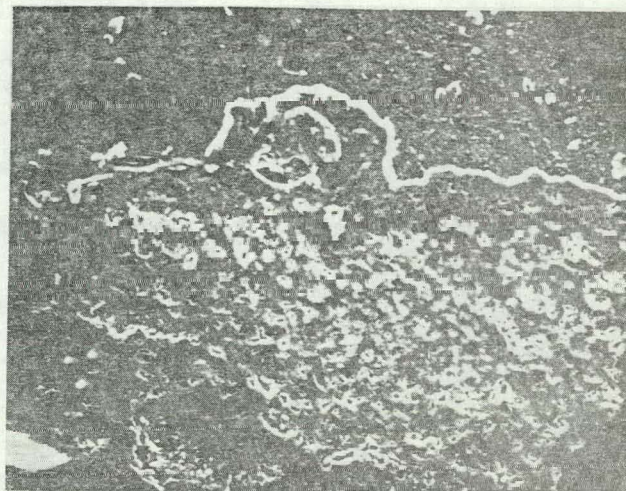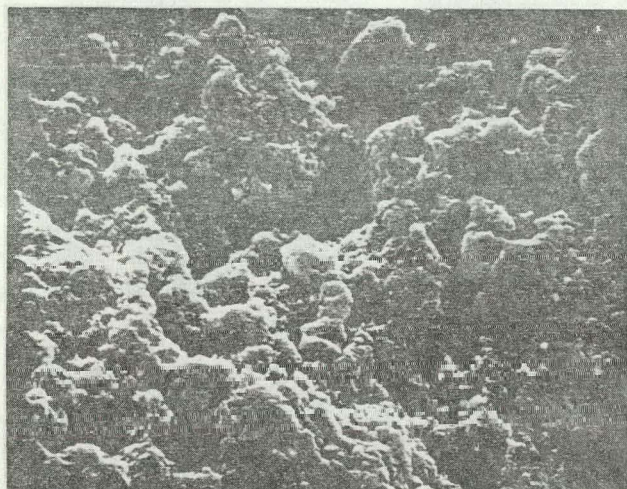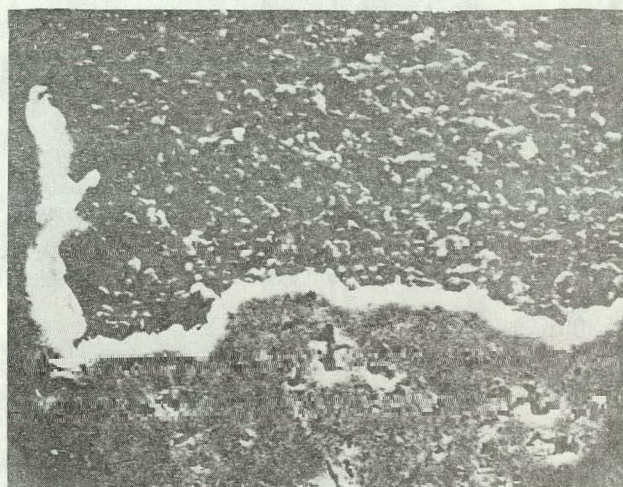
100 μm
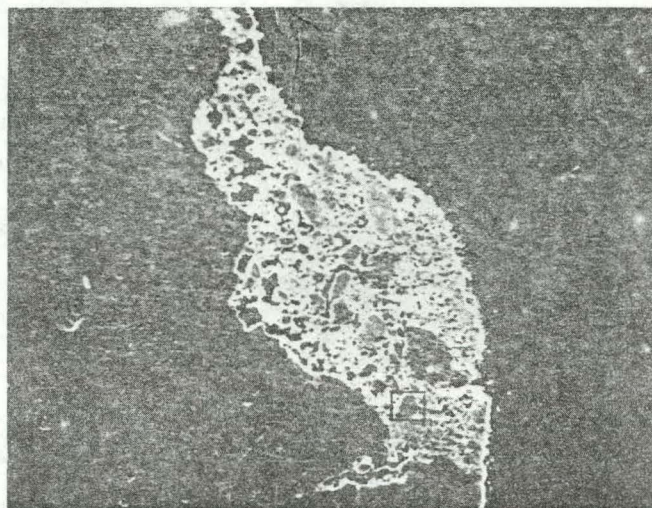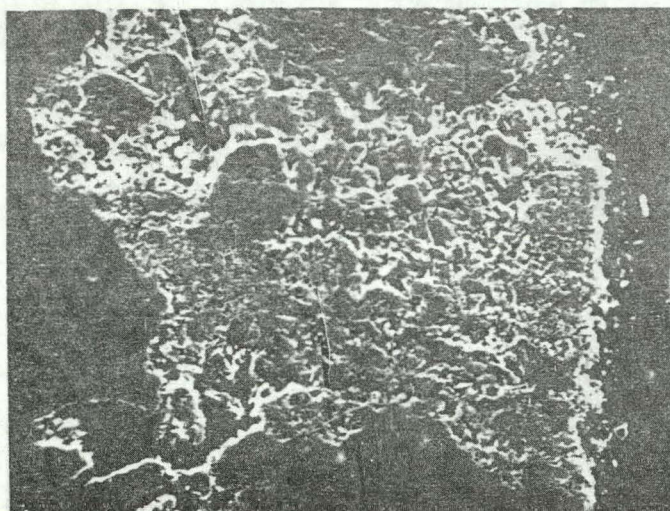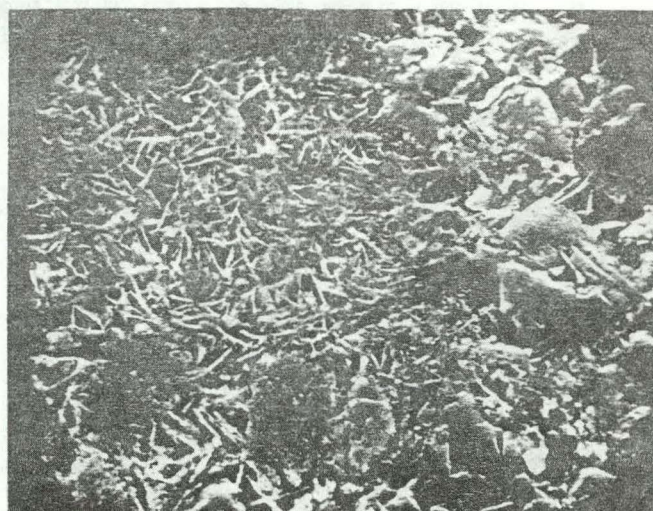
50 μm

10 μm

Figure 24. SEM of H-Coal Catalyst (Run 130-73) -- The right pictures
show a typical clear surface of the catalyst. EDAX results show
the edge of the catalyst contains primarily aluminum with small
amounts of titanium, molybdenum and traces of calcium, silicon,
ferrous sulfide, cobalt and potassium. The left pictures show the
typical interior deposition. The elements were determined by EDAX
to be primarily of aluminum, with small amounts of molybdenum,
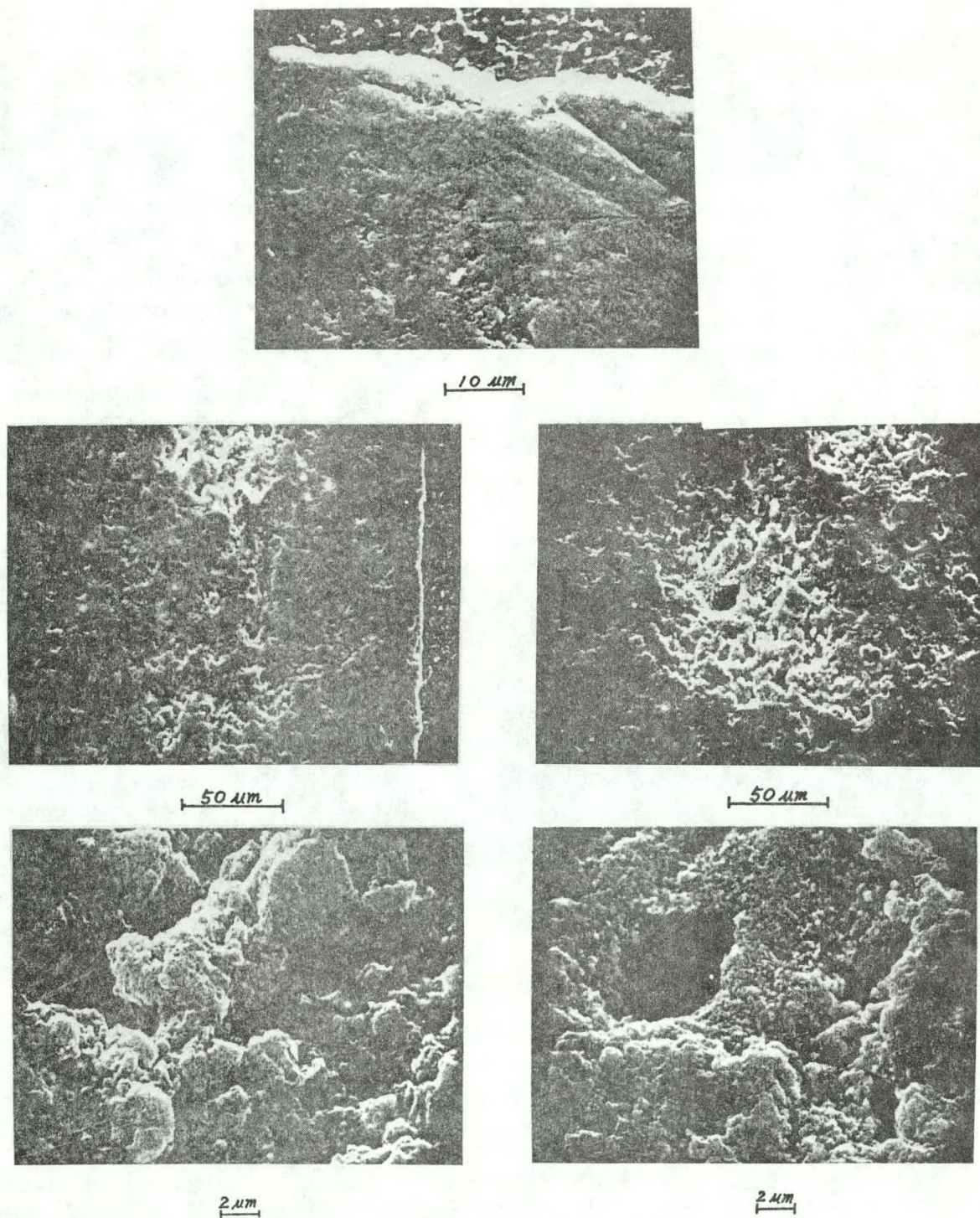titanium and traces of calcium, silicon, cobalt, potassium and iron.

Figure 25. SEM of H-Coal Catalyst (Run 130-78) -- The right
pictures show the interior deposition in the radical-sectioned
catalyst. The bubble is clean. EDAX results show that the blob
is made up primarily of aluminum, with small amounts of Mo and
traces of Ti, Co, Si and Fe. The upper picture shows the clean
surface in the transverse-sectioned catalyst. The left pictures
show the interior deposition of the catalyst. The blob material
was determined by EDAX to be composed of primarily Al, Mo with
traces of Ti, Ca, Co and Fe.

Figure 26. SEM of H-Coal Catalyst (Run 130-79) -- The catalyst
surface is clean, and the macropore structure of the catalyst can
be seen. The EDAX results show that the elements of the catalyst
edge are primarily of Al with small amounts of Ti and Mo and with
traces of Ca, Co, Si and ferrous sulfide.

Electron

Al

Mo

Co
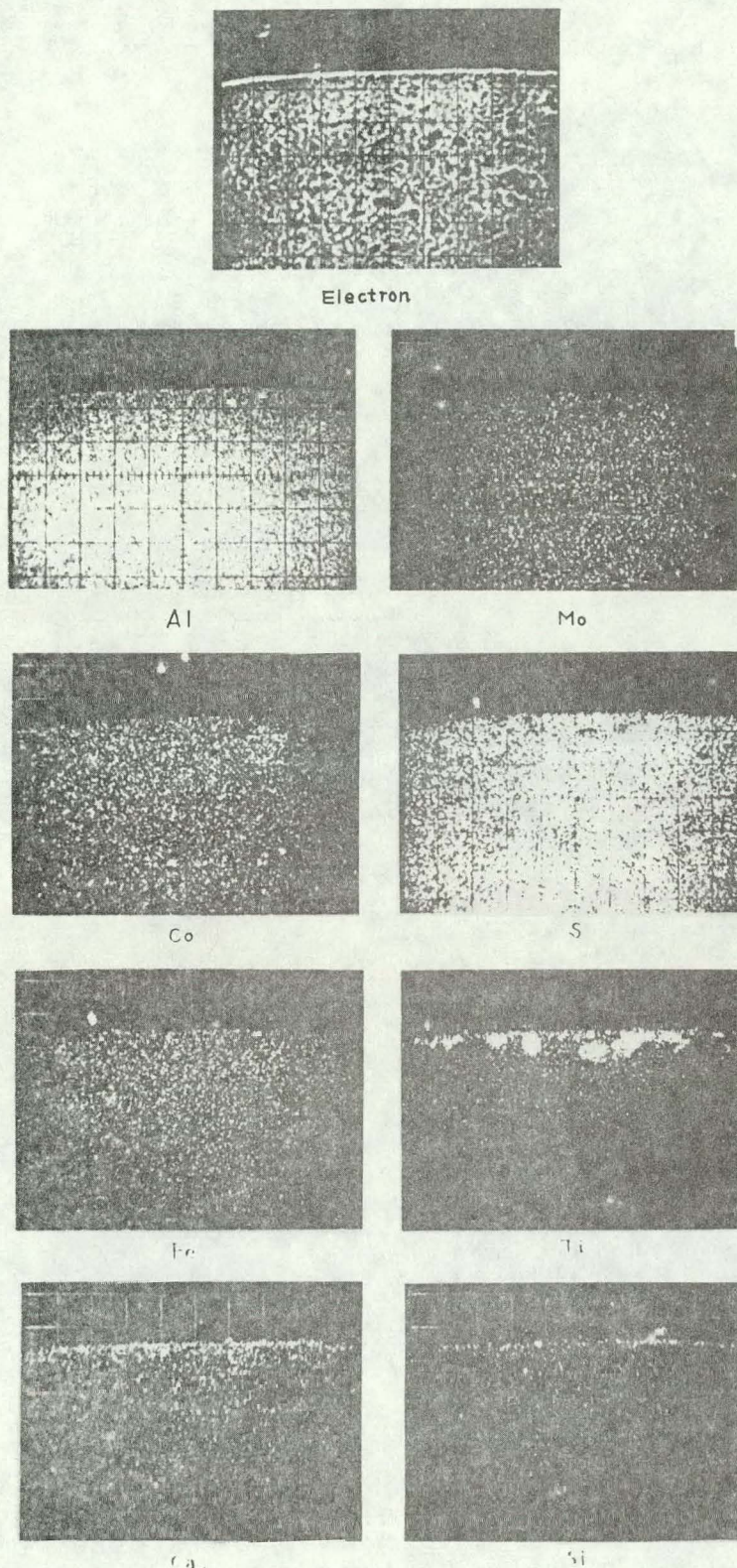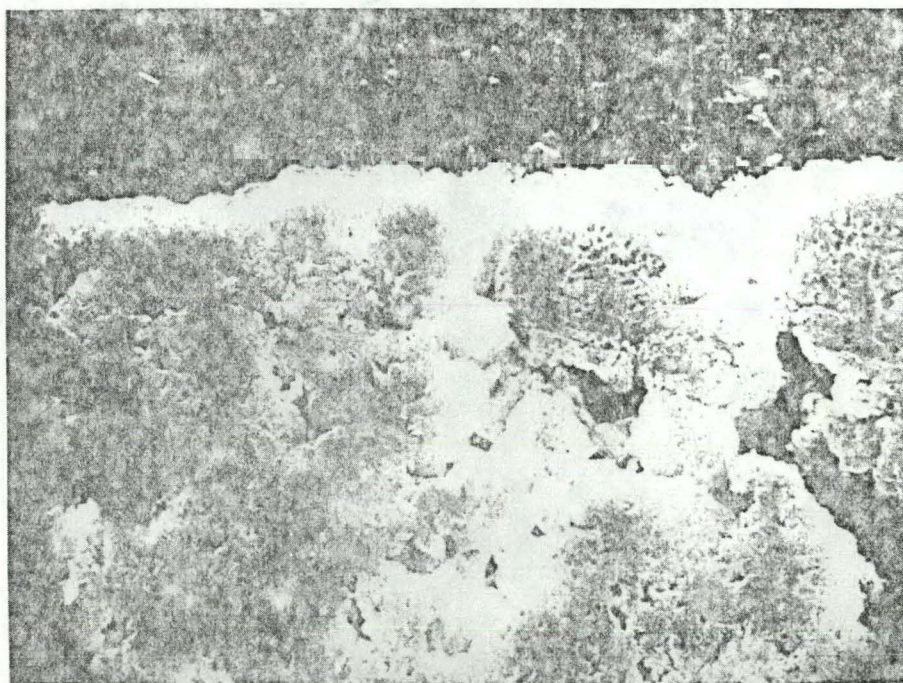

S

Fe

Ti

Ca

Si

Figure 27. SEM of H-Coal Catalyst (Fresh) -- This picture shows the
typical structure of fresh catalyst with both micropores and
macropores. The EDAX results show the elements are primarily of
Al, with small amounts of Mo and traces of Co and S.

10 um

10 um

Fig. 28 Electron Microprobe X-ray Images of H-coal Catalyst
(Run 130-79)--These pictures show the qualitative distribution
of the elements examined. The electron image shows a roughly
150µm thickness of organic crust. Al is observed to be quite
uniformly distributed except near the edge. The images of Mo,
Co and S show uniform distribution inside the catalyst pellet.
Fe is observed to decrease toward the interior of catalyst. Ti
and Ca appear to deposit primarily near the edge. The image of
Si shows trace amount of deposition near the edge.
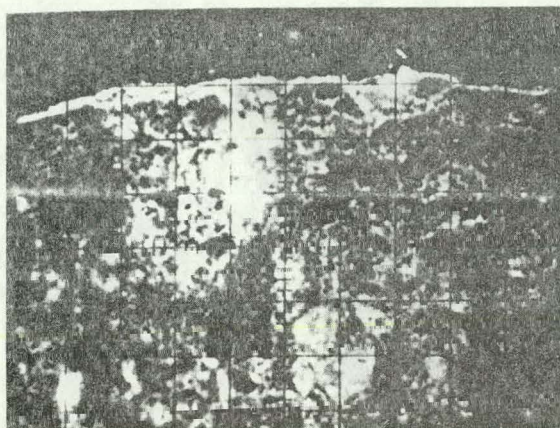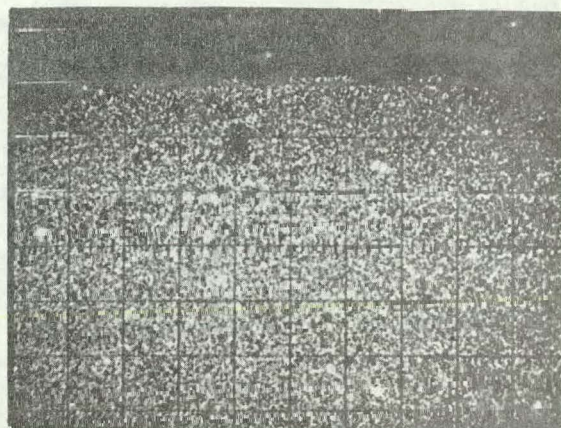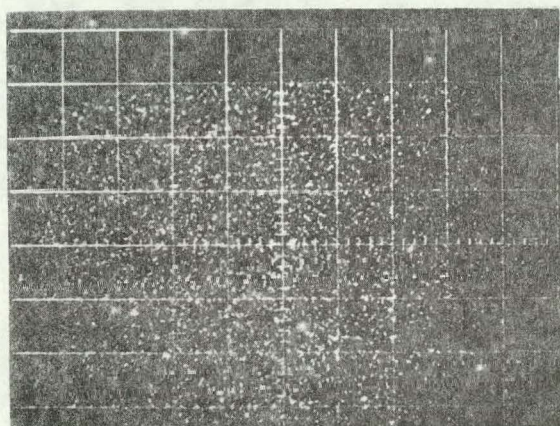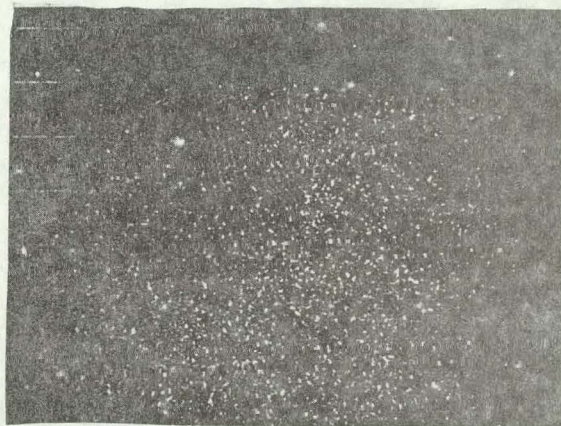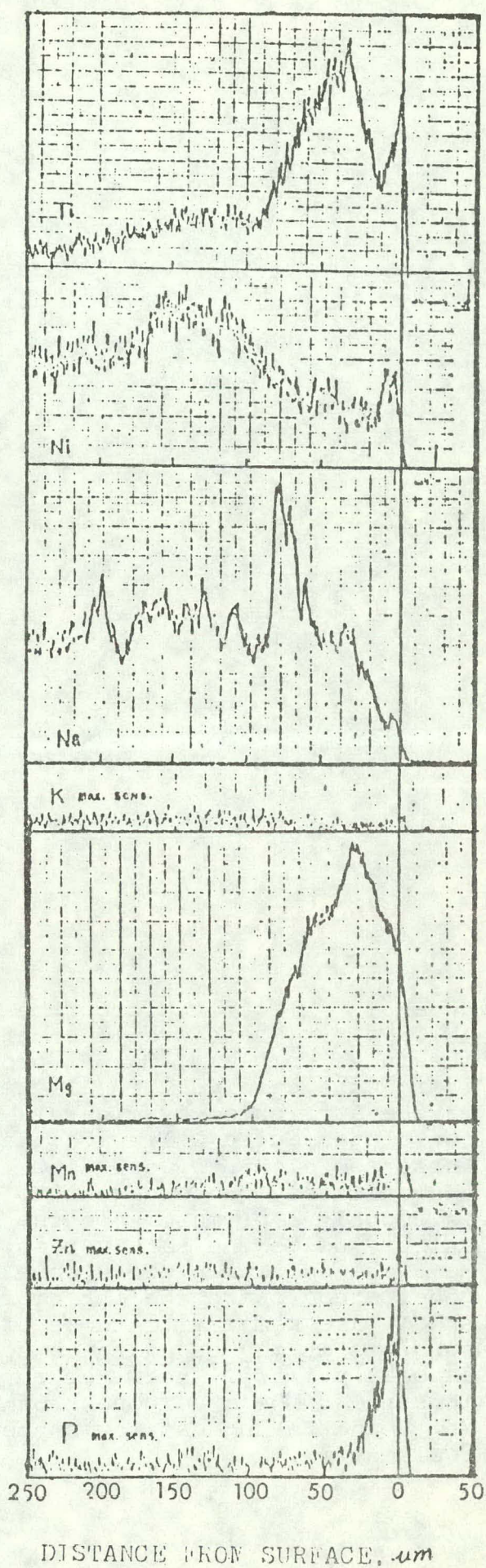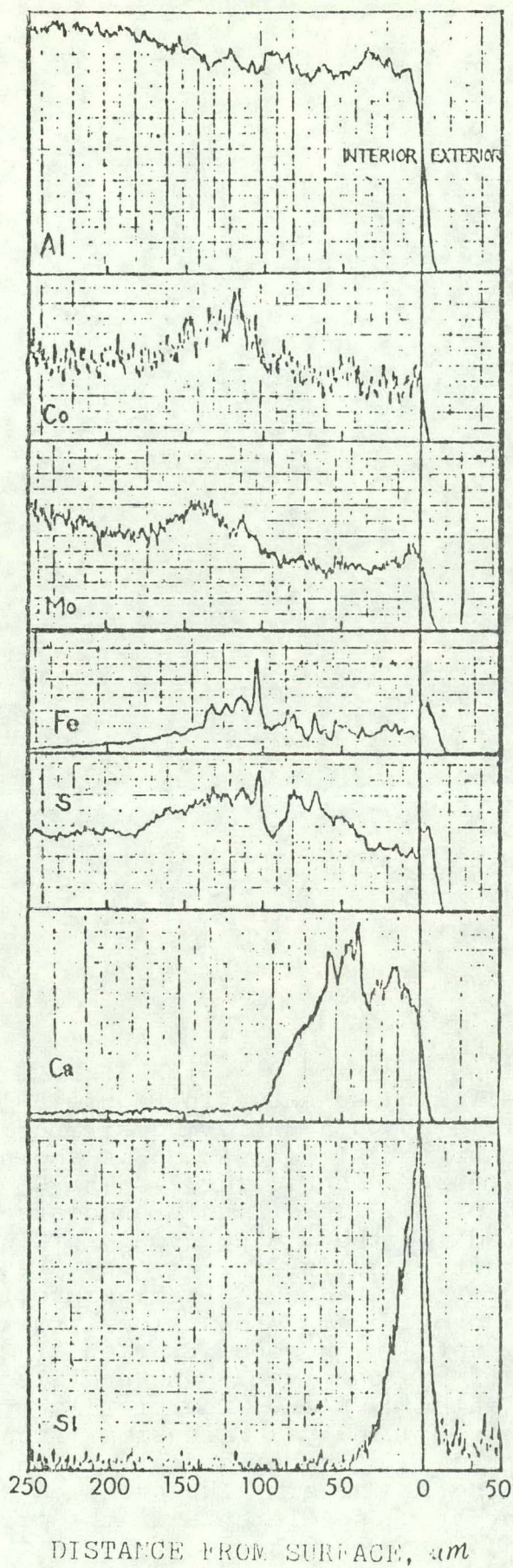
Electron

Al

Co

Mo

50 μm

Figure 29. Electron Microprobe X-Ray Images of H-Coal Catalyst
(Fresh) -- These pictures show the qualitative distribution of
selected elements. Al is observed to be quite uniformly dis-
tributed except near the edge. Co and Mo appear somewhat
uniformly distributed inside the catalyst.

Figure 30. Electron Microprobe Concentration Profiles of PP
   Catalyst (Inlet) -- The aluminum profile serves to identify
   the exterior catalyst surface and shows the variation inside
   the catalyst. The concentration profile of Co correlates
   quite well with that of Ni, which suggests they have been in
   the catalyst and been distributed proportionally. The iron
   profile is approximately proportional to that of sulfur from
   the crust toward the interior of the catalyst. The interior
   sulfur concentration exceeds iron since the catalyst is
   sulfided. The concentration profiles of Ca, Si, Ti and Mg
   suggest deposition of mineral matter. The profiles of Mn and
   Zn show the lower content of these materials in the original
   coal matrix, and the deposition is primarily in the crust.
   The concentration profile of phosphorous shows this element is
   primarily deposited at the outer edge of the catalyst, and the
   higher concentration than that of the middle and outlet samples
   indicates deposition takes place primarily in the inlet of a
   reactor.

SIGNAL SENSIVITY

DISTANCE FROM SURFACE, *um*

DISTANCE FROM SURFACE, *um*

Figure 31.   Electron Microprobe Concentration Profiles of PP Catalyst
   (Middle) -- These profiles parallel those shown in Figure 30 for
   the inlet samples.   The Al profile shows a uniform distribution
   inside the catalyst.   Small amounts of Al deposition is shown, which
   may be attributed by mineral matter as in Figure 32.   The Co profile
   correlates quite well with that of Ni.   This result suggests that
   these two elements were deposited together.   The iron profile is
   approximately proportional to that of sulfur in the crust, and it
   is deposited primarily in the crust.   The concentration profile of
   sulfur inside the catalyst is approximately proportional to that of
   Mo.   The calcium profile shows that a high concentration of Ca has
   penetrated toward the interior of the catalyst.   The profiles of Si
   and Ti are similar to those of inlet samples.   The profile of Na
   suggests it may be added to control acidity.   Magnesium is shown to
   deposit primarily near the outer edge of catalyst surface and is
   inferred to be a component of mineral matter.   The profiles of K,
   Mn, P and Zn suggest low content of these elements in the original
   coal matrix.

85

SIGNAL SENSITIVITY

INTERIOR EXTERIOR

Al

Co

Mo

Fe

S

Ca

Si

Tl

Ni

Na

K max. sens.

Mg

Mn max. sens.

Zn max. sens.

P max. sens.

250   200   150   100   50   0   50

DISTANCE FROM SURFACE, μm
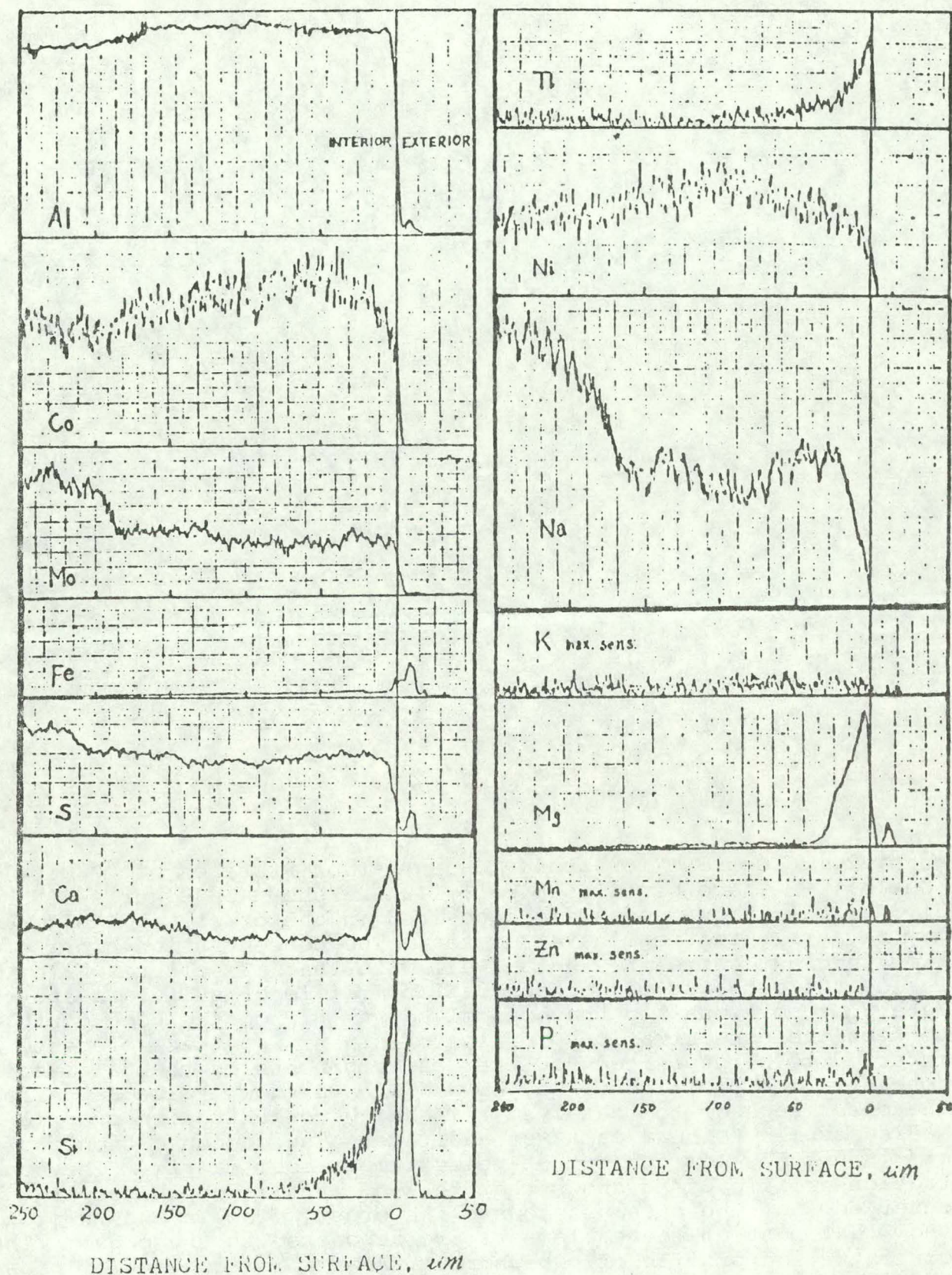
DISTANCE FROM SURFACE, μm

Figure 32. Electron Microprobe Concentration Profiles of PP Catalyst
    (Outlet) -- These profiles parallel those shown in Figures 30 and
    31. A small amount of Al is deposited in the crust, and this deposit
    may be attributed to mineral matter. The concentration profile of
    iron in crust correlates quite well with that of sulfur, while
    inside the catalyst the concentration profile of sulfur is approxi-
    mately proportional to that of molybdenum. From the good correlation
    between the concentration profiles of Ni and Co, these elements are
    inferred to be deposited together as components of the catalyst. The
    concentration profiles of Ca, Si and Ti are shown to be deposited at
    the outer edge of the catalyst. The high concentration profile of
    Na is assumed to be a catalyst additive. The concentration profile
    of K shows the low content of potassium in coal matrix. The concen-
    tration profile of Mg shows that this element is deposited at the
    outer edge of the catalyst toward the crust. The Mn and Zn profiles
    show that most of these elements are deposited in the crust. The
    concentration profile of phosphorous shows a low content of phos-
    phorous in the original matrix.

DISTANCE FROM SURFACE, μm

SIGNAL SENSIVITY

DISTANCE FROM SURFACE, μm

88
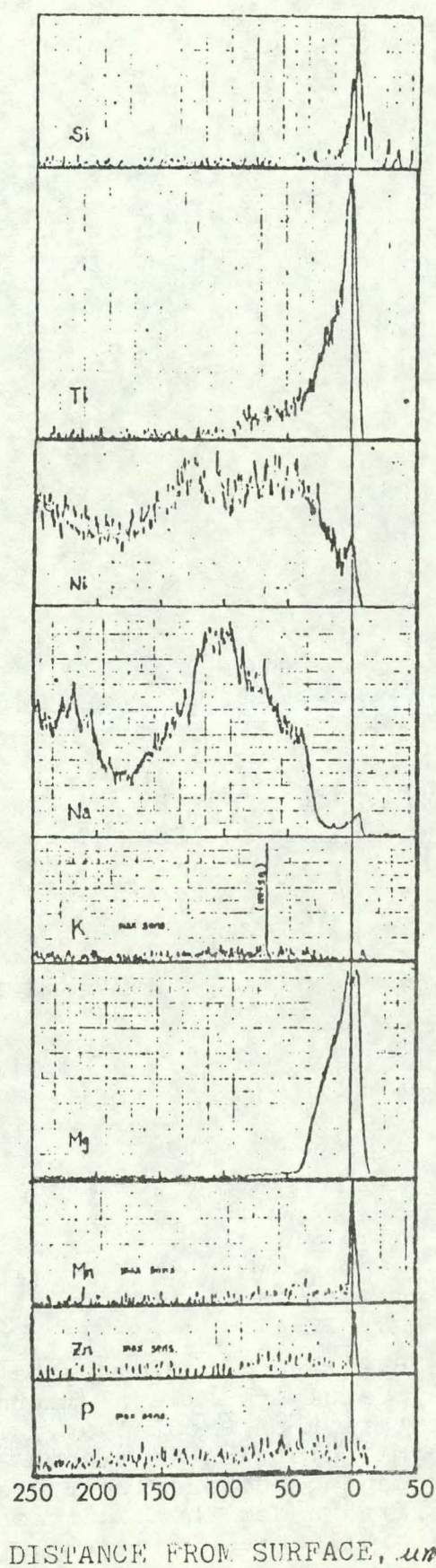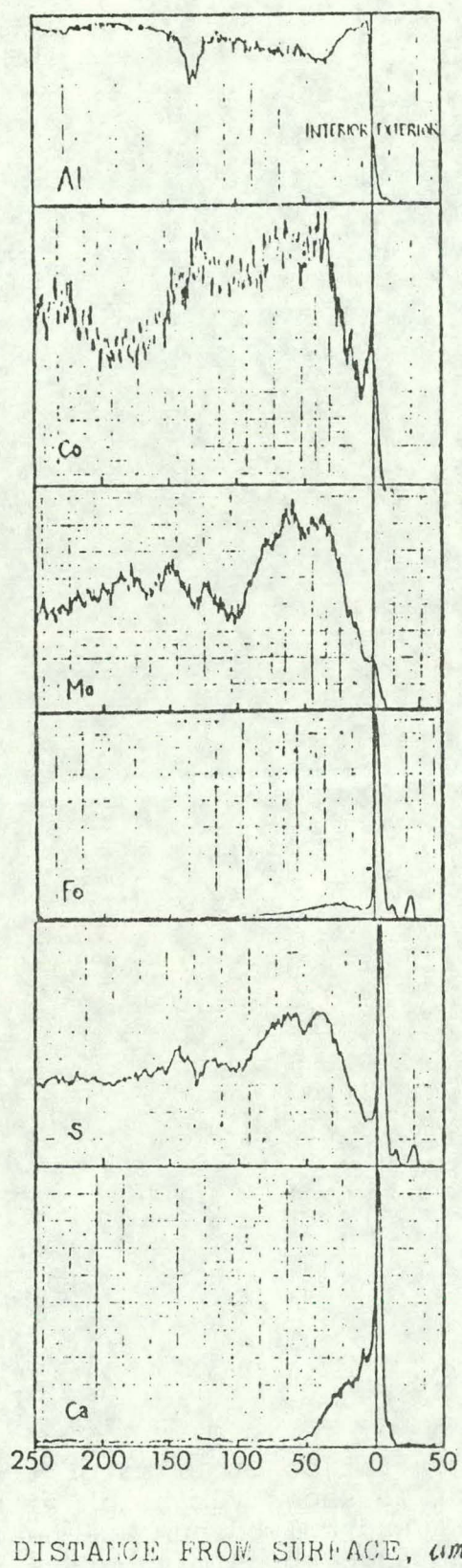
Figure 33. Electron Microprobe Concentration Profiles of the Fresh
   H-Coal Catalyst. The aluminum profile shows variation within
   the interior of H-catalyst. Cobalt and molybdenum are nearly
   uniformly distributed except at the edge which may be due to the
   heterogeneous porous structure of the catalyst. Sulfur is
   identified under the condition of maximum sensitivity; the catalyst
   is partially presulfided.

INTERIOR EXTERIOR

Al

Co

Mo

MAXIMUM SENSITIVITY

S

SIGNAL INTENSITY, arbitrary units

DISTANCE FROM SURFACE, μm.
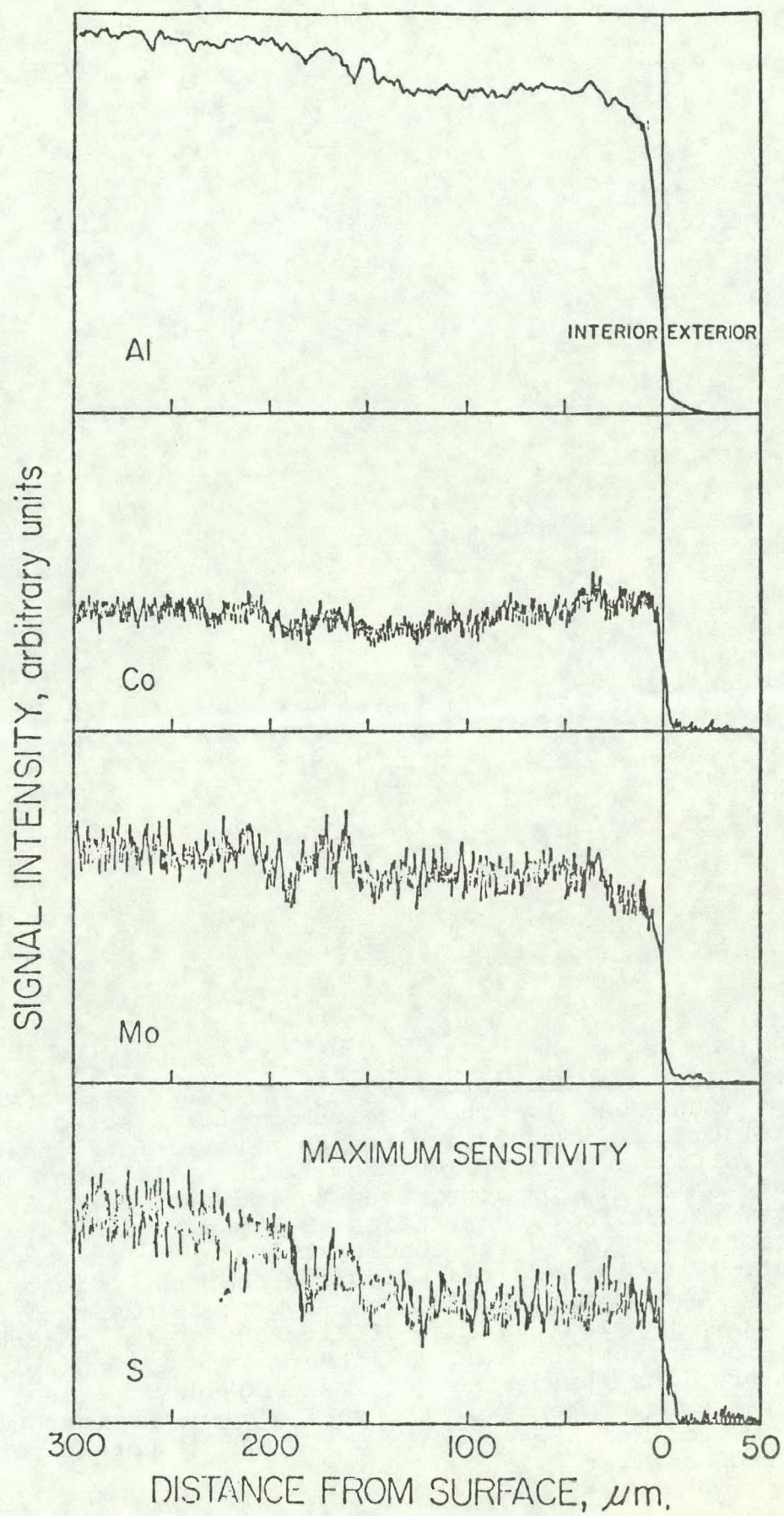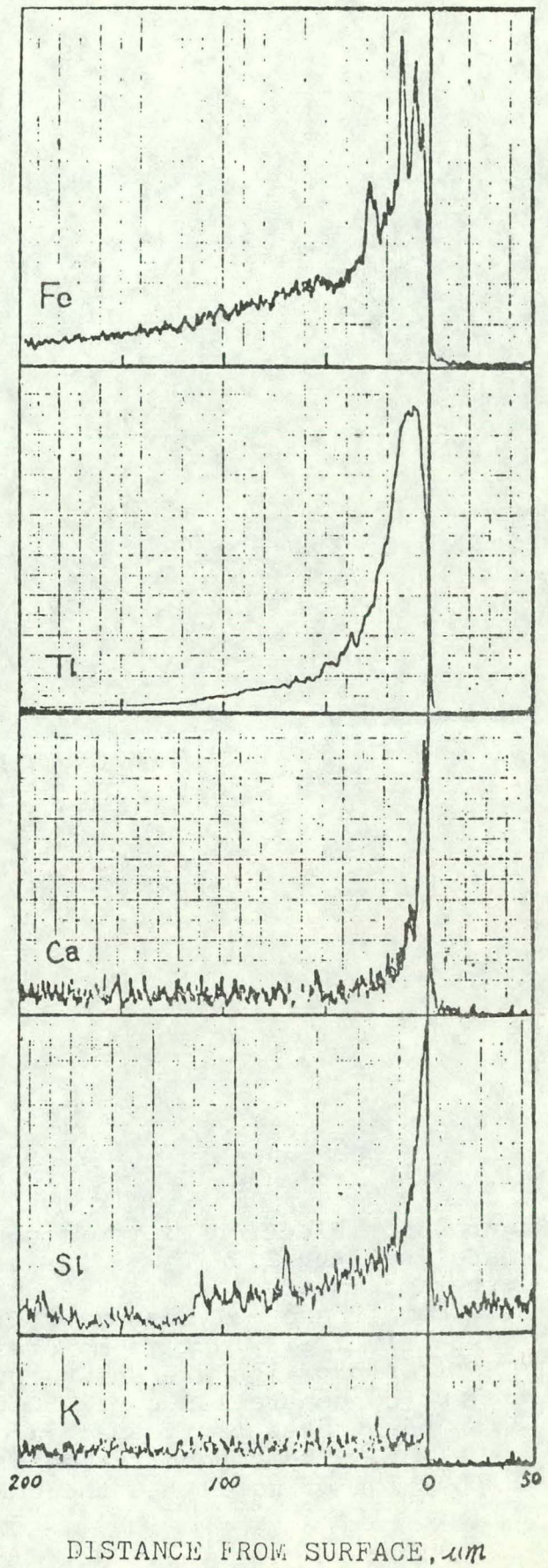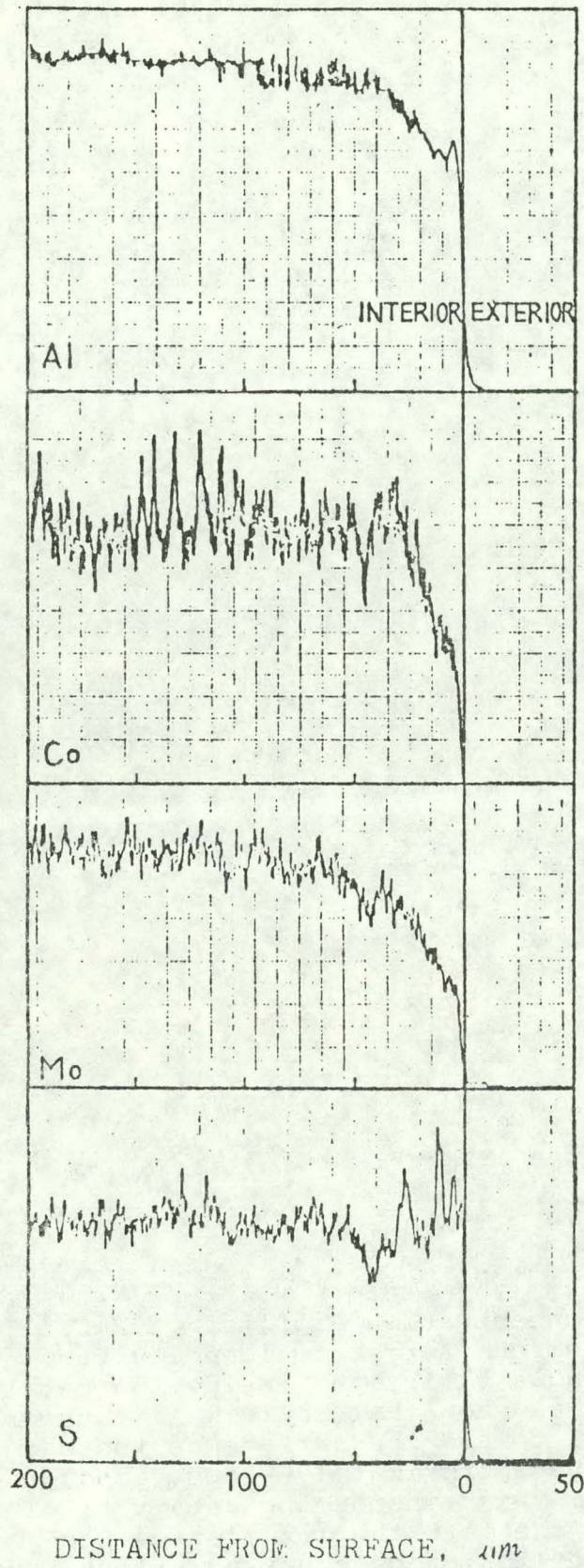
300   200   100   0   50

Figure 34. Electron Microprobe Concentration Profiles of H-Coal
Catalyst (Run 130-73). The aluminum profiles serve to identify
the exterior catalyst surface and show variations inside the
interior. Co and Mo profiles show large variations inside the
catalyst which may be attributed to low dispersion of these
elements. The iron concentration is shown to be approximately
proportional to the sulfur concentration up to 25 μm inside the
catalyst. Ti was deposited primarily near the edge of the
catalyst. The Ca and Si profiles show the similar concentration
distribution parallel to that of Ti, suggesting that these
elements come from the mineral matter. The irregularity of
silicon profiles inside the catalyst suggests the incorporation
of mineral constitutents of the coal within the macropores. The
potassium profile shows a trace of finely dispersed potassium
inside the catalyst.

91

DISTANCE FROM SURFACE, μm

DISTANCE FROM SURFACE, μm

SIGNAL SENSIVITY
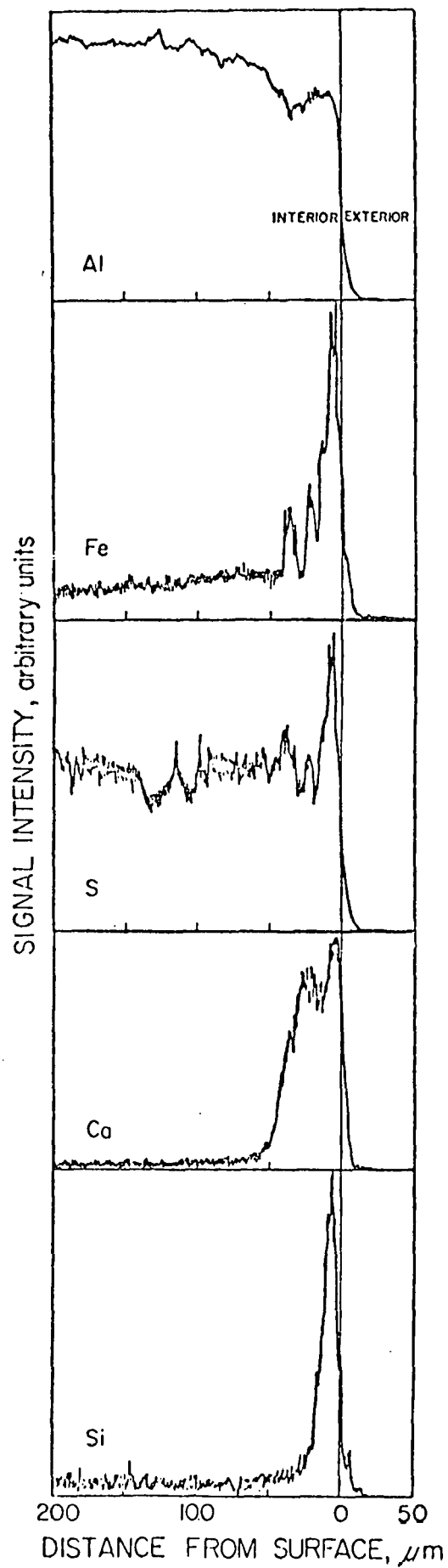
Figure 35.   Electron Microprobe Concentration Profiles of H-Coal
     Catalyst (Run 130-78) -- The aluminum serves to identify the
     exterior catalyst surface and shows variations inside the catalyst.
     The cobalt and molybdenum profiles show that there was transport
     of catalytically active material toward the surface of the catalyst.
     The iron profiles are shown to be approximately proportional to the
     sulfur concentration up to 50 μm thick inside the catalyst.   The
     iron pdnetrates far deeper into the into the interior of the
     catalyst.   The concentration profiles of calcium and silicon show
     deposition primarily at the outer edge of the catalyst.

INTERIOR EXTERIOR

Al

Fe

S

Ca

Si

SIGNAL INTENSITY, arbitrary units

200   100   0   50

DISTANCE FROM SURFACE, μm
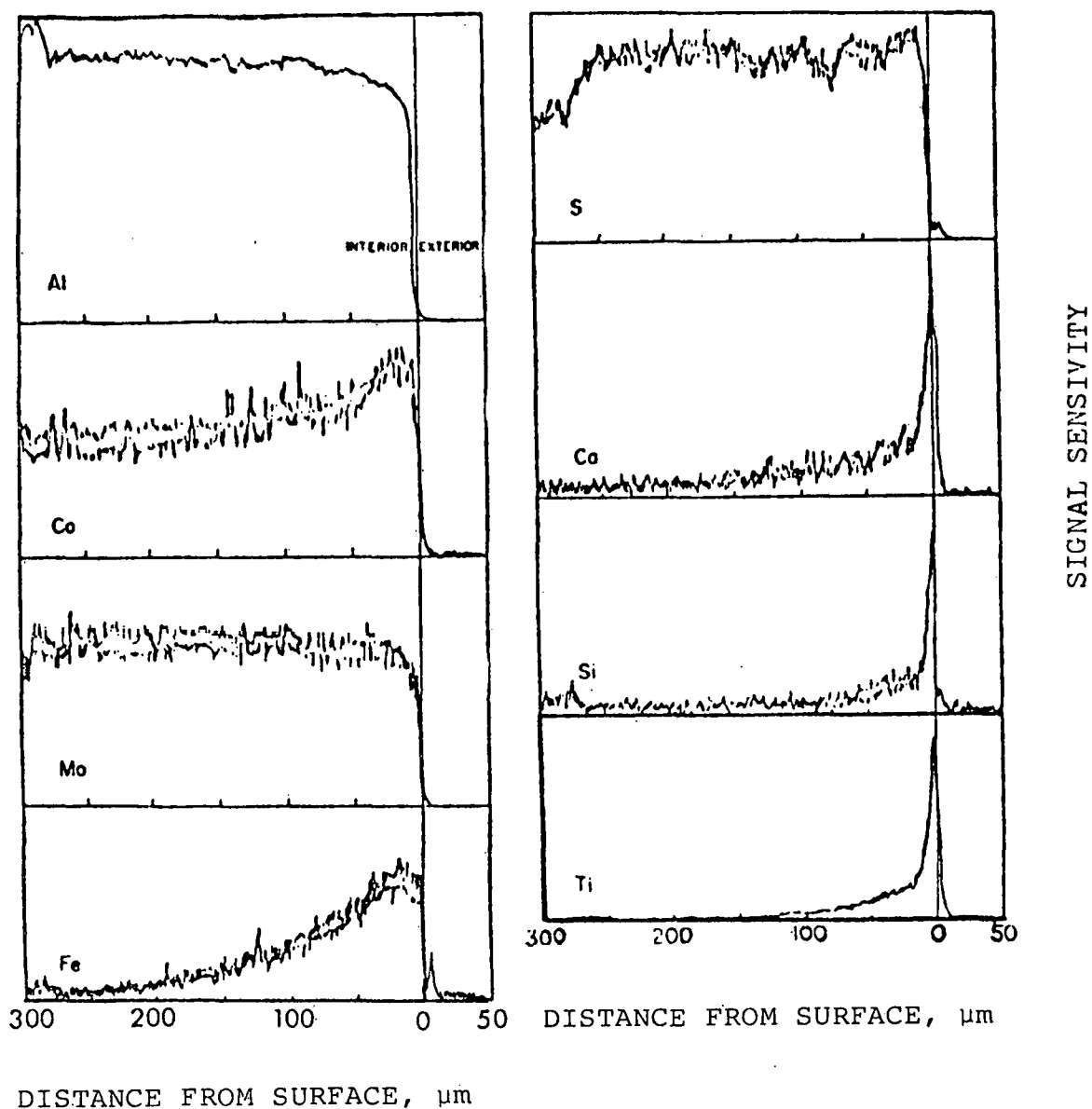
Figure 36. Electron Microprobe Concentration Profiles of H-Coal
Catalyst (Run 130-79) -- These profiles parallel those shown in
Figure 35. The profiles of Al and Mo show uniform distribution
inside the catalyst. The sulfur concentration profile is shown
to be approximately proportional to Co concentration. The iron
concentration is higher than that in Figures 34 and 35. The
concentration profiles of Ti, Ca and Si are shown to be deposited
primarily near the surface. The concentration profiles basically
parallel those of Figures 34 and 35.
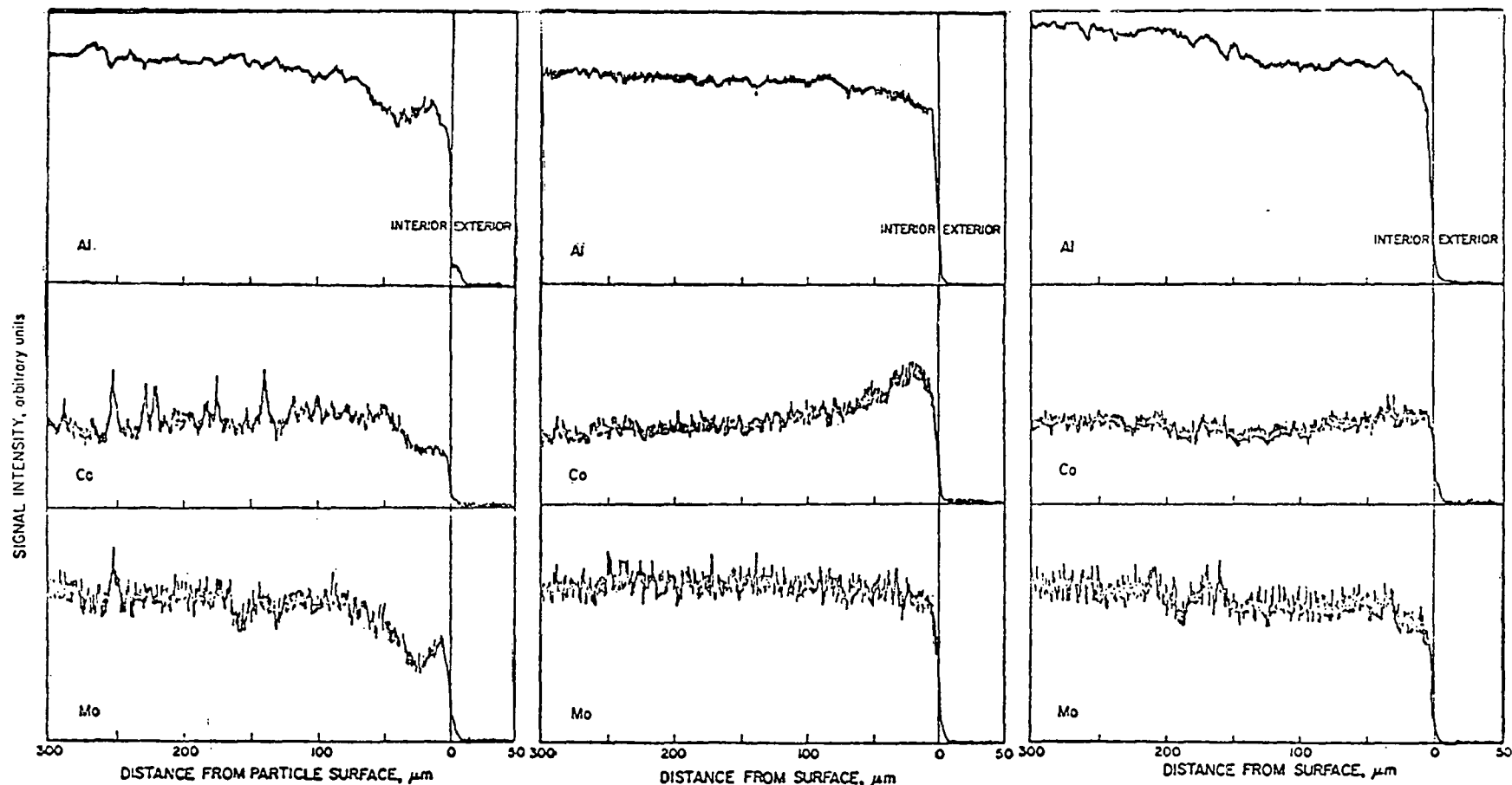
Figure 37. Dispersion of H-Coal Catalyst -- Electron Microprobe Concentration Profiles of H-Coal Catalysts (Run 130-78, 130-79 and fresh). This figure compares the Al, Co and Mo signals from the three samples at identical amplification. These figures show that cobalt does not correlate with molybdenum and hence appears to be added to the catalyst separately. There are large variations in the average concentration of catalytically active material. The spikes in the cobalt signal suggest sintering of the promoter during the run.

96

V. CONCLUSIONS

1. An experimental procedure for examining dibenzothiophene reaction kinetics has been developed. This procedure maintains the catalyst activity at the initial level for extended periods.

2. The detected organic reaction products of dibenzothiophene are sulfur free.

3. The reaction rate for 4,6-dimethyldibenzothiophene is about one-fifth of the rate for dibenzothiophene. The organic reaction products are sulfur free, and hence the C-S bond is the point of attack.

4. The major organic product of the hydrodenitrogenation of quinoline is o-propylcyclohexane amine, and the minor products are n-propyl benzene and three other unidentified materials. These products are consistent with preferred hydrogenolysis of the C-N bond in the hydrogenated hetrocyclic ring.

5. The rate of quinoline hydrodenitrogenation in the liquid-phase flow reactor is similar to the rates measured in stirred autoclave experiments.

6. The formation of external deposits on the surface of catalysts has been observed on a spent catalyst taken from a proprietary fixed-bed process for production of liquid fuel. These deposits are not present on catalyst samples from the H-Coal process.

7. Coal mineral matter deposits in the interior of all synthetic liquid fuel catalysts. The deposition occurs by cementing mineral matter just below the surface and also by a reactive transport deeper into the interior.

VI. LITERATURE CITED

1. Abou-Gheit, A. K., and Adbou, K., J. Institute Petroleum 59, 568 (1973).

2. Adkins, H., and Cramer, H. I., J. Amer. Chem. Soc. 52, 4349 (1930).

3. Cocchetto, J. F., and Satterfield, C. N., Ind. Eng. Chem. Process Design Develop. 15, 272 (1976).

4. Cox, K. E., and Berg, L., Chem. Eng. Progr. 56 (12), 53 (1962).

5. Doelman, J., and Vlugter, J. C., "Proceedings of the 6th World Petroleum Congress," Sect. III, p. 247, Frankfurt (1963).

6. Freifelder, M., Advan. Catal. 14, 203 (1963).

7. Flinn, R. A., Larson, O. A., and Beuther, H., Hydrocarbon Process 42 (9), 129 (1963).

8. Goudriaan, F., "Hydrodenitrogenation of Pyridine," Ph.D. Thesis, Twente University of Technology, 1975.

9. Goudriaan, F., Gierman, H., and Vlugter, J. C., J. Inst. Petrol. London 59 (565), 41 (1973).

10. Haensel, V., Pollitzer, E. L., and Watkins, C. H., "Proceedings of the 6th World Petroleum Congress," Sect. III, pp. 193-200, Hamburg (1963).

11. Hatch, L. F., Hydrocarbon Process 48 (2), 77 (1969).

12. Himmelblau, D., and Bischoff, K. B., I&EC Fundamentals 6, 539 (1967).

13. Hückel, W., and Stept, F., Ann. 453 (1927).

14. Landa, S., and Mrnkova, A., Coll. Tran. Chim. Tcheques. 2202 (1966).

15. Richter, F. P., Caesar, P. D., Meisel, S. I., and Offenhauer, R. D., Ind. Eng. Chem. 44, 2601, 1952.

16. Roberts, J. D., Stewart, R., and Caserio, M. C., Organic Chemistry, Benjamin, Inc., Menlo Park, CA, 1971.

17. Rollmann, L. D., preprint Fuel Division, San Francisco ACS meeting, August, 1976.

18. Sonnemans, J., Van Den Berg, G. H., and Mars, P., J. Catal. 31, 220 (1970).

19. Thomas, C. L., "Catalytic Processes and Proven Catalysts," pp. 157-172, Academic Press, New York 1970.

20. Urimoto, H., and Sakikawa, N., Sekiyu-Kagaku-Kyokaishi 15, (11), 926 (1972).

21. Vierhapper, F. W., and Eliel, E. L., J. Org. Chem. 60, 2729 (1975).

22. Vierhapper, F. W., and Eliel, E. L., J. Org. Chem. 40, 2734 (1975).

23. Von Braun, J., Gomelin, W., and Petzold, A., Ber 57, 302 (1924).

VII. PUBLICATIONS

1. Stanulonis, J. J., B. C. Gates, and J. H. Olson, "Catalyst Aging in a Process for Liquefaction and Hydrodesulfurization of Coal," A.I.Ch.E. Journal 19, 417 (1976).

2. Eliezer, Kenneth F., Manoj Bhinde, Marwan Houalla, Dennis Broderick, Bruce C. Gates, James R. Katzer, and Jon H. Olson, "A Flow Microreactor for Study of High-Pressure Catalytic Hydroprocessing Reactions," submitted to Ind. Eng. Chem. Fundamentals.

3. Chiou, M. J. and J. H. Olson, "A Method for Determining Catalytic Kinetics in a Pulse Microreactor System," submitted to Chem. Eng. Sci.

VIII. PERSONNEL

There has been one change in personnel this quarter: Ajit Sapre, a first-year graduate student, has joined the research group to work on HDS. To allow the expansion of the group, an NSF Energy Traineeship has been assigned to Dennis Broderick. Stuart Shih and Ed Reiff are expected to leave the group soon, and Dr. N. K. Nag will join it in February.